

S-1 MPC

S-1A & S-1B Annual Performance Report for 2017

Reference: MPC-0410
Nomenclature: DI-MPC-APR
Issue: 1.1
Date: 2018, Oct. 19

CLS (siège)
8-10 rue Hermès
Parc technologique du Canal
31520 Ramonville Saint-Agne
FRANCE

Tél. : +33 (0)5 61 39 47 00
Fax : +33 (0)5 61 75 10 14
Mél. : info@cls.fr
Web : www.cls.fr

CLS Brest Le Ponant
Avenue La Pérouse
29280 Plouzané
FRANCE

Tél. : +33 (0)2 98 05 76 80
Fax : +33 (0)2 98 05 76 90





Chronology Issues:

Issue:	Date:	Reason for change:	Author
0.1	26.03.18	First Draft	ESLs
1.0	01.10.18	Reviewed version	ESLs
1.1	19.10.18	Minor Revisions	ESLs

People involved in this issue:

Written by(*):	P. Meadows, BAE	Date + Initials:(visa or ref)
Checked by(*):	P.Vincent	Date + Initial:(visa ou ref) [Checker]
Approved by(*):	G.Hajduch	Date + Initial:(visa ou ref) [Approver]

**In the opposite box: Last and First name of the person + company if different from CLS*

**Index Sheet:**

Context:	Sentinel-1 Mission Performance Centre
Keywords:	Sentinel-1, Mission Performance Centre, Annual Report
Hyperlink:	

Distribution:

Company	Means of distribution	Names
CLS ESA	Notification	



List of tables and figures

List of tables:

Table 1: Noise power stability (3-sigma): period JAN 2017 - DEC 2017	27
Table 2: SM Azimuth and Slant Range Spatial Resolutions	29
Table 3: IW Azimuth and Slant Range Spatial Resolutions.....	30
Table 4: EW Azimuth and Slant Range Spatial Resolutions	30
Table 5: SM, IW & EW Sidelobe Ratios	31
Table 6: IW ENL & RR Measurements	31
Table 7: EW ENL & RR Measurements.....	31
Table 8: Azimuth Ambiguity Ratios.....	31
Table 9: SLC Relative Radar Cross-Section for the DLR transponders (dB)	32
Table 10: IW SLC Relative Radar Cross-Section for the DLR transponders (dB).....	32
Table 11: IW SLC Relative Radar Cross-Section for the DLR transponders (dB).....	32
Table 12: IW SLC Relative Radar Cross-Section for the Australian Corner Reflectors (dB)	33
Table 13: Gain Imbalance using the DLR transponders	36
Table 14: Phase Imbalance using the DLR transponders.....	37
Table 15: Polarimetric Calibration Measurements	37
Table 16: Cross-talk Measurements	37
Table 17: Results of the S-1A roll pointing analysis exploiting Elevation Notch acquisitions.	45
Table 18: S-1A/Radarsat-2 Mutual Interference during 2017	48
Table 19: Noise power stability (3-sigma): period JAN 2017 - DEC 2017	73
Table 20: SM Azimuth and Slant Range Spatial Resolutions	74
Table 21: IW Azimuth and Slant Range Spatial Resolutions	75
Table 22: EW Azimuth and Slant Range Spatial Resolutions	75
Table 23: SM & IW Sidelobe Ratios	76
Table 24: IW ENL & RR Measurements	76
Table 25: EW ENL & RR Measurements	76
Table 26: Azimuth Ambiguity Ratios	76
Table 27: SLC Relative Radar Cross-Section for the DLR transponders (dB).....	77
Table 28: SM SLC Relative Radar Cross-Section for the DLR transponders (dB).....	78
Table 29: IW SLC Relative Radar Cross-Section for the DLR transponders (dB).....	78
Table 30: IW SLC Relative Radar Cross-Section for the DLR transponders (dB).....	78
Table 31: IW SLC Relative Radar Cross-Section for the Australian Corner Reflectors (dB)	79
Table 32: Gain Imbalance using the DLR transponders	83
Table 33: Gain Imbalance using the DLR transponders	84
Table 34: Phase Imbalance using the DLR transponders.....	85
Table 35: SLC Polarimetric Co-registration.....	85
Table 36: Cross-talk Measurements	86



Table 37: Results of data DC analysis after attitude patches application.	90
Table 38: S-1B/Radarsat-2 Mutual Interference during 2017	92

List of figures:

Figure 1: H (top) and V (bottom) polarisation error matrixes on the 31 st December 2017. No TRM failures occurred during the whole 2017.	21
Figure 2: TX V antenna gain (left) and phase (right) variation due to tile #11 reconfiguration occurred on the 16-10-2017 (RDB#6).	22
Figure 3: TX H antenna gain (left) and phase (right) variation due to tile #11 reconfiguration occurred on the 16-10-2017 (RDB#6).	23
Figure 4: Gain (<i>top</i>) and phase (<i>bottom</i>) stability of the SAR antenna tiles (average of the RFC coefficients in TX H over rows). The Tile#11 reconfiguration on October can be recognized.	23
Figure 5: Gain (<i>top</i>) and phase (<i>bottom</i>) stability of the SAR antenna tiles (average of the RFC coefficients in TX V over rows). The Tile#11 reconfiguration on October can be recognized.	24
Figure 6: Gain (<i>top</i>) and phase (<i>bottom</i>) stability of the SAR antenna tiles (average of the RFC coefficients in RX H over rows).	24
Figure 7: Gain (<i>top</i>) and phase (<i>bottom</i>) stability of the SAR antenna tiles (average of the RFC coefficients in RX V over rows).	25
Figure 8: PG gain and phase over time. The colour represents the sub-swath.	26
Figure 9: EW HH (left) and HV (right) PG gain divided by sub-swath.	26
Figure 10: IW VV (left) and VH (right) PG gain divided by sub-swath.	27
Figure 11: Noise power versus time. The colour represents the different beams.	28
Figure 12: SM Azimuth and Slant Range Spatial Resolutions	29
Figure 13: IW Azimuth and Slant Range Spatial Resolutions	30
Figure 14: EW Azimuth and Slant Range Spatial Resolutions	30
Figure 15: IW SLC Relative Radar Cross-Section for the DLR transponders	32
Figure 16: IW SLC Relative Radar Cross-Section for the DLR Transponders and the BAE Corner Reflector	33
Figure 17: Permanent Scatter Calibration time series for TopSAR IW over Paris.	34
Figure 18: ALE estimates for S-1A IW SLC product time series acquired over the Swiss test sites using precise state vectors (AUX_POEORB). (a) products acquired in 2016; (b) products acquired in 2017. Product date ranges are shown in the figure inset. Point colours represent beam/subswath.	35
Figure 19: IW Gain Imbalance using the DLR transponders.	36
Figure 20: Phase Imbalance using the DLR transponders.	37
Figure 21: Difference in IW EAP gain between the new and previous EAPs.	38
Figure 22: Difference in EW EAP gain between the new and previous EAPs.	38
Figure 23: Difference in IW EAP gain between the new and previous EAPs.	39
Figure 24: Difference in EW EAP gain between the new and previous EAPs.	39
Figure 25: NESZ measures for IW. Blue is the measured NESZ and	40
Figure 26: NESZ measures for EW. Blue is the measured NESZ and the red lines are	42



Figure 27: S-1A Parallel (top) Normal (mid) and Along-Track (bottom) interferometric baseline during 2017. The hot colours represent the maximum value and the cold colours represent the minimum value for each orbit. The colours represent the track number. ..	43
Figure 28: S-1A IW (top) and EW (bottom) burst synchronization during 2017. The colour represents the number of points (light blue few points, purple many points). The black line is the average synchronization per day and the dashed lines are the S-1 requirement limits.	44
Figure 29: Doppler Centroid versus time. Average on a slice basis (dots) and daily average (red line). The star-trackers reconfigurations events are marked by the vertical black lines. The STT alignment campaign is marked by the vertical green lines.....	45
Figure 30: Doppler Centroid jump at sub-swath overlap versus time. Average on a slice basis (dots) and daily average (red line).....	46
Figure 31: An example of Radio Frequency Interference over Bangladesh & Bhutan.....	47
Figure 32: An example of S1/RS-2 Mutual Interference over Kazakhstan/China	48
Figure 33: S-1A/Satellite Interference 9th July 2017 (23:04 UT)	49
Figure 34: S-1A/Satellite Interference 11th July 2017 (11:53 UT).....	50
Figure 35: S-1A/Satellite Interference 31st October 2017 (11:20 UT)	51
Figure 36: S-1A/Satellite Interference 5th November 2017 (11:28 UT).....	51
Figure 37: SAR Wind speed compared with reference wind speed for IW mode VV polarisation.	53
Figure 38: S1A OWI wind speed performance as the function of the elevation angle demonstrating visible NESZ impact on the wind measurement.....	54
Figure 39: Ocean surface wind monthly performances for WV1 (a) and WV2 (b) and number of acquisitions co-located to reference data for validation for WV1 (bottom-left) and WV2 (bottom-right). For top panels, coloured thick solid lines stand for the mean difference between Sentinel-1 and ECMWF model wind speeds. Coloured thin solid lines are associated standard deviation.	55
Figure 40: Focus on ocean surface wind monthly performances for WV1 (a) and WV2 (b). Colored thick solid lines stand for the 7-days mean difference between Sentinel-1 and ECMWF model wind speeds.	56
Figure 41: scatter plot of wind speed from S-1A WV1 versus ECMWF Dec 2017 (left WV1 and right WV2).....	57
Figure 42: S-1A oswWindSpeed distribution per incidence angle. Red bars are WV1 and blue ones are WV2.....	57
Figure 43: scatter plot of effective significant wave height from S-1A WV1 versus WW3 significant wave height Dec 2017. The model outputs are considered as reference here. This is only valid from a statistical point of view	59
Figure 44: S-1A WV1 and WV2 Ocean Swell monthly performances as function of time.	59
Figure 45: Geophysical Doppler as included in the Level 2 products as a function of radial wind speed (wind speed projected in the line of sight of the radar) for WV1 and WV2. The colour code indicates the latitude.	61
Figure 46: Evolution of the Geophysical Doppler Centroid during the year 2017. The blue curve is the 7 days averaged Geophysical Doppler Centroid computed from Level2 RVL products for WV1 and red for WV2. Only measurements corresponding to ECMWF radial wind speed forecast is between -2 m/s and 2m/s are taken into account.....	62
Figure 47: S-1A WV OCN Doppler components from December 2017. The vertical bars are the spread in measured DC over the period. Note that the geometric DC is around zero and the EM DC bias is around -40Hz for S-1A.	62
Figure 48: (a,b) Doppler anomaly field from Sentinel 1A IW RVL product acquired over tropical cyclones in Caribbean. Here land areas are used to calibrate the Doppler anomaly. c) Acquisition areas.	63



Figure 49: S-1A HH EM DC offset computed from antenna model (full line) with error matrix corresponding to the day of acquisition and estimated from rain forest data using the Level 2 processor.....	64
Figure 50: Sentinel-1A geophysical relative RCS computed using CMOD-IFRv2+ECMWF for WV1 VV polarisation between 50° and -50° latitude. Panel 1 shows the mean bias between ECMWF and Sentinel-1A. Panel 2 shows the bias standard deviation. Panel 3 shows the number of SAFE used to perform the analysis.	65
Figure 51: Sentinel-A geophysical relative RCS computed using CMOD-IFRv2+ECMWF for WV2 VV polarisation between 50° and -50° latitude. Panel 1 shows the mean bias between ECMWF and Sentinel-1A. Panel 2 shows the bias standard deviation. Panel 3 shows the number of SAFE used to perform the analysis.	66
Figure 52: External Geophysical calibration evolution for 2017. WV1 (left) and WV2 (right) curves are showing the evolution of the bias between the level2 sigma0 and the sigma0 that CMOD-IFR2 model is giving. Green vertical lines are showing the date of AUX_PP1 update and IPF 2.84 deployment.	67
Figure 53: S-1B antenna status on 31/12/2016. The top charts refer to RX elements and the bottom charts refer to TX elements.....	68
Figure 54: Gain (<i>top</i>) and phase (<i>bottom</i>) stability of the SAR antenna tiles (average of the RFC coefficients in TX H over rows).	69
Figure 55: Gain (<i>top</i>) and phase (<i>bottom</i>) stability of the SAR antenna tiles (average of the RFC coefficients in TX V over rows).	69
Figure 56: Gain (<i>top</i>) and phase (<i>bottom</i>) stability of the SAR antenna tiles (average of the RFC coefficients in RX H over rows).	70
Figure 57: Gain (<i>top</i>) and phase (<i>bottom</i>) stability of the SAR antenna tiles (average of the RFC coefficients in RX V over rows).	70
Figure 58: Internal calibration parameters over time. The colour represents the sub-swath....	71
Figure 59: EW HH (left) and HV (right) PG gain divided by sub-swath.	72
Figure 60: IW VV (left) and VH (right) PG gain divided by sub-swath.	72
Figure 61: Noise power versus time. The colour represents the different beams.	73
Figure 62: SM Azimuth and Slant Range Spatial Resolutions.....	74
Figure 63: IW Azimuth and Slant Range Spatial Resolutions.....	75
Figure 64: EW Azimuth and Slant Range Spatial Resolutions.....	75
Figure 65: SM SLC Relative Radar Cross-Section for the DLR transponders.....	77
Figure 66: IW SLC Relative Radar Cross-Section for the DLR transponders.....	78
Figure 67: IW SLC Relative Radar Cross-Section for the DLR Transponders and the BAE Corner Reflector.....	79
Figure 68: S-1B Permanent Scatter Calibration time series for TopSAR IW over Paris.	80
Figure 69: ALE estimates for S-1B IW SLC product time series acquired over the Swiss test sites using precise state vectors (AUX_POEORB). (a) products acquired in 2016; (b) products acquired in 2017. Product date ranges are shown in the figure inset. Point colours represent beam/subswath.	81
Figure 70: ALE estimates for S-1B StripMap (SM), IW and EW SLC product time series acquired over the Swiss test sites using precise state vectors (AUX_POEORB). The left column shows ALE using previous post-processing methods; the right column shows more recent results after improved post-processing. Product date ranges are annotated in the figure inset text (N.B. no new S-1B SM or EW acquisitions were made over Switzerland in 2017; they are shown here to highlight the improved post-processing). Point colours represent beam/subswath. The S-1B SWST (range) bias (output of the respective commissioning and calibration phases) was applied in all cases.	83
Figure 71: Gain Imbalance using the DLR transponders.	84



Figure 72: Phase Imbalance using the DLR transponders.....	85
Figure 73: NESZ measures for IW. Blue is the measured NESZ and the red lines are.....	86
Figure 74: NESZ measures for EW. Blue is the measured NESZ and the red lines are.....	87
Figure 75: Parallel (top) Normal (mid) and Along-Track (bottom) interferometric baseline during 2017. The hot colours represent the maximum value and the cold colours represent the minimum value for each orbit. The colours represent the track number. ..	88
Figure 76: Doppler Centroid versus time. Average on a data-take basis (dots) and daily average (red line). The star-trackers reconfigurations events are marked by the vertical black lines.	89
Figure 77: (Left) Doppler Centroid versus ANX time during three different periods: blue before attitude patches application, red after relativistic aberration patch application and yellow after new AOCS filter gains application. (Right) Histogram of the DC estimates (same colour code).....	89
Figure 78: S-1B burst synchronization during 2017.	91
Figure 79: An example of Radio Frequency Interference	92
Figure 80: An example of Radarsat-2/Sentinel1-B Interference (3rd May 2017)	93
Figure 81: SAR Wind speed compared with reference wind speed for IW mode VV polarisation.	94
Figure 82: S1B OWI wind speed performance: bias as the function of the elevation angle (noticeable impact of the NESZ at high incidence angle: beam shaped profile)	95
Figure 83: S-1B WV1 and WV2 wind speed performances as function of time. Ocean surface wind monthly performances for WV1 (top-left) and WV2 (top-right) and number of acquisitions co-located to reference data for validation for WV1 (bottom-left) and WV2 (bottom-right). For top panels, coloured thick solid lines stand for the mean difference between Sentinel-1 and ECMWF model wind speeds. Coloured thin solid lines are for standard deviation.	96
Figure 84: S-1 Wind speed bias evolution for year 2017. Top panel represents WV1 measurements and resp. WV2 on bottom panel. Reference wind speed is ECMWF with a 0.125° resolution and 3-hourly temporal resolution. Dash line is the mean daily bias of OCN WV acquisitions. Black plain line is the 7-day mean and magenta line is the 30-day mean bias. The green vertical lines indicate technical facts linked to performance changes on WV. Green area delineates the period of HH acquisitions.	97
Figure 85: Scatter plot of wind speed from S-1B WV1 versus ECMWF Dec 2017. The model outputs are considered as reference here. This is only valid from a statistical point of view.	98
Figure 86: Sentinel-1 oswWindSpeed distribution per incidence angle. Red bars are WV1 and blue ones are WV2.	98
Figure 87: Significant wave height for the long waves performances for December 2017 in Wave Mode 1. The model outputs from WW3 are considered as reference here. This is only valid from a statistical point of view.	99
Figure 88: S-1B WV1 Ocean Swell monthly performances as function of time. For top panels, coloured thick solid lines stand for the mean difference between effective significant wave height from Sentinel-1 and from WW3 model. Coloured thin solid lines are for standard deviation.	100
Figure 89: Geophysical Doppler Centroid evolution. Light green area delineates the HH period of acquisition.	101
Figure 90: S-1B Geophysical Doppler as included in the Level 2 products as a function of radial wind speed (wind speed projected in the line of sight of the radar) for WV1 and WV2. The colour code indicates the latitude.	101
Figure 91: S-1B WV OCN Doppler components from December 2018. The vertical bars are the spread in measured DC over the period. Note that the geometric DC is around zero and the EM DC bias is around -15Hz for S-1B.	102



Figure 92: S-1B WV OCN Doppler versus range wind speed before (upper plots) and after (lower plots) attitude correction.....	103
Figure 93: S-1B IW OCN RVL mean DC bias as function of azimuth pixel. Data acquired over ocean areas.	103
Figure 94: S-1 B VV EM DC offset computed from antenna model (full line) with error matrix corresponding to the day of acquisition, and estimated from rain forest data using the Level 2 processor.....	104
Figure 95: Sentinel-1B geophysical relative RCS computed using CMOD-IFRv2+ECMWF for WV1 VV polarisation between 50° and -50° latitude. Panel 1 shows the mean bias between ECMWF and Sentinel-1B. Panel 2 shows the bias standard deviation. Panel 3 shows the number of SAFE used to perform the analysis.	105
Figure 96: External Geophysical calibration bias. WV1 (left) and WV2 (right) 7-days mean of sigma0 difference with a GMF are displayed. Green vertical line indicates the date of the AUX_PP1 calibration update and IPF 2.84 deployment.	105
Figure 97: S-1A and S-1B IW SLC Relative Radar Cross-Section for the BAE Corner Reflector..	106
Figure 98: PSCAL time series for IW DV acquisitions over Paris. The colour represents the sensor.....	107
Figure 99: ALE estimates for S-1A/B IW SLC product time series acquired over the Swiss test sites using precise state vectors (AUX_POEORB). (a) shows ALE using earlier post-processing methods; (b) shows more recent results after improved post-processing. Product date ranges are annotated. Point colours represent beam/subswath.	108
Figure 100: Parallel (top) Normal (mid) and Along-Track (bottom) interferometric baseline during 2017. The hot colours represent the maximum value and the cold colours represent the minimum value for each orbit. The colours represent the track number.	109
Figure 101: Comparison of S-1A (blue) and S-1B (red) daily average DC from data.	110
Figure 102: S-1B vs. S-1A burst synchronization error during 2017.	111



Applicable documents

[AD-01]	Sentinel-1 Product Specification, S1 RS-MDA-52-7441, Issue 3/3, October 2016
[AD-02]	Sentinel-1 Product Definition, S1-RS-MDA-57-7440, Issue 2/7, March 2016
[AD-03]	Sentinel-1 Level 1 Detailed Algorithm Definition, SEN-TN-52-7445, Issue 2/1, January 2017
[AD-04]	Sentinel-1 IPF Auxiliary Product Specification, S1-RS-MDA-52-7443, Issue 3/2, October 2016
[AD-05]	Sentinel-1 Doppler and Ocean Radial Velocity (RVL) ATBD, ISSN 1890-5226, Issue 01 , 09 May 2011
[AD-06]	Sentinel-1 Ocean Wind Fields (OWI) ATBD, S1-TN-CLS-52-9049, Issue 01, 27 April 2011
[AD-07]	Sentinel-1 Ocean Swell Wave Spectra (OSW) ATBD, S1-TN-NRT-52-7450, Issue 01, 27 April 2011



Reference documents

[S1-RD-01]	Nuno Miranda, Peter Meadows, Riccardo Piantanida, Andrea Recchia, David Small and Adrian Schubert and Pauline Vincent, 'The Sentinel-1 Constellation Product Performance Status' Proceedings of the ESA Fringe Workshop, 5-9 June 2017, Aalto University, Helsinki, Finland.
[S1-RD-02]	Nuno Miranda, Peter Meadows, Riccardo Piantanida, Andrea Recchia, David Small and Adrian Schubert and Pauline Vincent, 'The Sentinel-1 Constellation Performance Status', Proceedings of the CEOS SAR Workshop, November 7-9, 2017, Jet Propulsion Laboratory, California Institute of Technology, in Pasadena, California, USA.
[S1-RD-03]	Nuno Miranda, Andrea Recchia, Riccardo Piantanida, Niccolò Franceschi and Peter Meadows, 'Sentinel-1 New Thermal Noise Removal Approach', Proceedings of the CEOS SAR Workshop, November 7-9, 2017, Jet Propulsion Laboratory, California Institute of Technology, in Pasadena, California, USA.
[S1-RD-04]	Medhavy Thankappan, Ulrich Bals, Matthew Garthwaite, Christoph Gisinger, Peter Meadows, John Peter Merryman Boncori and Adrian Schubert, 'Calibration of Sentinel-1 and TerraSAR-X time-series SAR data over the Queensland Corner Reflector Array, Australia', Proceedings of the CEOS SAR Workshop, November 7-9, 2017, Jet Propulsion Laboratory, California Institute of Technology, in Pasadena, California, USA.
[S1-RD-05]	Schubert, A., D. Small, N. Miranda, D. Geudtner, E. Meier. Sentinel-1A Product Geolocation Accuracy: Commissioning Phase Results. Remote Sens. 2015, 7, 9431-9449. doi: 10.3390/rs70709431.
[S1-RD-06]	Schubert, A., D. Small, N. Miranda, D. Geudtner, E. Meier. Sentinel-1A Product Geolocation Accuracy: Beyond the Calibration Phase. Presented at CEOS SAR Calibration & Validation Workshop; Noordwijk, The Netherlands, 2015.
[S1-RD-07]	Pietro Guccione, Michele Belotti, Davide Giudici, Andrea Monti Guarnieri, Ignacio Navas-Traver Sentinel-1A: Analysis of FDBAQ Performance on Real Data, IEEE TRANSACTIONS ON GEOSCIENCE AND REMOTE SENSING, 2015.
[S1-RD-08]	Small, D., A. Schubert. Guide to ASAR Geocoding, UZH technical note for ESA-ESRIN, Contract No. 20907/07/I-EC, RSL-ASAR-GC-AD, Iss. 1.01; University of Zurich: Zurich, Switzerland, 2008, 36p.
[S1-RD-09]	GMES Sentinel-1 Team. GMES Sentinel-1 System Requirements Document, Ref. S1-RS-ESA-SY-0001, Iss. 3, Rev. 3, 2010.
[S1-RD-10]	Rodriguez-Cassola M. et al. Doppler-related distortions in TOPS SAR images, IEEE Trans. Geosci. Remote Sens. 2015, 53, 25-35.
[S1-RD-11]	Piantanida, R. Recchia, A., Franceschi, N., Valentino, A., Miranda, N., Schubert, A., Small, D., Accurate Geometric Calibration of Sentinel-1 Data, Proc. EUSAR 2018 (Abstract accepted at the time of this report)
[S1-RD-12]	Schubert, A., Miranda, N. Geudtner, D., Small, D., Sentinel-1A / B Combined Product Geolocation Accuracy. Remote Sensing 2017, 9, 1-16.
[S1-RD-13]	Sentinel-1A and -1B Annual Performance Report 2016, Issue 1.1, 04 April 2017

A set of technical documents, issued by S-1 Mission Performance Center, giving more information on the S-1A and S-1B products quality could also be cited as reference and is available on the [Sentinel Online Library](#). The full list is provided on Appendix B -.



List of Contents

1. Introduction.....	15
1.1. Purpose of the document	15
1.2. Structure of the document	15
2. Executive Summary	16
3. Processor Updates	19
4. S-1A Instrument Status	21
4.1. S-1A Antenna Status.....	21
4.2. S-1A Instrument Unavailability.....	25
4.3. S-1A Radar Data Base Updates	25
4.4. S-1A Internal Calibration	25
4.5. S-1A Noise Power	27
5. S-1A Products Status	29
5.1. S-1A Level 1 Products	29
5.1.1. Level 1 Basic Image Quality Parameters	29
5.1.1.1. Spatial Resolution.....	29
5.1.1.2. Sidelobe Ratios	30
5.1.1.3. ENL and Radiometric Resolution	31
5.1.1.4. Ambiguity Analysis.....	31
5.1.1.4.1. Azimuth Ambiguities	31
5.1.1.4.2. Range Ambiguities.....	31
5.1.2. Radiometric Calibration	31
5.1.2.1. Absolute Radiometric Calibration	32
5.1.2.2. Permanent Scatter Calibration	33
5.1.3. Geometric Validation	34
5.1.4. Polarimetric Calibration.....	36
5.1.4.1. Gain Imbalance.....	36
5.1.4.2. Phase Imbalance	36
5.1.4.3. Coregistration	37
5.1.4.4. Cross-talk	37
5.1.5. Elevation Antenna Patterns	38
5.1.6. Azimuth Antenna Patterns.....	39
5.1.7. Noise Equivalent Radar Cross-section	40
5.1.8. Interferometric Performances	42
5.1.8.1. S-1A Orbit Baseline	42
5.1.8.2. S-1A Burst synchronization	43
5.1.8.3. Instrument Pointing	44



5.1.9. Summary of Anomalies	46
5.1.9.1. Radio Frequency Interference	46
5.1.9.2. Radarsat-2/Sentinel1-A Mutual Interference	47
5.1.9.3. Other S-1A Interference	48
5.1.10. Quality Disclaimers	52
5.2. S-1A Level 2 products	52
5.2.1. Wind measurement	52
5.2.1.1. Image Mode (SM-IW-EW)	52
5.2.1.2. Wave Mode.....	55
5.2.2. Swell Measurement	58
5.2.2.1. Wave Mode.....	58
5.2.3. Radial Velocity Measurement	60
5.2.3.1. Wave Mode.....	60
5.2.3.2. TOPS Mode	63
5.2.4. Geophysical Calibration	65
5.2.4.1. Wave Mode.....	65
6. S-1B Instrument Status	68
6.1. S-1B Antenna Status	68
6.2. S-1B Instrument Unavailability	70
6.3. S-1B Radar Data Base Updates	71
6.4. S-1B Internal Calibration	71
6.5. S-1B Noise Power	73
7. S-1B Products Status	74
7.1. S-1B Level 1 Products	74
7.1.1. Level 1 Basic Image Quality Parameters	74
7.1.1.1. Spatial Resolution.....	74
7.1.1.2. Sidelobe Ratios	76
7.1.1.3. ENL and Radiometric Resolution	76
7.1.1.4. Ambiguity Analysis.....	76
7.1.1.4.1. Azimuth Ambiguities	76
7.1.1.4.2. Range Ambiguities.....	76
7.1.2. Radiometric Calibration	77
7.1.2.1. Absolute Radiometric Calibration	77
7.1.2.2. Permanent Scatter Calibration	80
7.1.3. Geometric Validation	80
7.1.4. Polarimetric Calibration	83
7.1.4.1. Gain Imbalance.....	83
7.1.4.2. Phase Imbalance	84
7.1.4.3. Coregistration	85



7.1.4.4. Cross-talk	85
7.1.5. Elevation Antenna Patterns	86
7.1.6. Azimuth Antenna Patterns.....	86
7.1.7. Noise Equivalent Radar Cross-section	86
7.1.8. Interferometric performances	87
7.1.8.1. S-1B Orbit Baseline	87
7.1.8.2. Instrument Pointing	88
7.1.8.3. S-1B Burst synchronization	90
7.1.9. Summary of Anomalies	91
7.1.9.1. Radio Frequency Interference	91
7.1.9.2. Radarsat-2/Sentinel1-A Mutual Interference.....	92
7.1.10. Quality Disclaimers	93
7.2. S-1B Level 2 products	93
7.2.1. Wind measurement.....	93
7.2.1.1. Image Mode (SM-IW-EW)	93
7.2.1.2. Wave Mode.....	95
7.2.2. Swell Measurement.....	99
7.2.2.1. Wave Mode.....	99
7.2.3. Radial Velocity Measurement	100
7.2.3.1. Wave Mode.....	100
7.2.3.2. TOPS Mode	103
7.2.4. Geophysical Calibration	105
7.2.4.1. Wave Mode.....	105
8. S-1A and S-1B Cross-comparison.....	106
8.1. Radiometric Calibration	106
8.1.1. Absolute Radiometric Calibration	106
8.1.2. Permanent Scatter Calibration.....	106
8.2. Geometric Validation.....	107
8.3. Interferometric Baseline	108
8.4. Instrument Pointing	109
8.5. Cross-interferometry Burst Synchronization.....	110
Appendix A - List of Acronyms	112
Appendix B - S-1A & S-1B Technical Reports	113
Appendix C - S-1A & S-1B Instrument Unavailability.....	115
Appendix D - S-1A & S-1B Quality Disclaimers	116
Appendix E - S-1A Orbit Cycles.....	117
Appendix F - S-1A Transmit Receive Module Failures	118



Appendix G - S-1A Auxiliary Data Files 119
Appendix H - S-1B Orbit Cycles..... 122
Appendix I - S-1B Transmit Receive Module Failures 123
Appendix J - S-1B Auxiliary Data Files..... 124



1. Introduction

1.1. Purpose of the document

The purpose of this document is to provide the status on the S-1A & S-1B instruments and products performance during 2017.

1.2. Structure of the document

The outline of this report is given below:

- Chapter 1 : this introduction
- Chapter 2 : Executive Summary
- Chapter 3 : Level 1 Processor Updates
- Chapter 4 : S-1A Instrument Status
- Chapter 5 : S-1A Products Status
- Chapter 6 : S-1B Instrument Status
- Chapter 7 : S-1B Products Status
- Chapter 8 : S-1A and S-1B Cross-comparison

The following appendices are also provided:

- Appendix A : List of Acronyms
- Appendix B : ESA S-1A & S-1B Technical Reports
- Appendix C : S-1A & S-1B Instrument Unavailability
- Appendix D : S-1A & S-1B Quality Disclaimers
- Appendix E : S-1A Orbit Cycles
- Appendix F : S-1A Transmit Receive Module Failures
- Appendix G : S-1A Auxiliary Data Files
- Appendix H : S-1B Orbit Cycles
- Appendix I : S-1B Transmit Receive Module Failures
- Appendix J : S-1B Auxiliary Data Files



2. Executive Summary

This report gives the status of the S-1A & S1-B instruments and product performance during 2017.

As will be seen in Chapter 2, Chapters 3 & 4 (S-1A), Chapters 5 & 6 (S-1B) and Chapter 7 (S-1A and S-1B Cross-Calibration) many aspects of the Instrument Processing Facility (IPF), instrument and products are considered with the aim of ensuring users receive high quality products.

A summary of the report is provided below:

IPF and Auxiliary Files

- During 2017, the IPF was updated twice for v2.82 to fixed throughput issues and v2.84 which is a major evolution of L2 processor (change in the language coding), but not aiming to change the Level 2 products performance.
- In addition, the AUX_CAL and AUX_PP1 auxiliary files were updated for both S1-A and S1-B for updates to noise calibration factors, elevation antenna patterns and processing gains.

Instrument Status

- The analysis of RFC, Internal Calibration and Noise products shows that S-1A instrument status is stable. No major events have been recorded during 2017.
- S-1A antenna was reconfigured on October 2017 in order to optimize the antenna electronic status after the tile 11 issue occurred on June 2016. The reconfiguration was performed updating a couple of RDB tables (RDB#6). The reconfiguration impact on the SAR performance was negligible.
- S-1A interferometric performances (interferometric baseline, instrument pointing and burst synchronization) are better than the requirements.
- On March 2017 the S-1A STTs have been re-aligned in order to avoid data DC jumps when STT configuration changes occur. The operation was successful.
- The analysis of RFC, Internal Calibration and Noise products shows that S-1B instrument status is stable. During 2017 a single TRM failure was recorded (mid-January 2017).
- On November 2017 an optimization of the on board attitude control system was performed. The optimization aimed at improving the agreement between DC estimates from the data and from the annotated attitude in order to enable L2 applications (RVL estimation). The optimization was successful, resulting in a reduction of the data DC estimates spread of the 50%, but L2 RVL estimation is still not possible. The same optimization has been performed for S-1A beginning in 2018.

Level 1 Product Status

- The various image quality parameters such as spatial resolution, sidelobe parameters, equivalent number of looks and ambiguity ratios derived using DLR transponders & corner reflectors, the BAE corner reflector and the Australian corner reflector array all give nominal results.
- The IW radiometric measurements using the DLR transponders give an overall relative radar cross-section of -0.06 ± 0.27 dB although there are some small variations with polarisation (i.e. gain imbalance) and IW sub-swath. Phase imbalance, image coregistration and cross-talk all give good results.
- Permanent scatter IW results over Paris show consistent results with the RCS measurements for the BAE corner reflector.
- For the geometry absolute localisation accuracy, results indicate that given bias compensations, the localisation performance was much better than the original requirements. The most important improvements made in 2017 to the geolocation estimation process itself were:



- For TOPS mode products, a range timing bias correction was implemented within the geolocation estimation processing chain, whose magnitude depends on the reference target's relative azimuth position within a burst (the greater its offset from mid-burst, the greater the Doppler frequency and the greater the corresponding range bias).
- Sensor motion during the interval from echo Tx to Rx causes an azimuth timing error if not properly corrected during product generation. The S-1 processor makes use of a single range reference time to perform subswath-specific timing corrections. However, the reference time used by the S-1 processor for its correction was shown not to be the one annotated in the products, causing subswath-dependent relative azimuth shifts of up to several metres (in TOPS products, less in SM products). Correcting for this processor-internal timing error (we call this the "bulk bistatic correction") improves the relative azimuth geolocation accuracy between subswaths.
- There were two small updates to the S-1A elevation antenna patterns (EAPs) during 2017. The first related to the outcome of re-calibration activities related to the refinement of the antenna model while the second were for the period after the tile 11 anomaly in mid-2016.
- S-1B interferometric performances (interferometric baseline, instrument pointing and burst synchronization) are better than the requirements.
- Several updates to the noise calibration vectors were performed during 2017 to ensure that image noise could be successfully removed by users. Noise equivalent radar cross section measurements were made - all were consistent with previous measurements.
- A few examples of interference occurred during 2017 from sources on the ground, mutual interference with Radarsat-2 and an unknown source(s) causing long-duration interference. These were primarily for S1-A with no long-duration interference occurring for S1-B.

Level 2 Product Status

- The performance of L2 appeared stable during 2017. The major evolution was done with IPF 2.84 which includes a change in the coding language of the L2 processor. This has had no impact on the L2 performances but allowed to increase the rate of products processed up to L2, production has increased during October/November 2017 to become global.
- Wind products on Image Mode (IW/SM/EW) show good correlation with reference wind speeds, and are better than the requirements in term of global statistics (Wind speed RMS is nominal lower than 2m/s, Direction lower than 30°; respecting the products requirement) However, they show artefacts due to the current choice of the wind GMF (Cmod-lfr2, Quilfen et al., 2004):
 - General negative bias -0.3 to -0.7 m/s (depending on the reference data used for the comparison) on VV polarization (reduced/balanced on HH due to cumulative impact of noise)
 - Dependency of the performances with the wind speed
 - Trends to overestimate zero wind speed value (at low incidence angle)

In addition, the impact of noise profile is clearly visible on HH polarization or for high incidence angles.

- Wave Mode Wind Measurements: 2017 was the first complete year for routine acquisition in Wave mode with both S1A and S1B. The performances are very similar for S1A and S1B. In WV1 and WV2 wind speed bias with respect to ECMWF 0.125° are about -0.14 and -0.07 m/s with mean RMSE of about 1.56m/s and 1.54m/s, respectively. Those performances are better than the Sentinel-1 mission requirements for ocean surface wind speed (RMSE<2m/s).

The limitations observed from both missions are:

- Wind speed performances are wind speed dependent for both WV1 and WV2.
- The presence of null wind speed obtained with WV1. This is due to the use of CMOD IFR2 for the wind inversion.



- These two issues are related to the Wave Mode calibration and the choice of the Geophysical Model Function in the inversion scheme.
- Swell Measurements: In 2017, Sentinel-1 acquisitions in wave mode have been performed at global scale over the oceans in a routine configuration during the whole year. It leads to about 480000 acquisitions of acquisitions every cycle. Sentinel-1 significant wave height performances with respect to WW3 numerical model forecasts are better than the mission requirements regarding the bias but not for the RMSE (specifications are $RMSE < 0.5m$ and $bias < 0.1m$). In WV1 and WV2, a mean bias of respectively about 0.15m and 0.20m, with a RMSE of about 0.38m is observed. The issue with the bias is related to the modulation transfer function applied in the inversion, and further investigation is undertaken.
- Radial Velocity: The Level 2 Doppler anomaly and radial velocity measurements are at present colored by the attitude Doppler. The attitude Doppler computed from the downlinked quaternions is around zero, and do not reflect the actual attitude Doppler. This prevents calibrated radial velocity extraction.

In late November 2017 ESA performed a STT Aberration Correction and an AOCS Fine Attitude Tuning on Sentinel-1B. A similar exercise was performed in February for S1A. A positive impact was observed on both the S1A and the S-1B OCN Doppler product. A significant increase in correlation between OCN Doppler and radial wind speed was observed. After the SST corrections, the performance of the S1A and B OCN Doppler are similar.

Another problem observed in the IW and EW Level 2 Doppler is a scalloping with burst period. Attempt to account for the antenna deformation during sweep did not provide the expected results, and further investigations are undertaken.



3. Processor Updates

The main improvements introduced in the Level-1 and Level-2 Processor and impacting data quality are here below described, classified according to the release in which they have been included. The full description of IPF upgrade is available on the Release note for end users document link provided in Appendix B - . For information the IPF 2.8.0 version (released in November 2016) has been listed. This version was never made operational due to a throughput issue (excessive filter length) related to the new normalization strategy implemented for TopSAR SLC products generation. The IPF 2.8.2 & 2.8.4 included all IPF 2.8.0 features and restored previous performance.

IPF v2.8.0 (15/11/2016)

- Introduced full review of processor normalization approach for TopSAR data
- Solved issue in the management of Doppler Centroid estimations causing the presence of radiometric artefacts in TopSAR data (darker bursts)
- Review and correction of terrain height different annotations in L1 products

IPF v2.8.2 (28/03/2017)

- Fixed throughput issues introduced by IPF V2.8.0 (IPF V2.7.2 performances restored).

IPF v2.8.4 (22/08/2017)

- No Upgrade of the Level 1 processor, changes concerned only L2 part
- The aim of this delivery is to provide an IPF version for Level 2 in Python, replacing the previous IDL versions of the Level 2, without degradation of the quality performances. Minor additional changes are :
 - Fixed ice mask on OWI
 - Fixed the missing variables owiElevationAngle, owiNesz when OWI processing is not performed
 - Introduction of fill values for OSW variables

In addition to the described L1 and L2 Processor upgrades, a summary of Auxiliary Data Files (ADFs) updates during the reporting period is provided, together with an explanation of the updates, in Appendix G - for S1-A and Appendix J - for S1-B. The main ones are here below summarised:

AUX_INS

- No updates during 2017

AUX_CAL

During 2017 the S1-A AUX_CAL auxiliary files were updated on three occasions:

- 28th March 2017: updates of (a) IW & EW Noise Calibration Factors and (b) Elevation Antenna Pattern to implement the outcome of recalibration #2 activity related to the refinement of the antenna model
- 22nd May 2017: updated SM, IW and EW Elevation Antenna Patterns following the Tile 11 Anomaly in June 2016
- 13th October 2017: update to be compliant with RDB#6

During 2017 the S1-B AUX_CAL auxiliary files were updated on two occasions:



- 16th January 2017: update of Noise Calibration Factors for IW and EW mode
- 28th March 2017: update of IW and EW Noise Calibration Factors to implement the outcome of recalibration #2 activity performed in preparation to IPF v2.8.2 deployment

AUX_PP1

During 2017 the S1-A AUX_CAL auxiliary files were updated on two occasions:

- 28th March 2017: Update of Processing Gains for IW and EW modes to implement the outcome of recalibration #2 activity performed in preparation to IPF V282 deployment
- 13th October 2017: Processing gains updated for WV mode to introduce an offset compensating the WV1/WV2 bias characterised through the analysis of data NRCS.

During 2017 the S1-B AUX_CAL auxiliary files were updated on three occasions:

- 16th January 2017: Update of Processing Gains for IW and EW modes to implement the outcome of recalibration #2 activity performed in preparation to IPF V282 deployment
- 28th March 2017: Scaling LUT updated for SM, IW and EW modes, only QL decreasing them of 1.44dB to compensate extra-brightness w.r.t. S-1A QL
- 3rd October 2017: Processing gains updated for WV mode to introduce an offset compensating the WV1/WV2 bias characterised through the analysis of data NRCS



4. S-1A Instrument Status

Hereafter, the status of the S-1A instrument during 2017:

4.1. S-1A Antenna Status

The Antenna status is routinely monitored using the dedicated RFC calibration mode. The RFC products are processed in order to generate the Antenna Error Matrix from which it is possible to retrieve the failure and drift of each TRM.

Figure 1 shows the antenna Transmit/Receive Module (TRM) status at the end of 2017. No major changes in the antenna status occurred during the whole 2017. Ten (10) failures are counted in total among TX-RX and H-V (the antenna elements marked with a star in the plot). The figure also shows that half of tile 11 (TRMs from 1 to 10) is transmitting with reduced power (-10 dB) in both polarizations since the antenna issue on June 2016. This antenna configuration is required to reduce instrument power consumption and hence ensuring SAR operation. To ensure negligible impacts on SAR performance a new S-1A AUX-CAL was endorsed on March 2017 (see also Section 3). The new AUX-CAL file included Elevation Antenna Patterns evaluated with the S-1 Antenna Model considering the new instrument status.

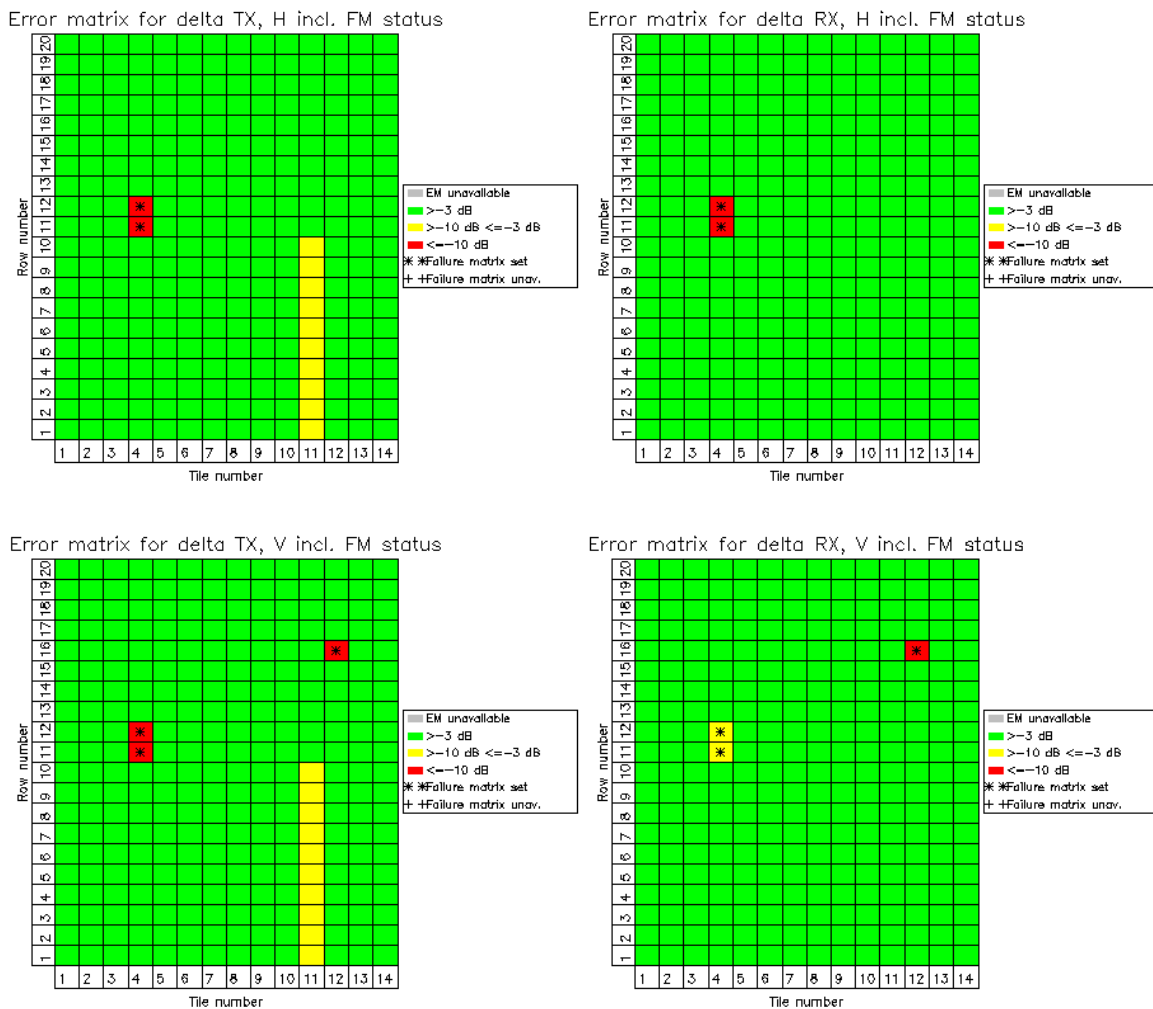


Figure 1: H (top) and V (bottom) polarisation error matrixes on the 31st December 2017. No TRM failures occurred during the whole 2017.



On the 16th October 2017, the configuration of antenna tile 11 was modified to improve the antenna electronic configuration. The resulting updated configuration was captured in the RDB#6. The following changes occurred:

- Only tile 11 status was modified
- The gain of TMRs from 1 to 10 was further decreased of about 3 dB
- The gain of TMRs from 11 to 20 was slightly increased in order to be re-aligned with the other TRMs
- The phase of TMRs from 11 to 20 was re-aligned with the other TRMs

The change in the antenna status are highlighted in Figure 2 (V pol) and Figure 3 (H pol), representing the variation of the gain (plot on the left) and of the phase (plot on the right) of the TRMs in TX configuration. The variation measured on the 19th October 2017 has been measured w.r.t. the antenna status on the 16th October 2017 (before the reconfiguration).

The antenna reconfiguration did not require to generate a new S-1A AUX-CAL file since the impact on the EAPs predicted by the S-1 AM is lower than ± 0.1 dB.

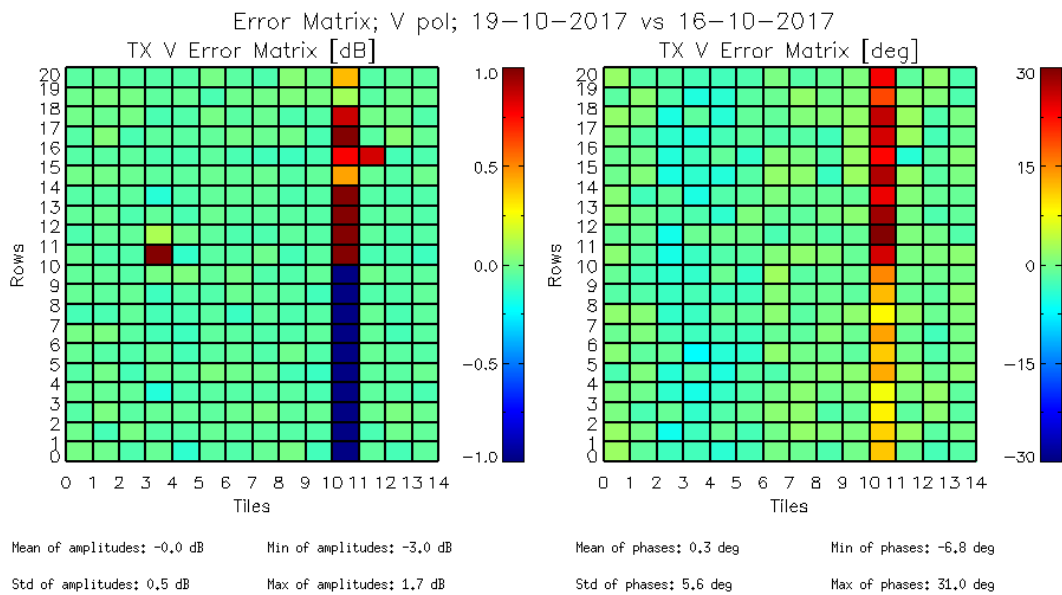


Figure 2: TX V antenna gain (left) and phase (right) variation due to tile #11 reconfiguration occurred on the 16-10-2017 (RDB#6).

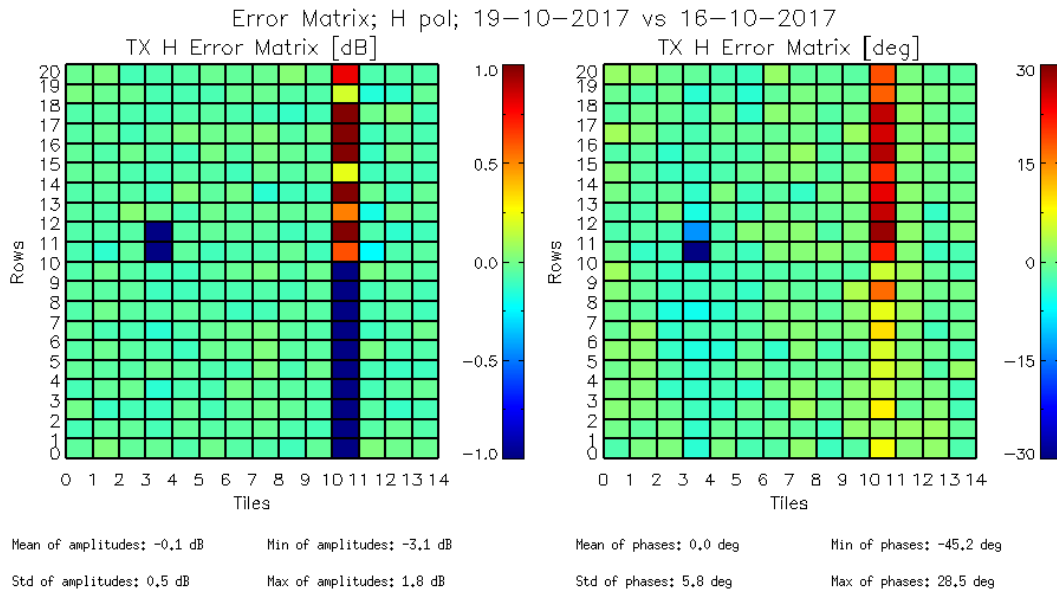


Figure 3: TX H antenna gain (left) and phase (right) variation due to tile #11 reconfiguration occurred on the 16-10-2017 (RDB#6).

The following plots show the TX excitation coefficients (averaged per tile) obtained processing RFC products of 2017. Tile 11 shows a small gain increase of about 0.2 dB and a phase jump of about 30° after the reconfiguration. Please note that other tiles show a small decrease of their average gain due to the fact that, during RFC processing, the coefficients are normalized. The plots showing the RX excitation coefficients have also been reported. No events related to RDB#6 can be noticed. Excluding the tile 11 reconfiguration, the antenna shows overall a stable behaviour: 0.4 dB of average temporal stability for the gain and 5° for the phase have been computed. Finally, it is worth to mention that the antenna reconfiguration led to no meaningful changes in the SAR performance.

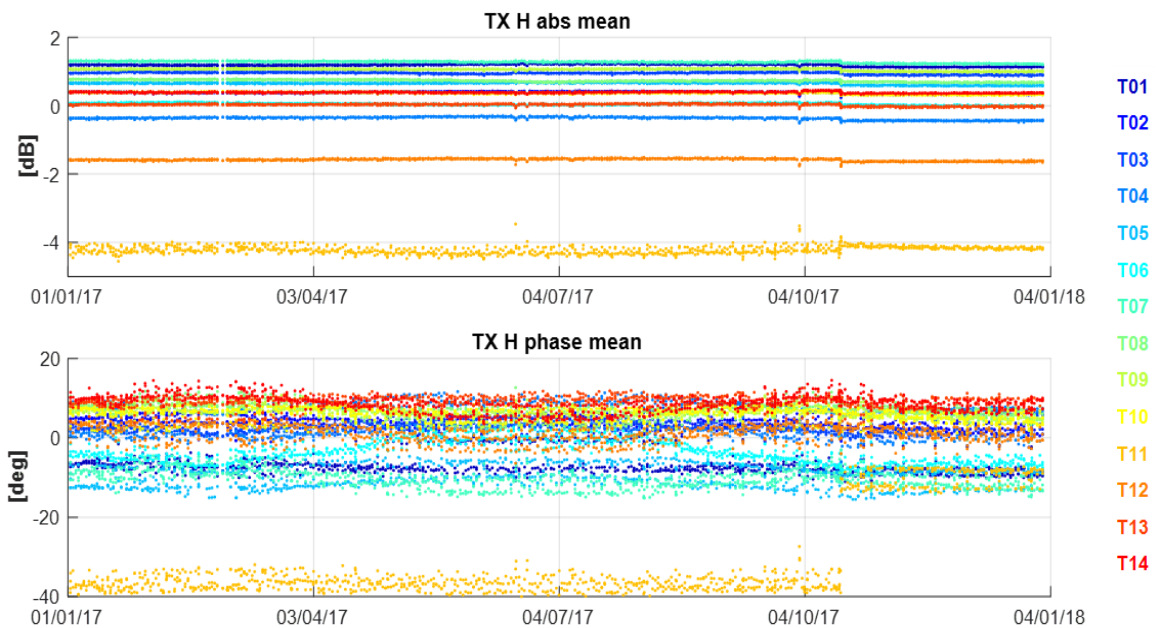


Figure 4: Gain (top) and phase (bottom) stability of the SAR antenna tiles (average of the RFC coefficients in TX H over rows). The Tile#11 reconfiguration on October can be recognized.

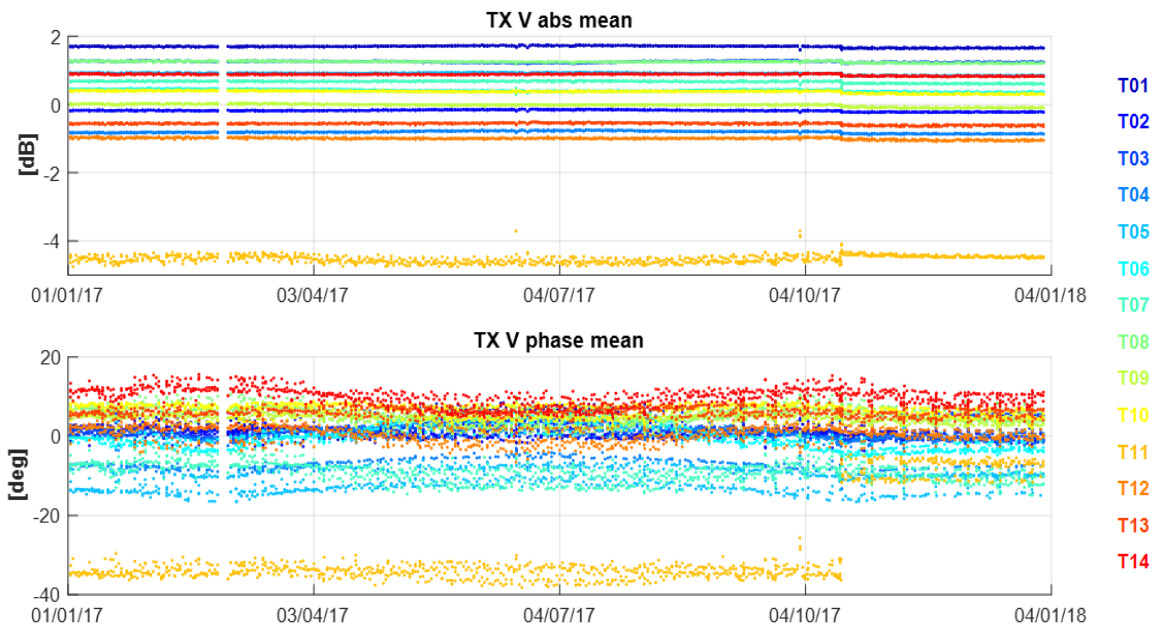


Figure 5: Gain (top) and phase (bottom) stability of the SAR antenna tiles (average of the RFC coefficients in TX V over rows). The Tile#11 reconfiguration on October can be recognized.

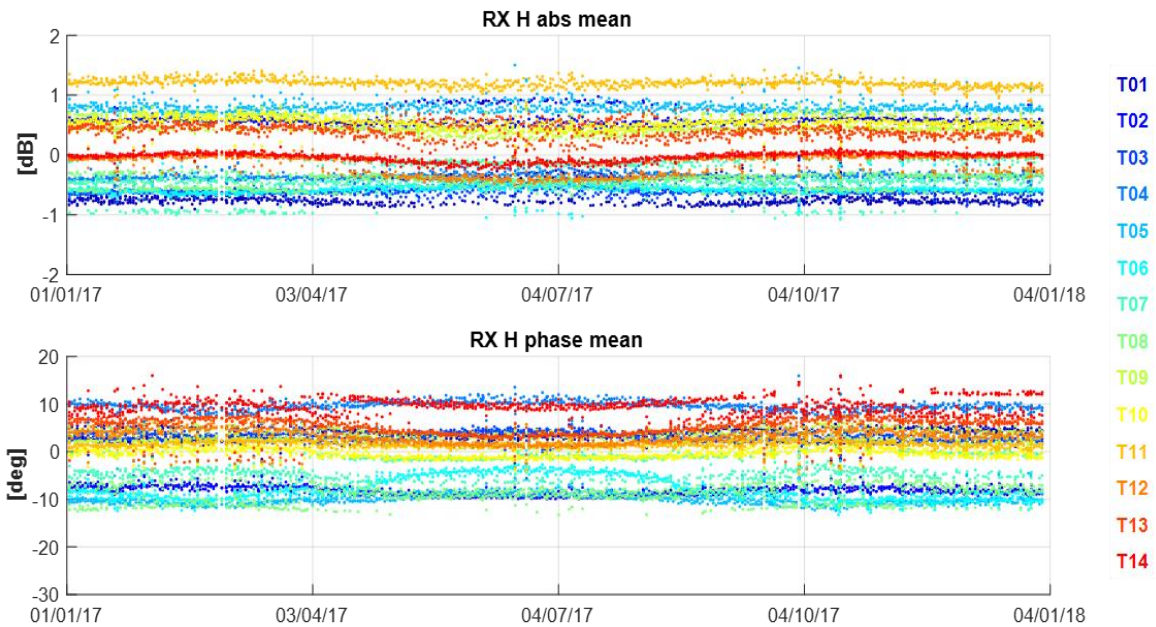


Figure 6: Gain (top) and phase (bottom) stability of the SAR antenna tiles (average of the RFC coefficients in RX H over rows).

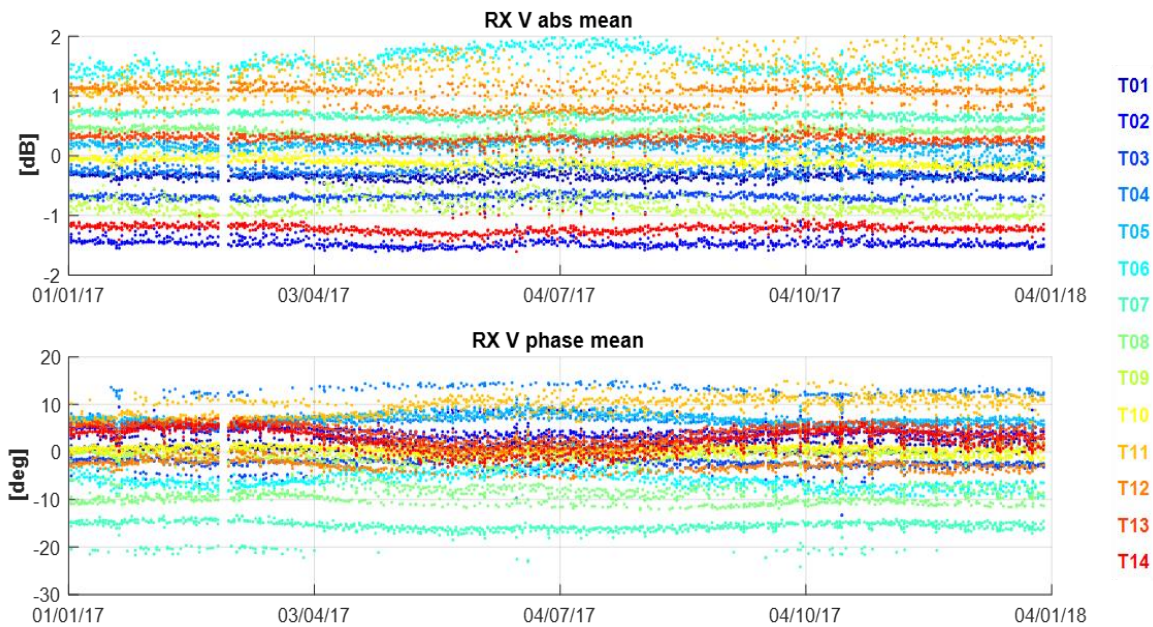


Figure 7: Gain (top) and phase (bottom) stability of the SAR antenna tiles (average of the RFC coefficients in RX V over rows).

4.2. S-1A Instrument Unavailability

A list of S-1A instrument unavailabilities during 2017 is given in Appendix C -.

4.3. S-1A Radar Data Base Updates

The RDB version #6 was endorsed on 16 October 2017. The new RDB version captured new antenna status after tile 11 reconfiguration described in Section 4.1. In particular, the the following updates were included in the new RDB:

- TA redundancy Tile 11 updated in the Redundancy Configuration Table (SAS)
- Modification of the Nearest State Tables (TX only) for tile 11 with the new gains (SES)

4.4. S-1A Internal Calibration

The instrument stability over time is monitored through the internal calibration signals. The plot in Figure 8 shows the main parameters monitored: PG gain and phase. The colour in the plot represents the different sub-swaths.

The PG gain is quite stable in the reporting period. The observed different levels pertaining to the same mode (e.g. two different PG levels observed in particular for EW beams) are related to the different RX polarization as detailed in the following plots.

The observed PG phase jumps are expected. They occur at every instrument switch off due to a different initialization of the ADC. They are not an issue since they only provide a phase constant in the SAR data.

Figure 9 and Figure 10 show a more detailed picture of the PG trend during the reporting period for EW DH and IW DV acquisitions. No particular trends can be identified during the reporting period,



even if some slow fluctuations can be observed in particular for RX H beams (EW HH and IW VH). Such fluctuations are in any case quite small with a peak to peak variation around 0.1 dB. In all the plots, it is possible to see a small jump in the PG gain of less than 0.1 dB after the tile 11 reconfiguration (see Section 4.1). This small PG increase is due to the phase re-alignment of the nominally working TRMs of tile 11.

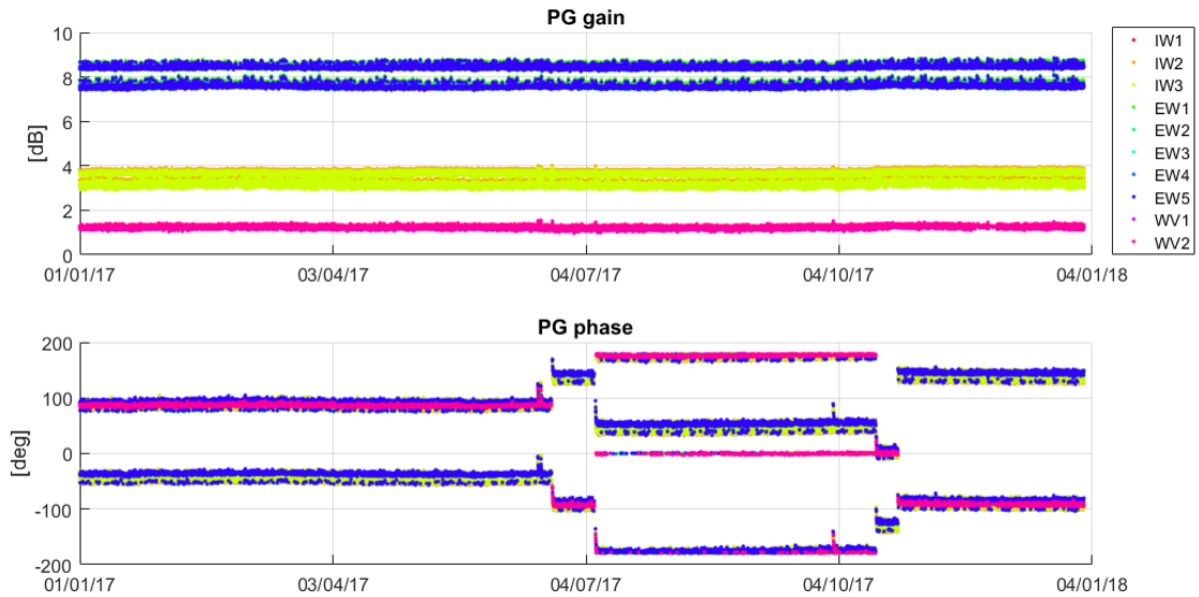


Figure 8: PG gain and phase over time. The colour represents the sub-swath.

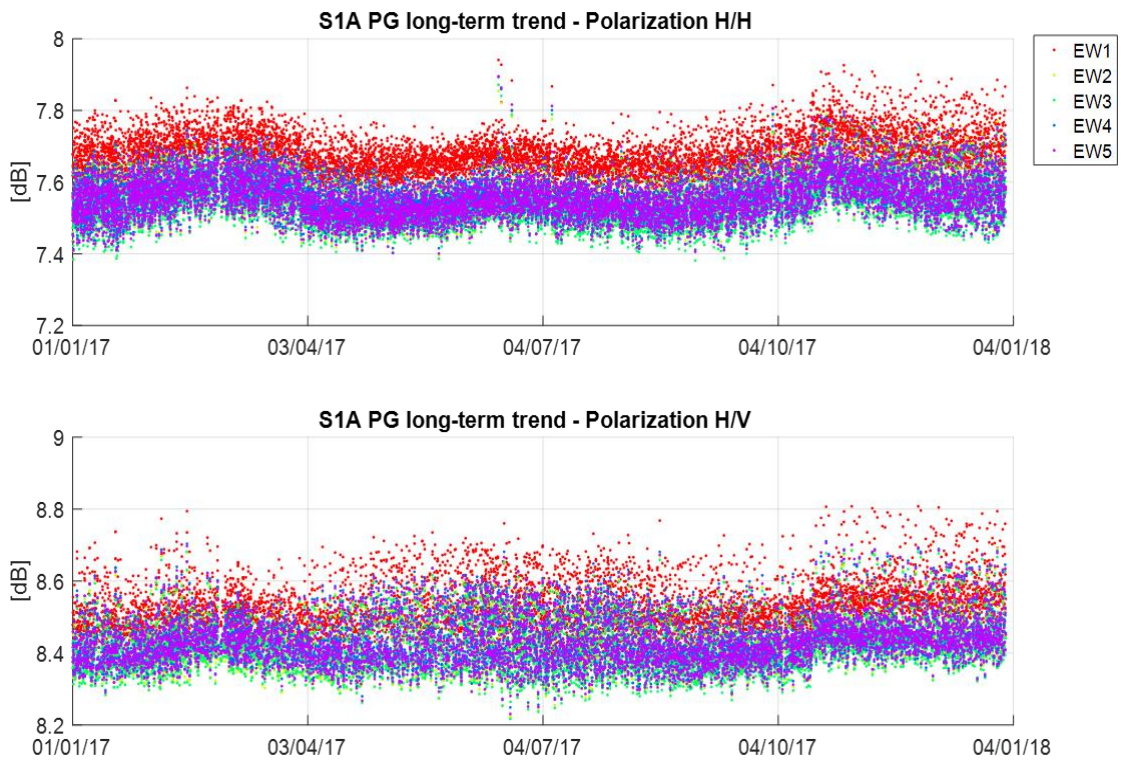


Figure 9: EW HH (left) and HV (right) PG gain divided by sub-swath.

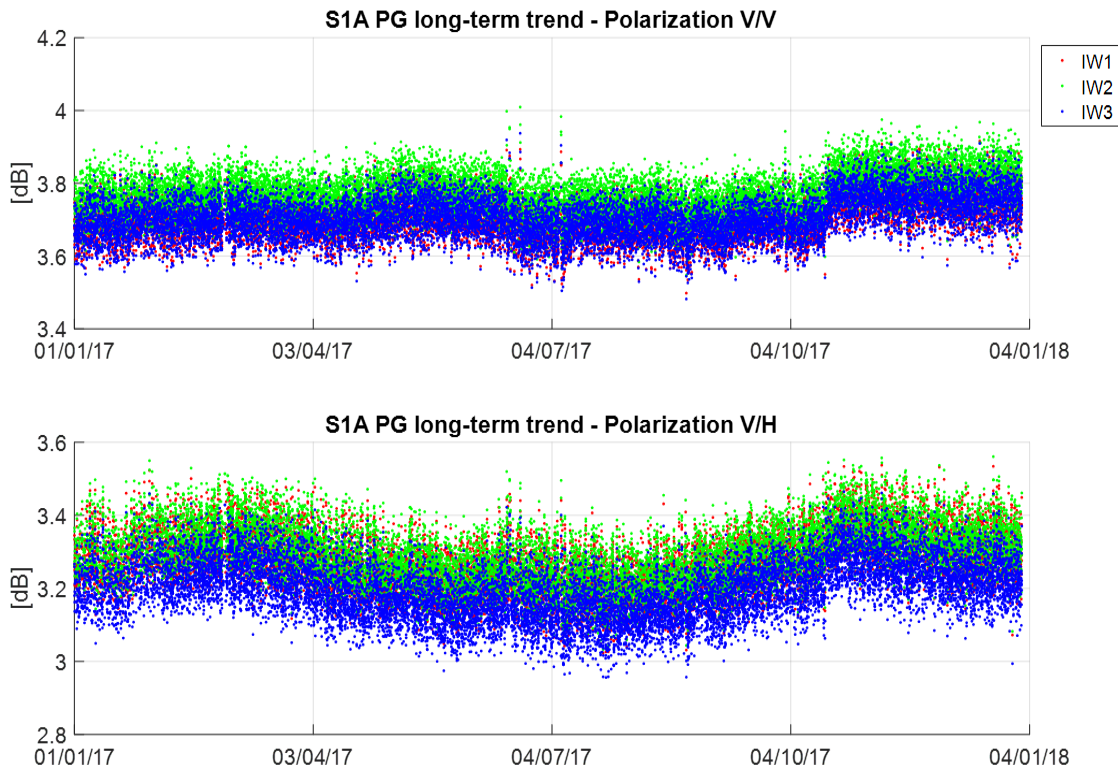


Figure 10: IW VV (left) and VH (right) PG gain divided by sub-swath.

4.5. S-1A Noise Power

The noise power is monitored through the dedicated RX-only pulses embedded at the start/stop of each data-take. Figure 11 shows the noise power versus time in the period January-December 2017. The noise power is stable in the reporting period. Table 1 reports the noise power stability (3σ) averaged over the full reporting period. The number in the parenthesis is the number of considered products.

Acquisition mode	Noise power stability [dB]
IW	HH: 6.6 ± 1.1 (13938) VV: 7.4 ± 1.3 (91537) HV: 7.4 ± 1.0 (5691) VH: 6.6 ± 1.45 (88189)
EW	HH: 5.2 ± 1.0 (87275) VV: 6.0 ± 0.66 (5585) HV: 6.3 ± 0.9 (63103) VH: 4.8 ± 0.76 (5555)
WV	HH: N/A (0) VV: 6.2 ± 0.9 (49446)

Table 1: Noise power stability (3-sigma): period JAN 2017 - DEC 2017

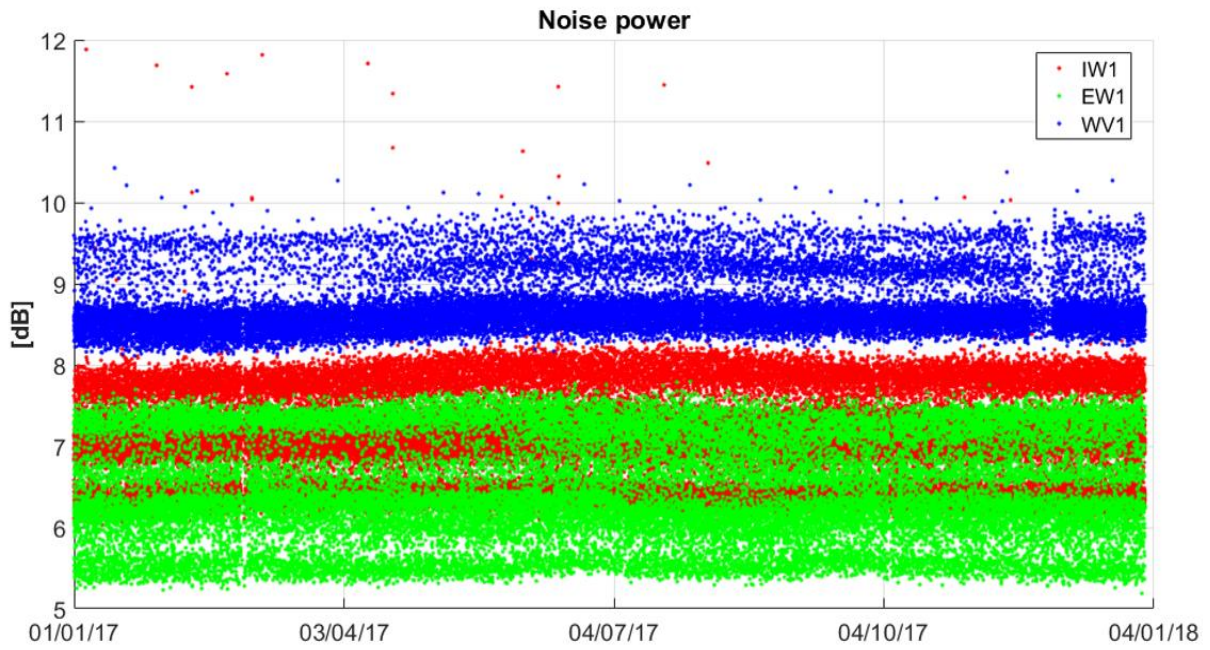


Figure 11: Noise power versus time. The colour represents the different beams.



5. S-1A Products Status

Hereafter, the status of the S-1A products during 2017:

5.1. S-1A Level 1 Products

A general summary of status of S-1A Level 1 products was presented at several conferences and workshops (see [S1-RD-01], [S1-RD-02], [S1-RD-03] and [S1-RD-04]).

5.1.1. Level 1 Basic Image Quality Parameters

The DLR Transponders & Corner Reflectors, the BAE Corner Reflector and the Australian Corner Reflector array have been used to assess various impulse response function parameters as described below. The products analysed were acquired in 2017 and processed with the Sentinel-1 IPF v2.7.2, v2.8.2 or v2.8.4.

5.1.1.1. Spatial Resolution

The Figures and Tables below give the azimuth and range spatial resolutions derived from SM, IW and EW SLC data. The numbers in brackets indicate the number of measurements.

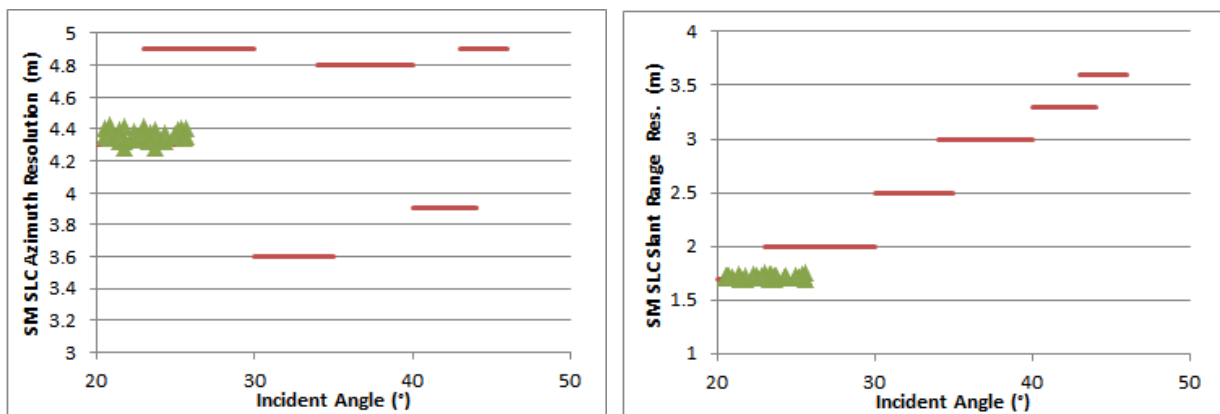


Figure 12: SM Azimuth and Slant Range Spatial Resolutions

Mode/Swath	Azimuth Spatial Resolution (m)	Slant Range Spatial Resolution (m)
S1	4.36±0.03(48)	1.72±0.01 (48)

Table 2: SM Azimuth and Slant Range Spatial Resolutions

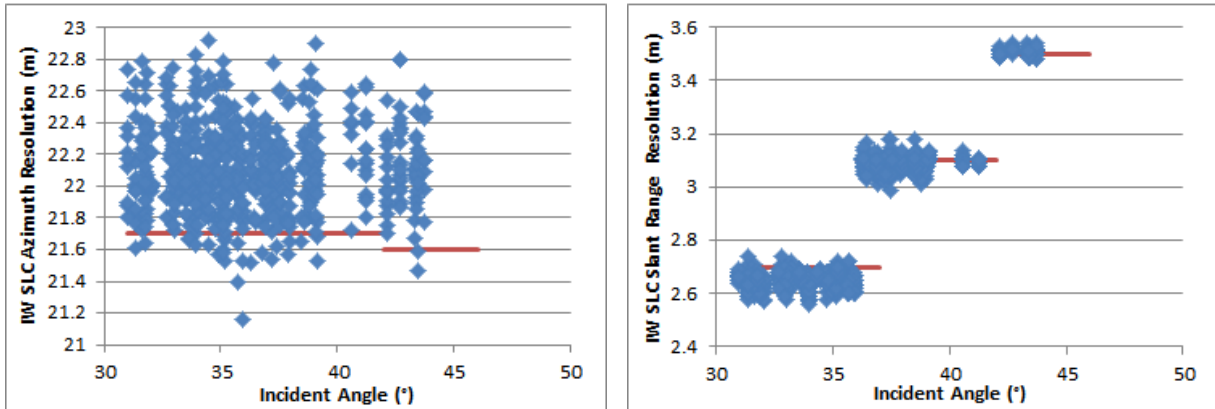


Figure 13: IW Azimuth and Slant Range Spatial Resolutions

Mode/Swath	Azimuth Spatial Resolution (m)	Slant Range Spatial Resolution (m)
IW1	21.76±0.21(689)	2.65±0.03 (689)
IW2	21.88±0.19(424)	3.09±0.03 (424)
IW3	21.72±0.12(165)	3.51±0.01 (165)

Table 3: IW Azimuth and Slant Range Spatial Resolutions

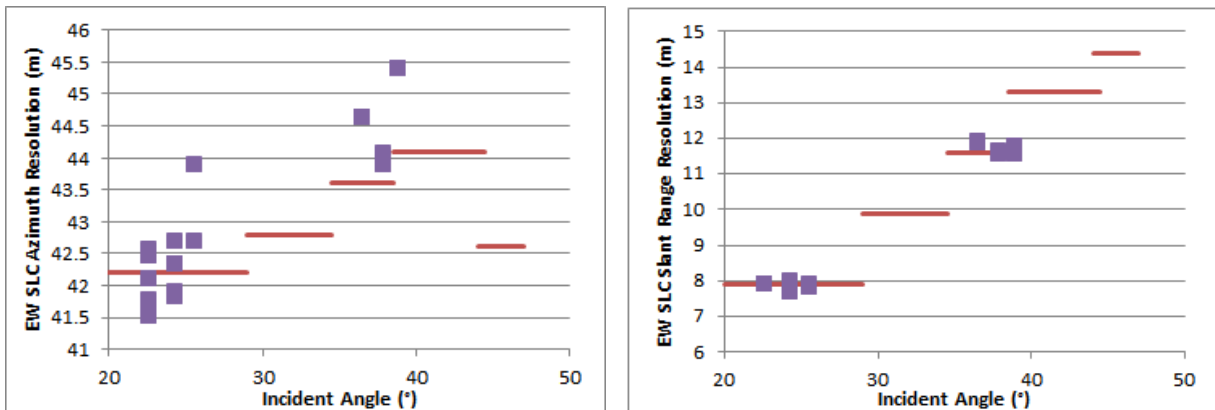


Figure 14: EW Azimuth and Slant Range Spatial Resolutions

Mode/Swath	Azimuth Spatial Resolution (m)	Slant Range Spatial Resolution (m)
EW1	42.30±0.59(14)	7.87±0.07(14)
EW3	44.67±0.64 (6)	11.71±0.16 (6)

Table 4: EW Azimuth and Slant Range Spatial Resolutions

5.1.1.2. Sidelobe Ratios

Table 5 below gives the measured impulse response function sidelobe ratios derived from SM, IW and EW SLC data - these indicate acceptable values.



Mode/Swath	Integrated Sidelobe Ratio (dB)	Range ISLR (dB)	Azimuth ISLR (dB)	Peak Sidelobe Ratio (dB)	Spurious Sidelobe Ratio (dB)
SM	-14.19±3.78	-16.32±1.02	-16.36±0.86	-19.79±0.98	-24.37±2.46
IW	-11.37±3.24	-15.78±1.29	-16.42±1.53	-19.65±1.26	-23.16±3.53
EW	-10.77±4.25	-17.12±3.26	-18.39±4.13	-19.68±2.39	-19.33±2.28

Table 5: SM, IW & EW Sidelobe Ratios

5.1.1.3. ENL and Radiometric Resolution

Large uniform distributed targets are used to measure the equivalent number of looks (ENL) and radiometric resolution (RR) in imagery as given in Table 6 and Table 7 below. For each swath/sub-swath and product type, the first number is the ENL while the second is the RR in dB.

	IW1	IW2	IW3
GRDH	4.55, 1.67	4.60, 1.66	4.73, 1.64

Table 6: IW ENL & RR Measurements

	EW1	EW2	EW3	EW4	EW5
GRDH	2.52, 2.12	2.51, 2.12	2.51, 2.13	2.61, 2.09	2.54, 2.11

Table 7: EW ENL & RR Measurements

5.1.1.4. Ambiguity Analysis

5.1.1.4.1. Azimuth Ambiguities

Table 8 below gives mean azimuth ambiguity ratio for DLR transponder targets acquired in IW mode.

	IW
Early Azimuth Ambiguity Ratio (dB)	-27.61±2.55
Late Azimuth Ambiguity Ratio (dB)	-27.84±2.79

Table 8: Azimuth Ambiguity Ratios

5.1.1.4.2. Range Ambiguities

No imagery suitable for range ambiguity measurements were identified during 2017.

5.1.2. Radiometric Calibration

The DLR Transponders & Corner Reflectors, the BAE Corner Reflector and the Australian Corner Reflector array have been used to measure their radar cross-section as described below. The products analysed were acquired in 2017 and processed with the Sentinel-1 IPF v2.72, v2.82 or v2.84.



5.1.2.1. Absolute Radiometric Calibration

DLR Transponders have been used to calculate the relative radar cross-section for IW mode during 2017. The results are shown in Table 9 where mean (radiometric accuracy) and standard deviation (radiometric stability) of the relative radar cross-section in dB are given. The number of measurements is given in brackets. All the transponder measurements are for IW mode and dual V (VV/VH) polarisation which reflects the acquisition planning strategy over land for S-1A during 2017. Note that the IW radiometric accuracy is close to zero while the radiometric stability is better than 0.3dB.

IW
-0.06±0.27 (376)

Table 9: SLC Relative Radar Cross-Section for the DLR transponders (dB)

The following results are also for the DLR transponders, and have been separated by polarisation. The IW results below indicate a good radiometric calibration with many mean relative radar cross-section values close to zero (the radiometric accuracy) and a standard deviation of typically 0.3dB (the radiometric stability). The differences between polarisations are also small (see also Section 5.1.4.1).

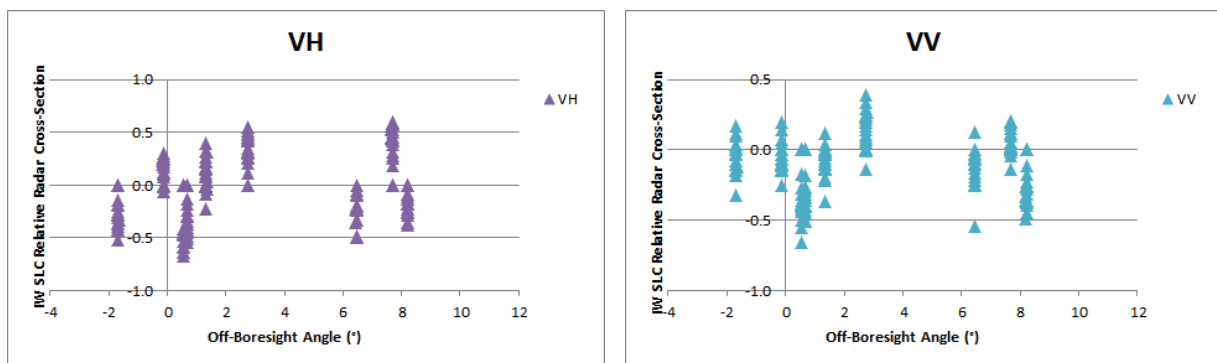


Figure 15: IW SLC Relative Radar Cross-Section for the DLR transponders

	VH	VV	HH	HV
IW	-0.02±0.32 (188)	-0.10±0.20 (188)	No measurements	No measurements

Table 10: IW SLC Relative Radar Cross-Section for the DLR transponders (dB)

	IW1	IW2	IW3
VH	-0.23±0.29 (104)	0.08±0.35 (38)	0.10±0.35 (46)
VV	-0.26±0.22 (104)	-0.03±0.21 (38)	-0.15±0.21 (46)

Table 11: IW SLC Relative Radar Cross-Section for the DLR transponders (dB)

The radiometric calibration results using the DLR Transponders and the BAE Corner Reflector for IW SLC products are shown in Figure 16 from imagery acquired during 2017. The derived relative radar cross-section for the DLR transponders during the same period is -0.09 ± 0.29 dB while from the BAE corner reflector is -0.19 ± 0.17 dB.



Figure 16: IW SLC Relative Radar Cross-Section for the DLR Transponders and the BAE Corner Reflector

An array of 40 corner reflectors has been deployed near Brisbane, Australia as a component of the Australian Geophysical Observing System (AGOS) - see [S1-RD-04] for further details. The CRs are size 1.5m (34), 2.0m (3) and 2.5m (3) with fixed orientations. Given that these corner reflectors have a fixed elevation and azimuth orientation they will not be pointing directly at S-1A. However, for IW acquisitions the reduction in radar cross-section compared to the case of a perfect orientation is small at less than 0.05dB. Table 12 gives the radiometric accuracy and stability for all corner reflector measurements during 2017 together with results for IW1 and IW2 sub-swaths and for HH polarisation (no imagery was acquired in VV polarisation). The numbers in brackets refer to the number of measurements. The results indicate an accuracy close to zero while the stability is less than 0.5dB but larger than the one derived from the DLR transponders above.

All	IW1	IW2	IW1 HH	IW2 HH
0.13±0.55 (637)	0.13±0.53 (381)	0.14±0.58 (256)	0.13±0.53 (381)	0.14±0.58 (256)

Table 12: IW SLC Relative Radar Cross-Section for the Australian Corner Reflectors (dB)

5.1.2.2. Permanent Scatter Calibration

Figure 17 shows a recent IW VV Permanent Scatter Calibration series over Paris. The series covers almost 2 years from January 2016 to November 2017. The PSCAL results are consistent with the time series from the BAE corner reflector (Figure 16). In particular, it can be noticed a small RCS



reduction (about 0.2 dB) around March 2017. Further analyses showed that such RCS reduction was recovered during 2018. This implies that the origin of this reduction is probably a small fluctuation of the instrument gain not properly captured by the Internal Calibration. The origin of the issue is under investigation but in any case the peak to peak fluctuation is quite reduced and the radiometric stability of the instrument is good.

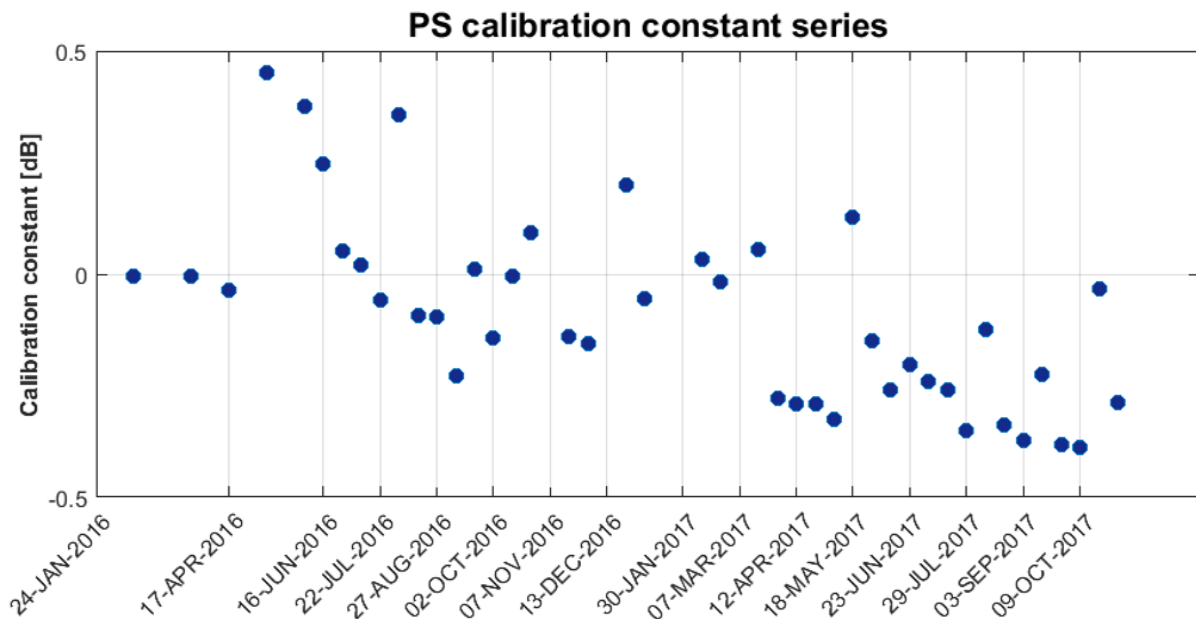


Figure 17: Permanent Scatter Calibration time series for TopSAR IW over Paris.

5.1.3. Geometric Validation

S-1A geolocation quality was monitored regularly throughout 2017 using SLC products from the IW mode. EW- and SM-mode acquisitions, while not acquired during 2017 over Swiss targets, were obtained during the earlier S-1A calibration and validation campaign. They were generally re-analysed whenever new, significant timing biases had been implemented in post-processing. The trihedral corner reflectors (CRs) whose positions had been installed and surveyed with cm-level accuracy at the Swiss test sites *Torny-le-Grand* and *Dübendorf* during the S1-B calibration campaign continued to serve as reference targets in 2017.

For a given CR visible in an S-1A image product, its predicted azimuth and slant range image pixel position was calculated as follows:

- The surveyed CR position was adjusted for acquisition-time “epoch” plate **tectonic drift** and **solid Earth tide** (SET), as described in [S1-RD-05].
- The relevant timing annotations were extracted from the product annotations; these included the azimuth zero-Doppler time stamps, the orbital state vectors, the near-range fast time, and the range and azimuth sample spacing’s.
- Range-Doppler geolocation was performed for the CR coordinate as described e.g. in [S1-RD-13], giving range and azimuth times as the output.
- The slant range prediction was corrected by adding the modelled **atmospheric path delay**, and the azimuth time was corrected by subtracting the **bistatic residual**. These effects and their associated corrections are described in more detail in [S1-RD-05].



ALE estimates for products from all three modes, which included the range and azimuth timing corrections mentioned in the above point, were published in mid-2017 [S1-RD-18]. By the end of 2017, the ALE estimates at UZH operationally included two further post-processing corrections:

- For TOPS products (IW and EW), a range shift dependent on the target azimuth position within the TOPS burst was shown to be affecting the corresponding ALE estimates [S1-RD-10]. Correcting for these biases on a target-by-target basis resulted in a lower range ALE spread, and slightly shifted the mean bias.
- The beam-dependent azimuth biases previously observed in IW and EW analyses were shown to be caused by an error in the way the S-1 IPF was interpreting the azimuth timing annotations (during the so-called *bulk bistatic correction*). While this was most visible in TOPS-mode product analyses, the error was shown to affect SM mode products as well [S1-RD-11].

The above steps resulted in a range-azimuth *predicted* position for each target that could be compared to the position of the peak intensity in the image raster itself, i.e., the *measured* CR position. The differences between predicted and measured positions were then plotted. For example, the IW SLC product time series for 2016 and 2017 are shown in Figure 18. Please refer to [S1-RD-05] and [S1-RD-06] for details on the evolution of the standard IPF processing and the geolocation methodology. Both the range and azimuth ALE has improved for all modes.

The ALE plots in Figure 18 indicate that given bias compensations, the localisation performance was much better than the original requirements (according to sections 5.5.2.1 and 5.5.2.2 in [S1-RD-09]). A method for integrating azimuth bias compensation annotations in the IPF is under study.

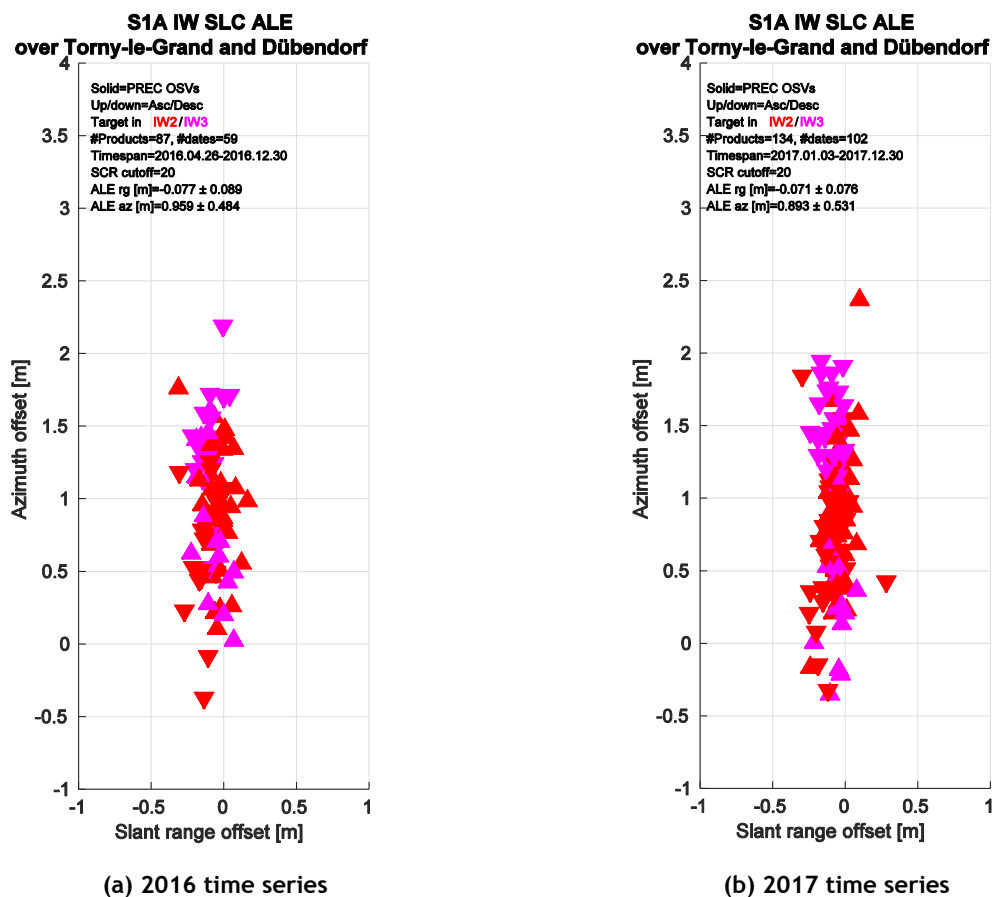


Figure 18: ALE estimates for S-1A IW SLC product time series acquired over the Swiss test sites using precise state vectors (AUX_POEORB). (a) products acquired in 2016; (b) products acquired in 2017. Product date ranges are shown in the figure inset. Point colours represent beam/subswath.



5.1.4. Polarimetric Calibration

5.1.4.1. Gain Imbalance

The DLR transponders have also been used to calculate the gain imbalance (the difference in radar cross-section between the two polarisations of dual polarisation products). Table 13 gives a summary of the gain imbalance for IW mode and VV/VH polarisation while Figure 19 shows the gain imbalance for IW.

	Gain Imbalance (dB)
IW (VV/VH)	0.10±0.21 (188)

Table 13: Gain Imbalance using the DLR transponders

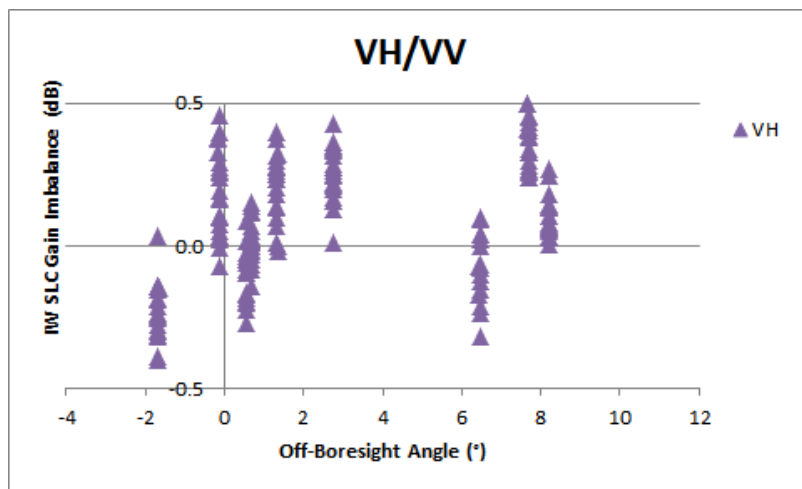


Figure 19: IW Gain Imbalance using the DLR transponders.

5.1.4.2. Phase Imbalance

The DLR transponders have been used to calculate the phase imbalance (the difference in peak phase between the two polarisations of dual polarisation products). Figure 20 and Table 14 give the gain imbalance for IW acquisitions during 2017 (there were no acquisitions of the DLR transponders in SM & EW modes). As expected the phase difference is close to zero.

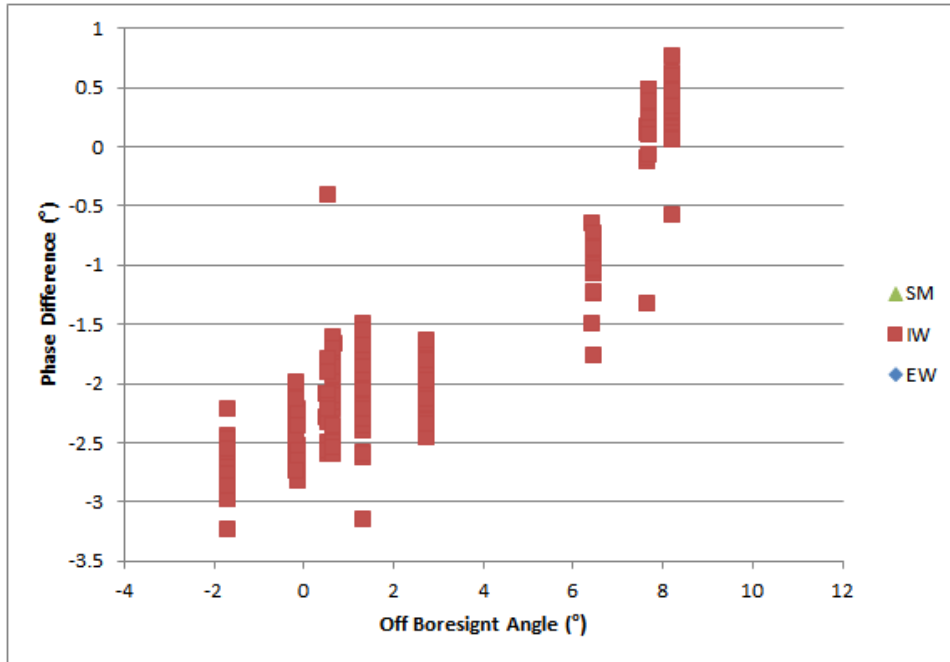


Figure 20: Phase Imbalance using the DLR transponders.

	Phase Difference (°)
IW	-1.52±1.13 (188)

Table 14: Phase Imbalance using the DLR transponders

5.1.4.3. Coregistration

The DLR transponders provide an impulse response in both polarisations of dual polarisation imagery which enables coregistration to be performed between the two polarisation images. Table 15 below shows that the average measured polarimetric co-registration derived from SLC products acquired during 2017 is very small (the IRF peak position is measured to a 1/8 of a pixel).

Mode/Swath	Range Co-registration Accuracy (m)	Azimuth Co-registration Accuracy (m)	Number of Measurements
IW	0.03±0.08	0.00±0.00	66

Table 15: Polarimetric Calibration Measurements

5.1.4.4. Cross-talk

The DLR corner reflectors enable the S1-A cross-talk to be measured since they provide an impulse response in only one polarisation (HH or VV) of dual polarisation imagery. Table 16 gives the IW cross-talk derived using SLC products - the measured cross-talk is acceptably low.

Corner Reflector Cross-talk (dB)	Number of Measurements
-37.5±4.2	16

Table 16: Cross-talk Measurements



5.1.5. Elevation Antenna Patterns

There were two updates to the S-1A elevation antenna patterns (EAPs) during 2017. The first related to the outcome of re-calibration activities related to the refinement of the antenna model while the second were for the period after the tile 11 anomaly in mid-2016.

Figure 21 and Figure 22 below show the difference in the EAPs for IW and EW mode before and after the IPF v2.82 re-calibration. As can be seen the difference is dependent on mode and polarisation.

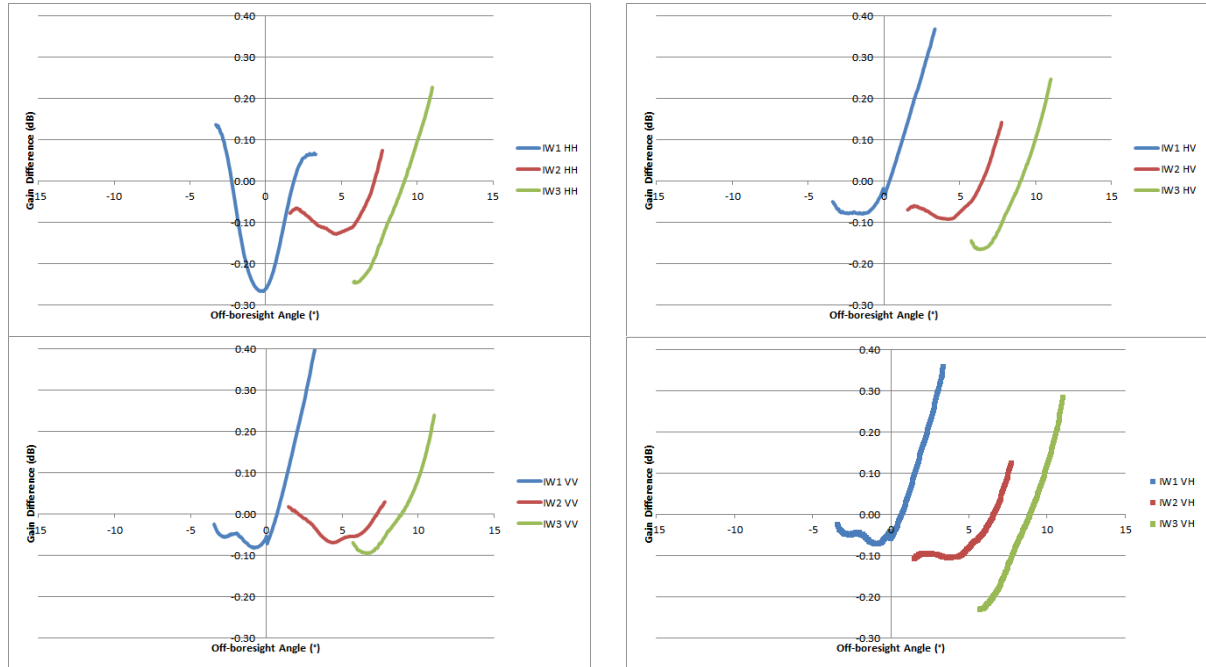


Figure 21: Difference in IW EAP gain between the new and previous EAPs.

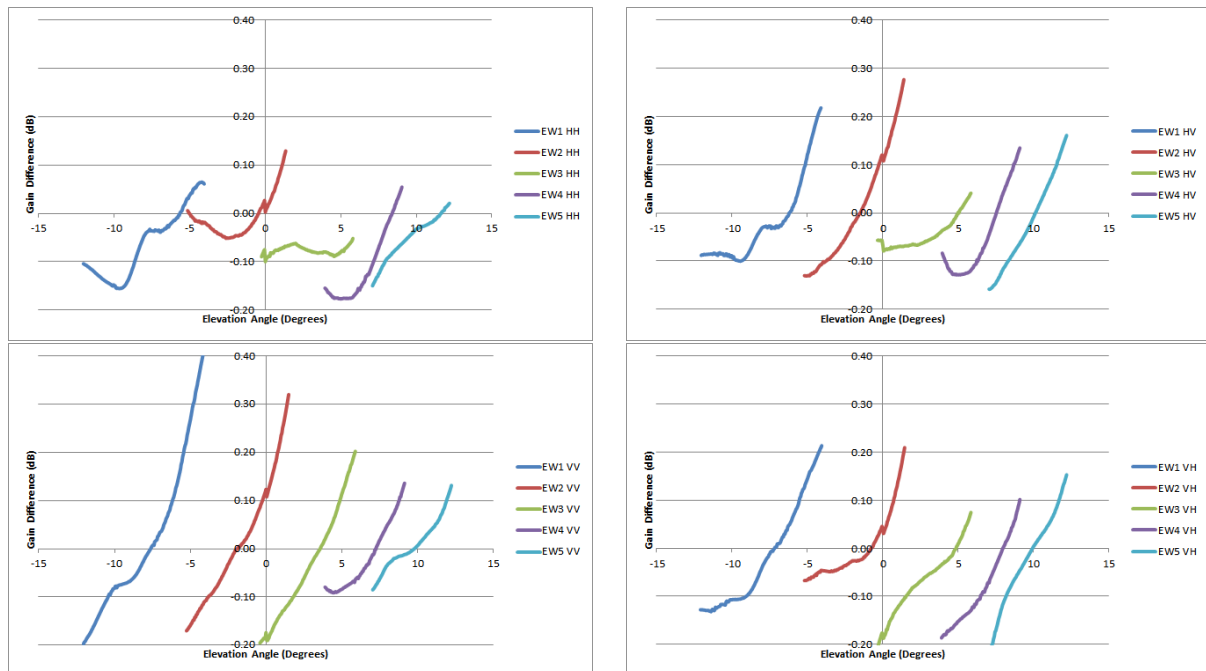


Figure 22: Difference in EW EAP gain between the new and previous EAPs.



The EAPs updates following the Tile 11 Anomaly in June 2016 are shown in Figure 23 and Figure 24 below - here the difference between the new and previous EAPs for IW and EW modes are shown. Since the inverse of the EAP is applied in the IPF, the relative RCS of distributed and point targets will in general increase depending on their incident angle.

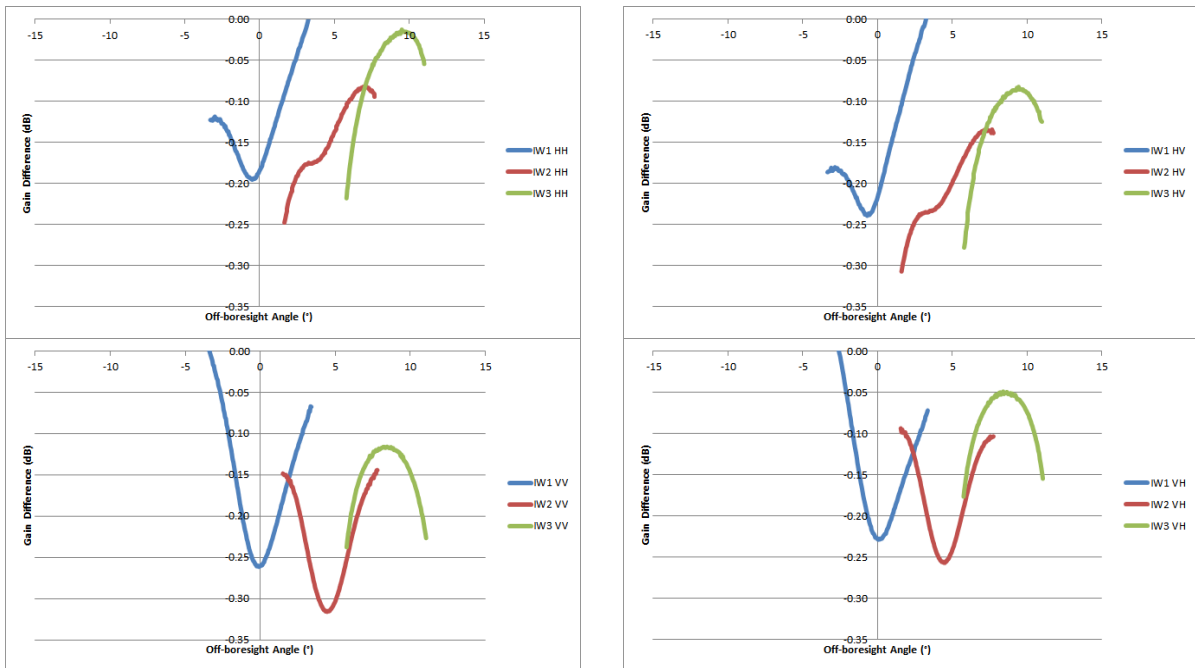


Figure 23: Difference in IW EAP gain between the new and previous EAPs.

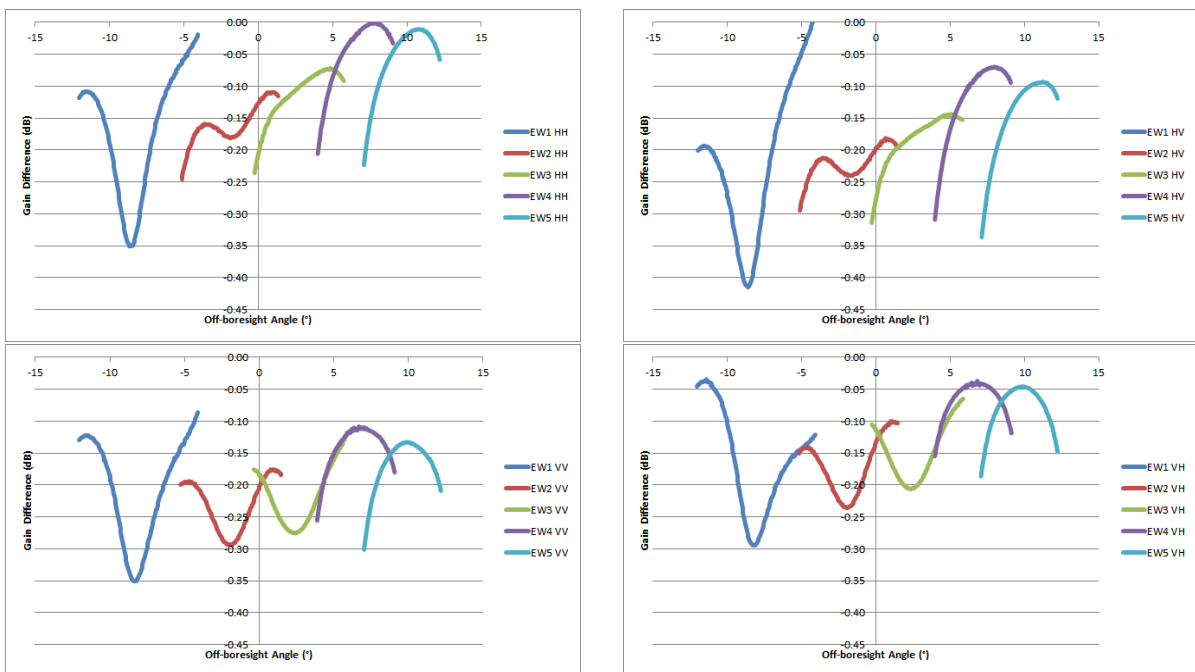


Figure 24: Difference in EW EAP gain between the new and previous EAPs.

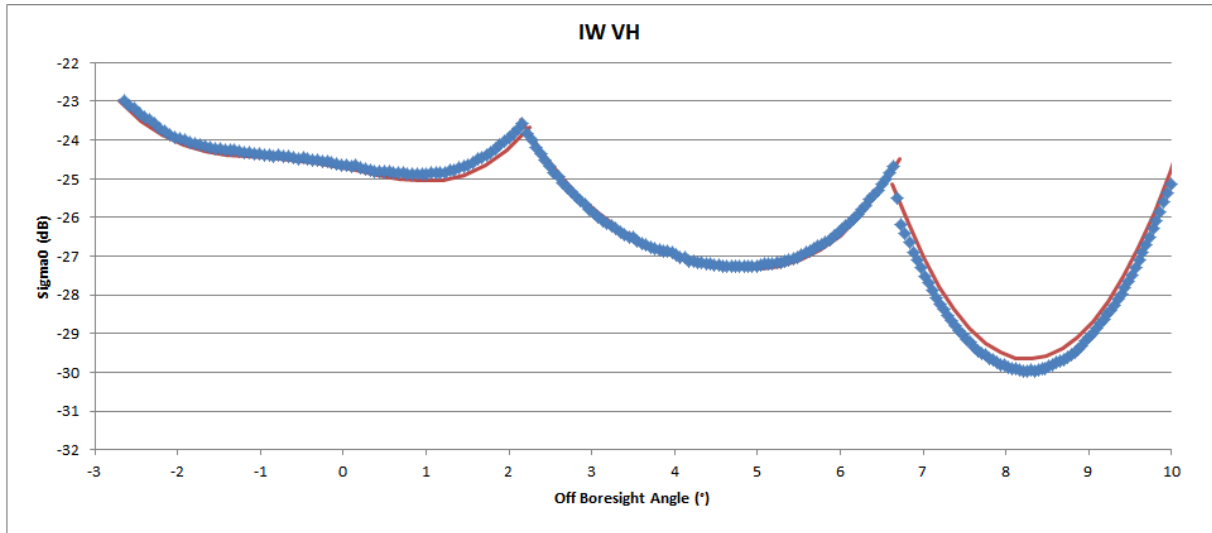
5.1.6. Azimuth Antenna Patterns

There were no updates to the S-1A azimuth antenna patterns during 2017.

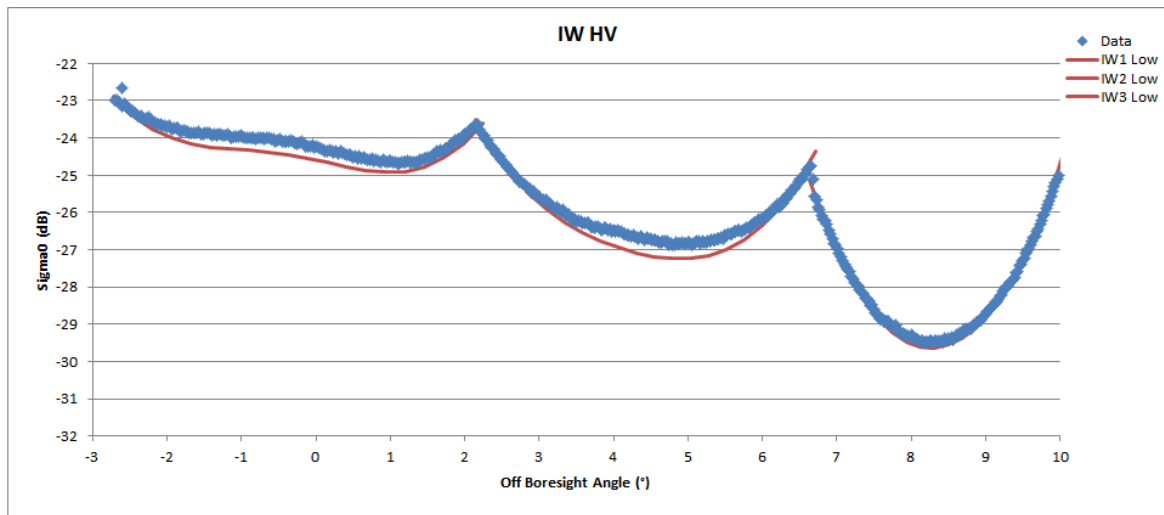


5.1.7. Noise Equivalent Radar Cross-section

S-1A imagery with low ocean backscatter can be used to estimate the Noise Equivalent Radar Cross-Section (NESZ). Figure 25 and Figure 26 show example NESZ measurements for IW and EW mode derived from data acquired in 2017. For the EW imagery a special acquisition campaign over the Pacific Doldrums was performed to acquire low backscatter imagery. The requirement that the NESZ should be below -22 dB is met at all sub-swaths. For IW the measurements are slightly better than the prediction (red curves) while for EW the measurements are slightly worse than the prediction.

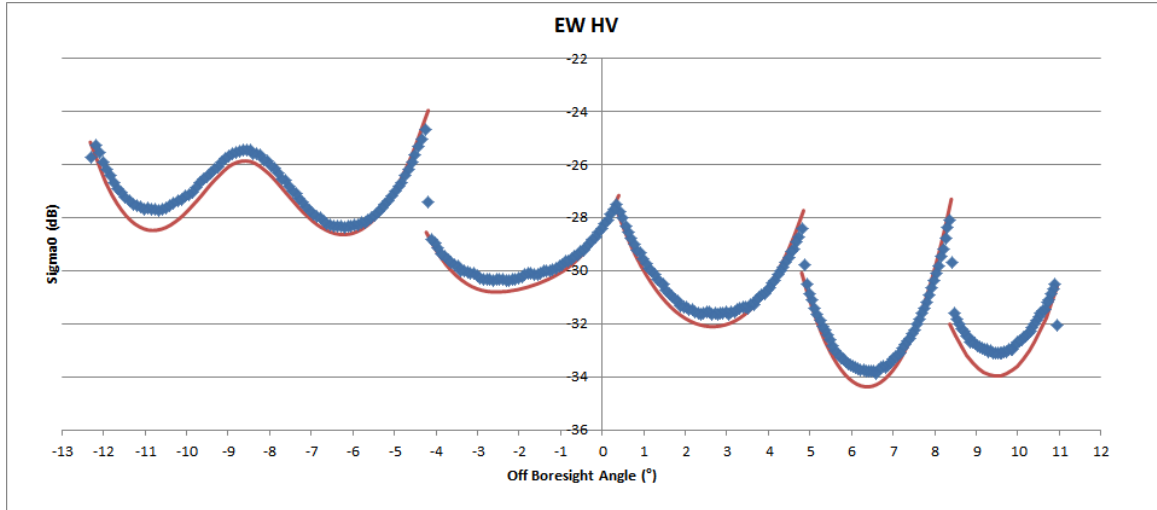


S1A_IW_GRDH_1SDV_20170112T043943_20170112T044008_014794_018180_C9AF.SAFE

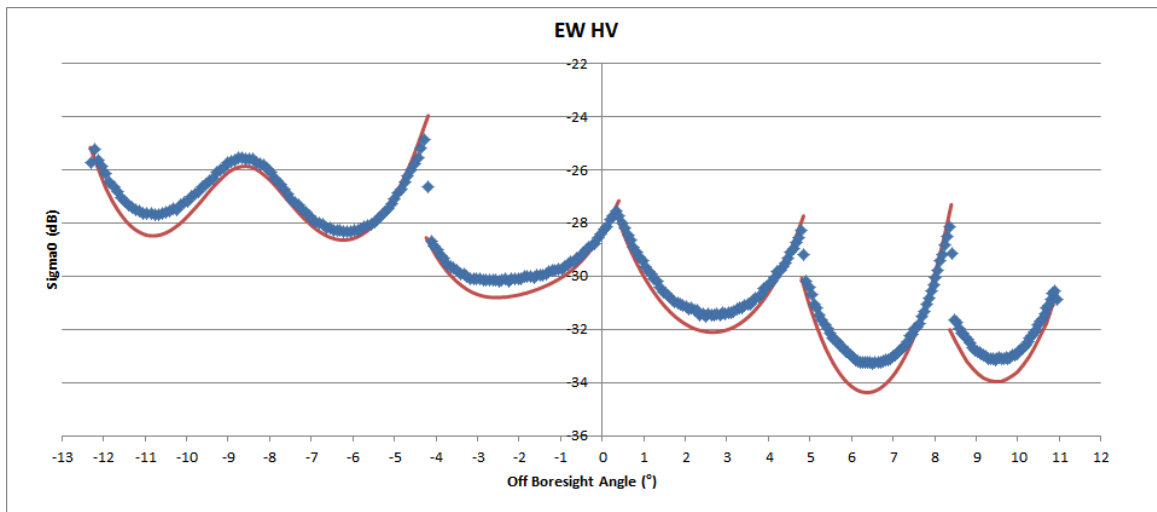


S1A_IW_GRDH_1SDH_20170603T121350_20170603T121418_016869_01COE3_80AE.SAFE

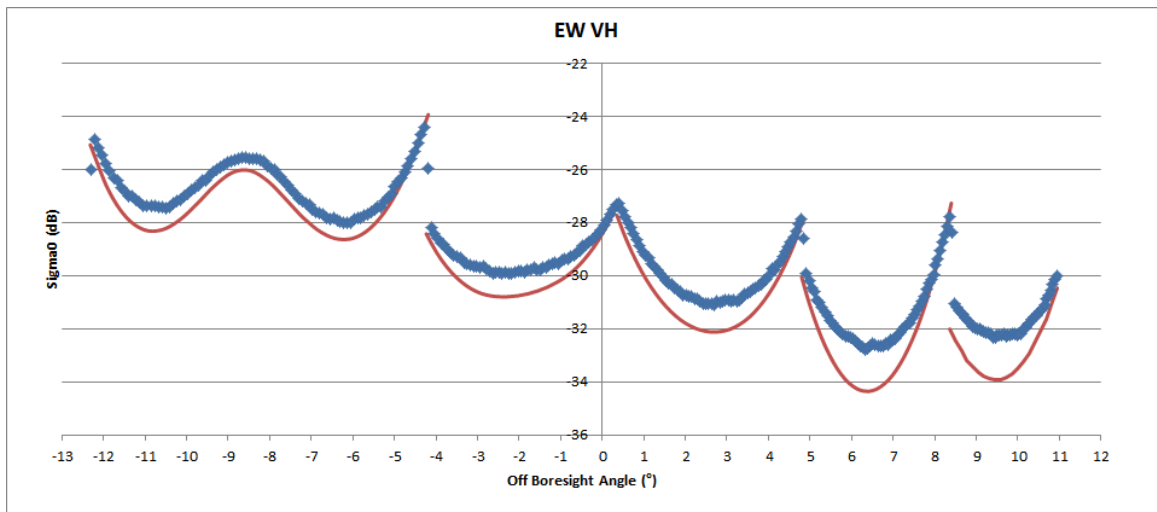
Figure 25: NESZ measures for IW. Blue is the measured NESZ and the red lines are the predicted NESZ.



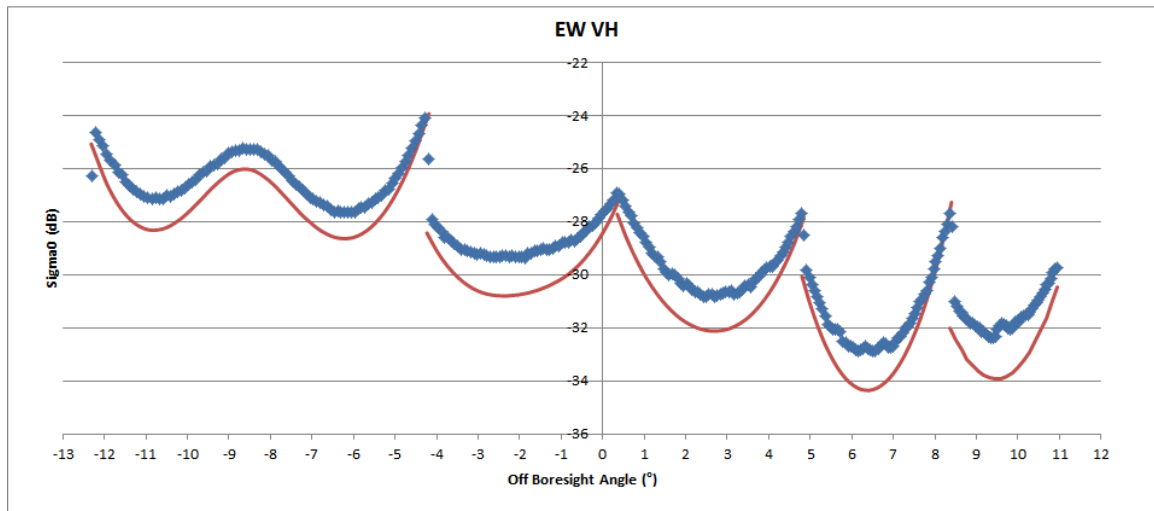
S1A_EW_GRDH_1SDH_20170807T122145_20170807T122233_017817_01DDD6_3EEA.SAFE



S1A_EW_GRDH_1SDH_20170808T004343_20170808T004447_017825_01DE13_D0F5.SAFE



S1A_EW_GRDH_1SDV_20170820T004343_20170820T004448_018000_01E35F_7227.SAFE



S1A_EW_GRDH_1SDV_20170907T121341_20170907T121426_018269_01EB7E_CA87.SAFE

Figure 26: NESZ measures for EW. Blue is the measured NESZ and the red lines are the predicted NESZ.

5.1.8. Interferometric Performances

The interferometric performances, and in particular, the coherence level of an interferogram between two S-1 images, depend on several factors including:

- Stability of the imaged scene (temporal coherence)
- Thermal noise level of the considered acquisitions (see section 5.1.7)
- Volumetric decorrelation due to different acquisition geometry (orbit baseline)
- Stability of the sensor pointing to ensure Doppler spectrum overlap
- Synchronization of the acquisitions (for TOPSAR modes only)

The S-1A performances related to the last three points are reported in the next sections.

5.1.8.1. S-1A Orbit Baseline

Repeat pass interferometry requires that acquisitions at different times are performed with a similar orbit to ensure high coherence interferograms. The “distance” between the orbits of a pair of interferometric acquisition is called interferometric baseline. The interferometric baseline is continuously monitored by the PDGS OBS tool, which compares the S-1B orbits with an arbitrary selected reference cycle (for S-1A it's cycle number 60, 30 September - 12 October 2015).

Figure 27 shows the three interferometric baseline components (Parallel on top, Normal in the mid and Along-Track on the bottom) evolution during 2017. The hot colours represent the maximum baseline value and the cold colours represent the minimum baseline value measured for each orbit. The different colours represent the track number evolving for each cycle from 1 to 175.

The most critical baseline component for the interferometric coherence is the normal one, which shall be lower than a certain threshold named critical baseline (about 5 km for S-1 and depending on the considered swath). The measured normal baseline (mid plot) shows that the worst-case coherence loss due to the interferometric baseline is always well below 5%.

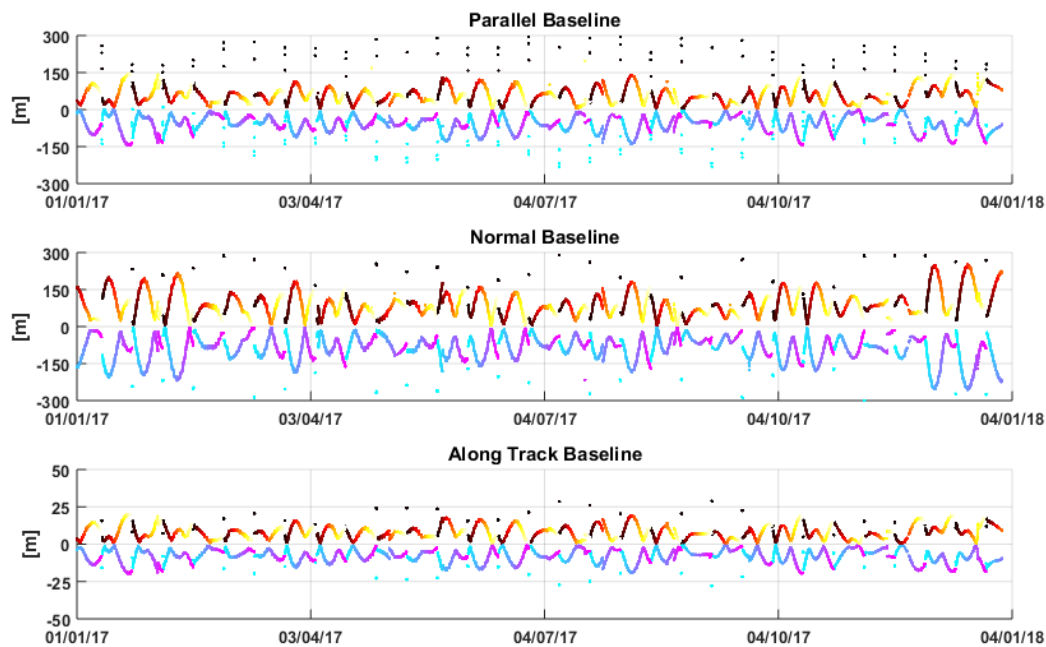


Figure 27: S-1A Parallel (top) Normal (mid) and Along-Track (bottom) interferometric baseline during 2017. The hot colours represent the maximum value and the cold colours represent the minimum value for each orbit. The colours represent the track number.

5.1.8.2. S-1A Burst synchronization

The burst synchronization between repeat pass interferometric acquisitions is relevant for the TOPSAR modes (IW and EW), to provide an indication of the quality of the interferometric phase that can be expected. The SAR acquisition start time is planned over a discrete set of points round orbit with precision down to milliseconds. The performance of the synchronization is monitored by the PDGS OBS tool.

Figure 28 shows the burst synchronization error over time for IW and EW mode, considering as reference cycle number 60 (30 September - 12 October 2015). The colour of the dots represents the number of repeat pass acquisitions falling in a certain temporal and burst synchronization interval (light blue meaning few points and purple meaning many points).

The daily average synchronization is reported with a continuous black line. It can be noticed that the average synchronization is always very good with a small seasonal trend (less than 5 ms peak to peak). A similar trend can be observed also for S-1B burst synchronization (see Figure 78), suggesting a common origin due to some long-term orbit perturbation.

The black dashed lines represent the S-1 synchronization requirement (about ± 7 ms). This value is obtained starting from the timing requirement for single acquisitions (5 ms) and multiplying it by $\sqrt{2}$ due to the fact that all the values in the image are obtained by combining the timing error of two independent acquisitions. The synchronization performance is quite good with 94% of IW acquisitions and 93.9% of EW acquisitions being better than the timing requirement.

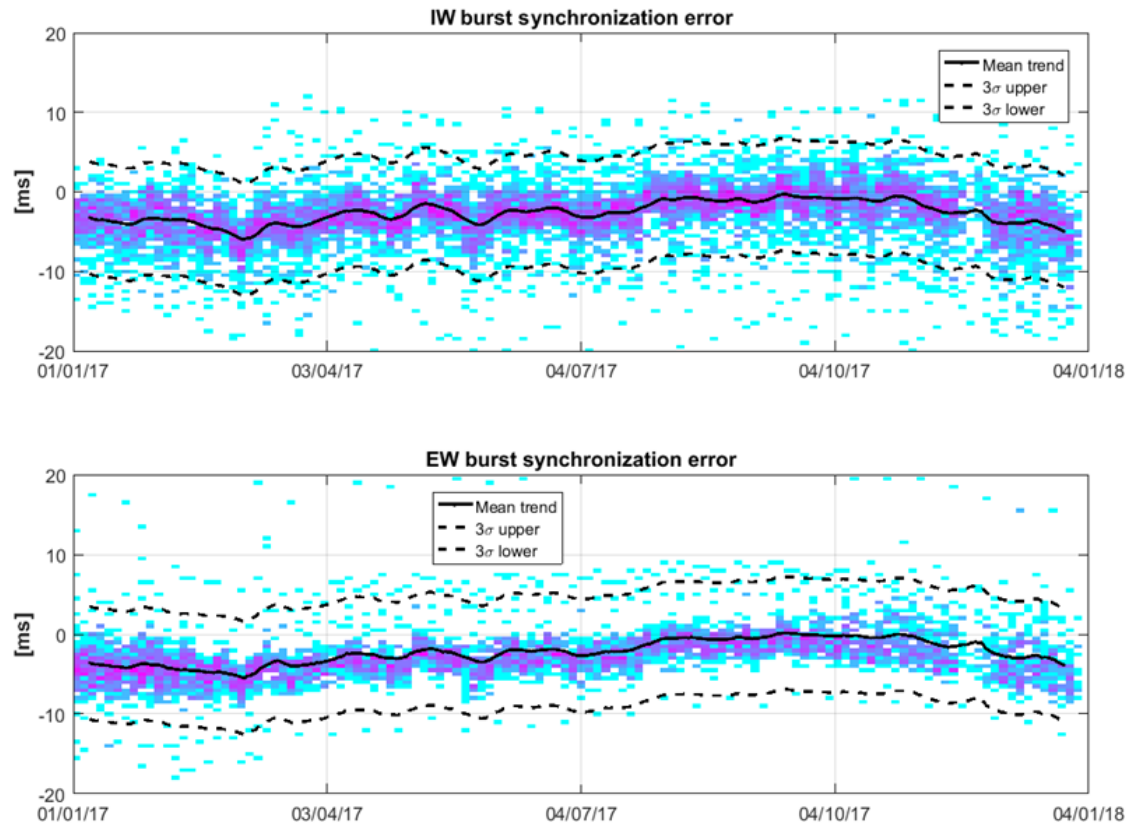


Figure 28: S-1A IW (top) and EW (bottom) burst synchronization during 2017. The colour represents the number of points (light blue few points, purple many points). The black line is the average synchronization per day and the dashed lines are the S-1 requirement limits.

5.1.8.3. Instrument Pointing

The instrument pointing is continuously monitored exploiting the attitude quaternions annotated in the SAR packets and the DC estimates from the data. The annotated attitude shows very small deviations w.r.t. the nominal attitude (Total Zero Doppler + Roll Steering) and does not allow predicting the short-term fluctuations of the DC estimates from the data as required for some L2 applications. This is related to the working of the on-board attitude control system (AOCS). An optimization of S-1B AOCS has been performed for S-1B during 2017 (see section 7.1.8.2) whereas S-1A AOCS optimization has been performed at begin 2018 and hence is not covered in the present report.

Figure 29 shows the average Doppler Centroid on a data-take basis (dots) and on a daily basis (red line) versus time. During the past years DC jumps were observed at every STT configuration change (vertical dashed black lines) due to a residual mis-alignment of the on-board STTs. For this reason, at the end of March 2017, the STTs were realigned (vertical dashed green lines). A clear reduction of the DC jumps after the STT alignment can be observed.

Figure 30 shows the DC jumps at sub-swath overlap (along range) as a function of time. The DC jumps are defined as the average DC data difference in the range overlapping region of two adjacent sub-swath (e.g. IW2 w.r.t. IW1). The DC jumps are computed both on a slice basis (blue dots) and on a daily basis (red line). It is worth to note the step in the IW2-IW1 DC jump around October 2017 due to the tile 11 reconfiguration (RDB#6). The step of about 4 Hz indicate that the new antenna configuration resulted in a slightly different azimuth pointing for IW1 and IW2 beams. On the other hand, the step is almost negligible for IW3-IW2 DC jump.

Following the STT alignment campaign, three Elevation Notch acquisitions were performed to verify that no mispointing in the elevation direction had been introduced. The following table shows a



resume of the results of the S-1A roll pointing analysis. The roll mispointing is quite small (lower than 10 mdeg) for ascending pass acquisitions in both STT1+3 and STT2+3 configurations. On the other hand, roll mispointing is higher (almost 20 mdeg) for the only available descending pass acquisition. This is probably due to the missing STT relativistic aberration correction which will be introduced for S-1A during 2018.

DT ID	Date	Pol.	Pass	Abs. orbit	Rel. Orbit	STT	Duration [s]	ANX start [s]	Scene Altitude [m]	Roll bias [mdeg]
1A355	28th March	DV	A	15898	76	1+3	20	5793.8	213.3	7.5
1A3EF	30th March	DV	D	15920	98	1+3	11	3088.6	221.1	17.3
1A423	30th March	DV	A	15927	105	2+3	21	5798.4	133.9	2.3

Table 17: Results of the S-1A roll pointing analysis exploiting Elevation Notch acquisitions.

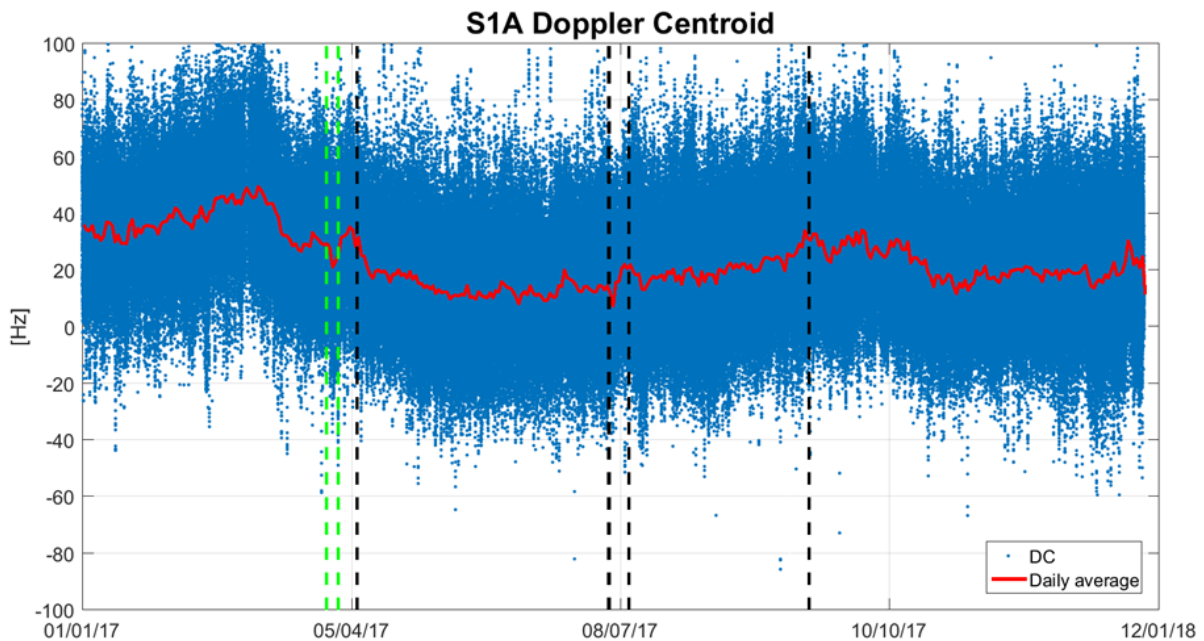


Figure 29: Doppler Centroid versus time. Average on a slice basis (dots) and daily average (red line). The star-trackers reconfigurations events are marked by the vertical black lines. The STT alignment campaign is marked by the vertical green lines.

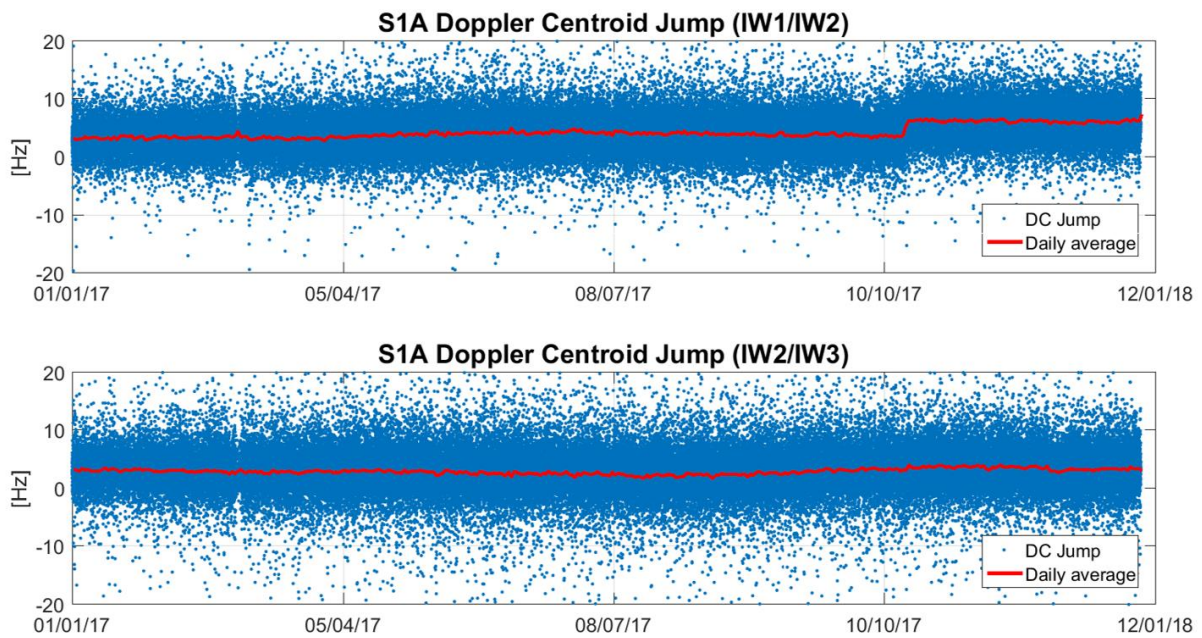


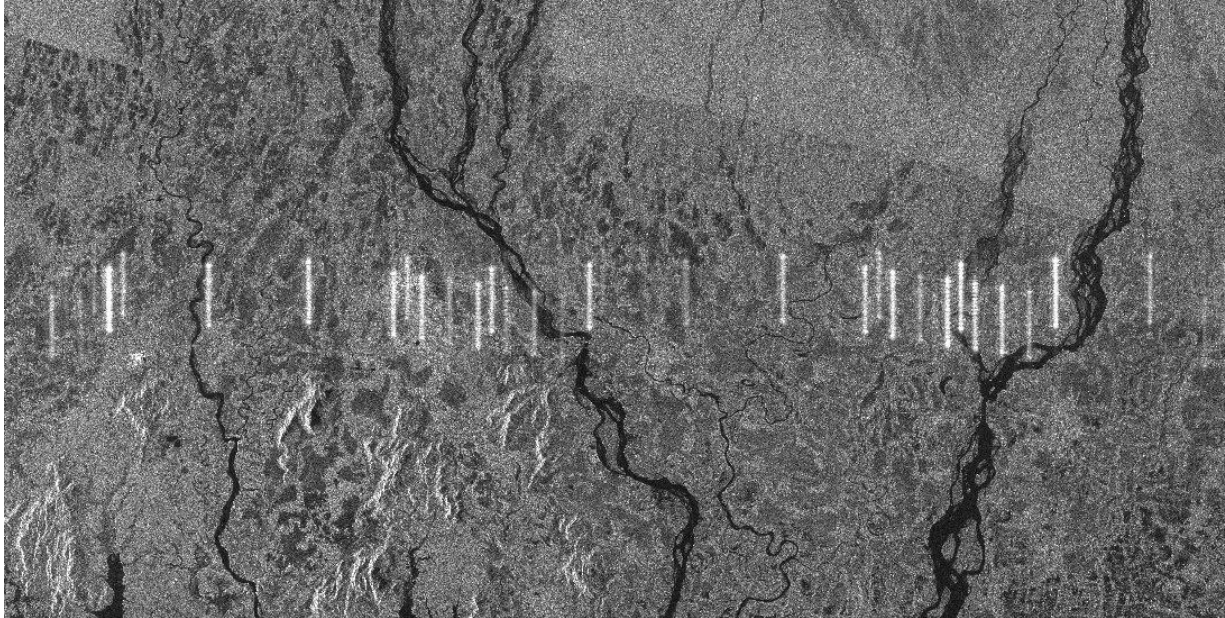
Figure 30: Doppler Centroid jump at sub-swath overlap versus time. Average on a slice basis (dots) and daily average (red line).

5.1.9. Summary of Anomalies

5.1.9.1. Radio Frequency Interference

As small percentage of Sentinel-1A imagery is affected by the presence of Radio Frequency Interference from the ground. An example from 2017 is shown below over Bangladesh & Bhutan (full scene and detail for VH polarisation). Usually RFI only affects a few range lines of raw data.





S1A_IW_GRDH_1SDV_20170822T120459_20170822T120524_018036_01E472_FFD0.SAFE

Figure 31: An example of Radio Frequency Interference over Bangladesh & Bhutan

5.1.9.2. Radarsat-2/Sentinel1-A Mutual Interference

Although the orbit altitude of Radarsat-2 and Sentinel1-A are quite different (789 km and 693 km respectively) their repeat periods are a multiple of each other (24 days and 12 days respectively) and their equatorial crossing times are almost the same (~18:00 hrs at the ascending node). Another similarity is that both SARs operate at the same frequency.

The repeat period and crossing times mean that every 24 days, Radarsat-2 will be directly above Sentinel-1 and hence both may be imaging the same region of the Earth's surface at the same time. If this occurs then mutual interference is detected. Further examples of such mutual interference occurred during 2017 as indicated in Table 18 with example images from 5th February 2017 are shown in Figure 32. More details and examples could be also found in a specific technical note on Sentinel-1 RadarSat-2 mutual interference (link is provided in Appendix B -)

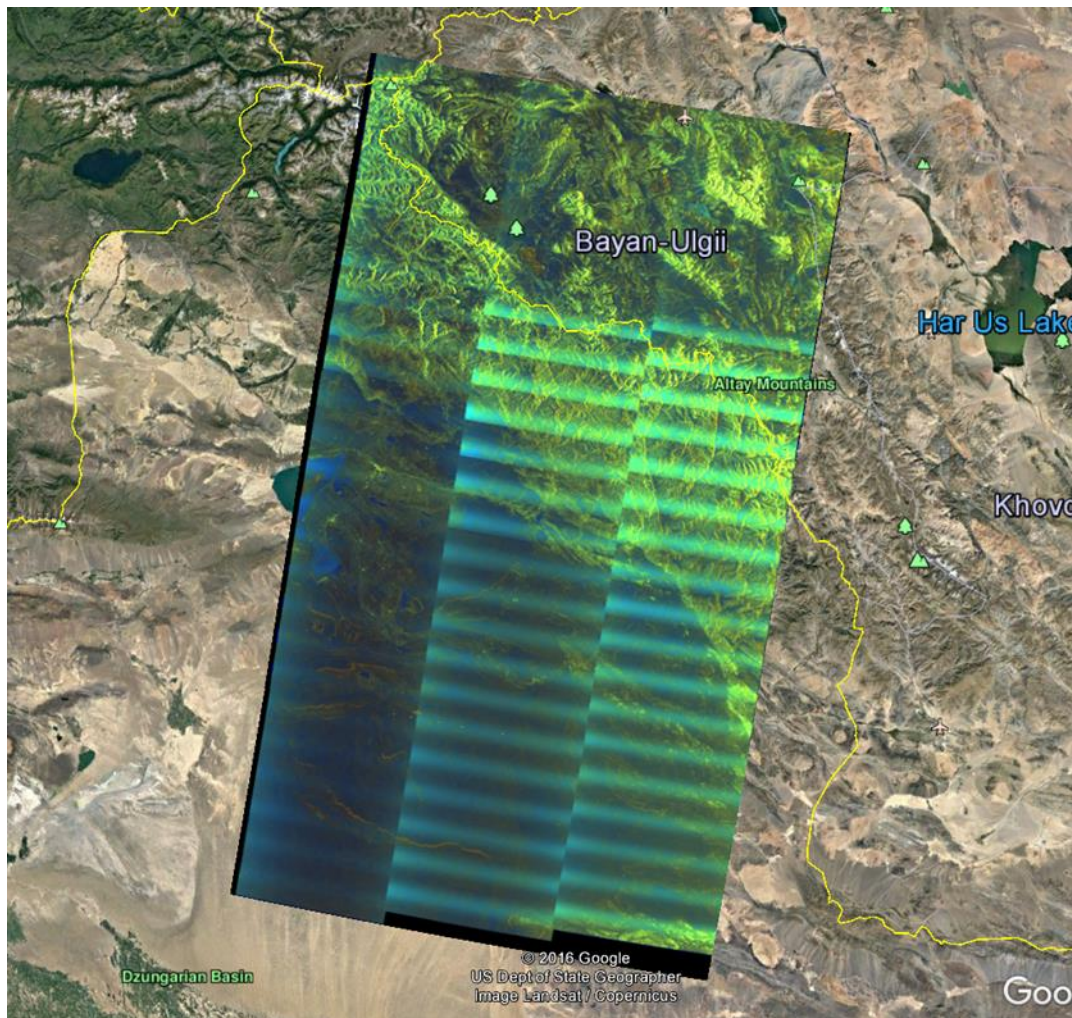
Satellite	Orbit	Relative Orbit	Acquisition Date	Start Time (UT)	End Time (UT)	Approx. Latitude	Approx. Location
S1-A	14691	94*	5th January 2017	03:38	03:39	50° N	Ukraine/Russia
S1-A	15141	19*	5th February 2017	00:13	00:14	47° N	Kazakhstan/China
S1-A	15291	169*	15th February 2017	07:05	07:05	48° N	North Atlantic
S1-A	15491	19*	1st March 2017	00:14	00:16	40° N	China
S1-A	15741	94*	18th March 2017	03:42	03:43	34° N	Cyprus
S1-A	15792	144*	21st March 2017	13:59	14:00	36° N	US West Coast
S1-A	15841	19*	25th March 2017	00:15	00:17	36° N	North China
S1-A	15941	119	31st March 2017	20:51	20:52	36° N	Japan



S1-A	16191	19*	18th April 2017	00:17	00:18	30° N	China
S1-A	16541	19*	12th May 2017	00:19	00:20	25° N	North India
S1-A	16891	19*	5th June 2017	00:21	00:22	20° N	India

*Descending pass

Table 18: S-1A/Radarsat-2 Mutual Interference during 2017



S1A_IW_GRDH_1ADV_20170205T001329_20170205T001354_015141_018C43_CE25.SAFE
 S1A_IW_GRDH_1ADV_20170205T001354_20170205T001419_015141_018C43_8E8B.SAFE
 S1A_IW_GRDH_1ADV_20170205T001419_20170205T001435_015141_018C43_D40C.SAFE

Figure 32: An example of S1/RS-2 Mutual Interference over Kazakhstan/China

5.1.9.3. Other S-1A Interference

Further examples of another type of interference found in S-1A imagery were seen during 2017 (the only previous example was on 8th December 2016 over Florida, USA). The dates of the 2017 examples, also over southern USA, the Gulf of Mexico, the Caribbean and Central America are:

- 9th July 2017, orbit 17401 (data take 01D117), ascending pass
- 11th July 2017, orbit 17423 (data take 01D1C6), descending
- 31st October 2017, orbit 19056 (data take 0203AE), descending
- 5th November 2017, orbit 19129 (data takes 0205E3 & 0205E4), descending.



Images from these dates are shown in Figure 33 to Figure 36. This type of interference is >1000 km in azimuth extent and it has a visual appearance that is quite different from the S-1A/Radarsat-2 interference. The source of the interference has not been identified.

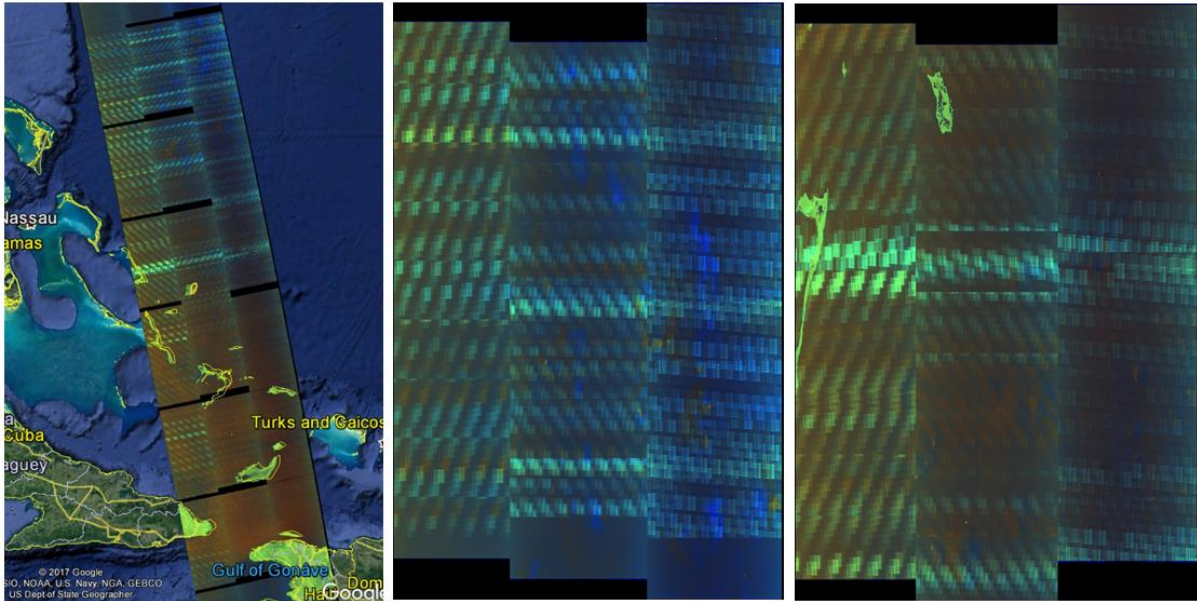


Figure 33: S-1A/Satellite Interference 9th July 2017 (23:04 UT)

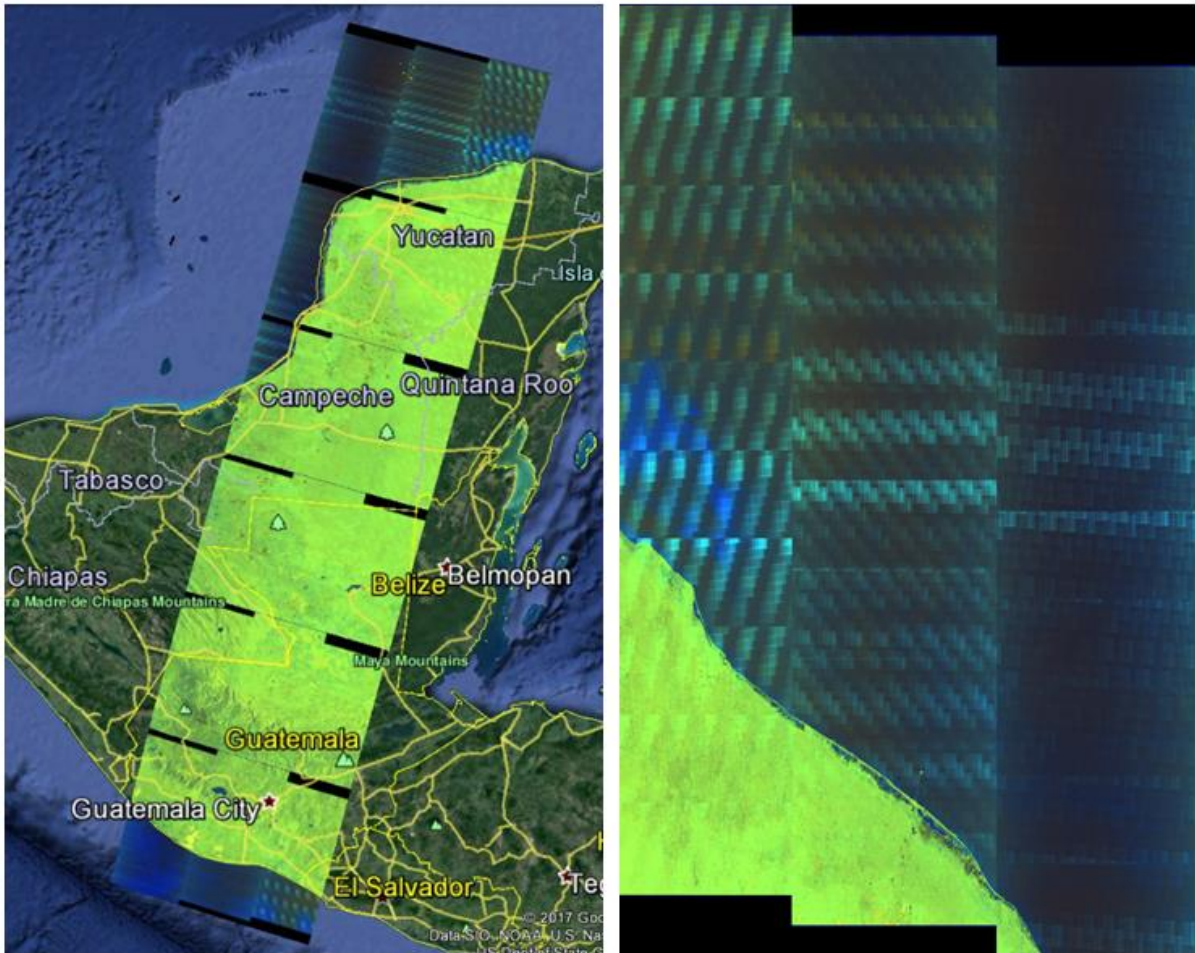


Figure 34: S-1A/Satellite Interference 11th July 2017 (11:53 UT)



Figure 35: S-1A/Satellite Interference 31st October 2017 (11:20 UT)



Figure 36: S-1A/Satellite Interference 5th November 2017 (11:28 UT)



5.1.10. Quality Disclaimers

S-1A Quality disclaimers issued during 2017 are given in Appendix D -.

5.2. S-1A Level 2 products

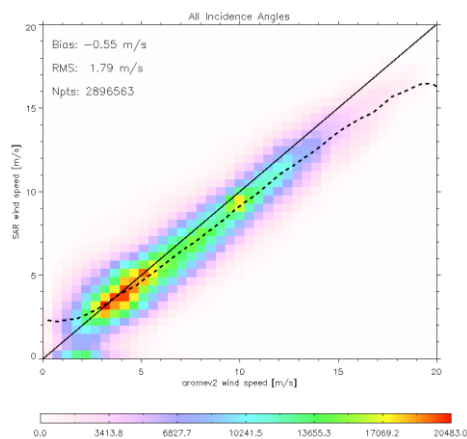
5.2.1. Wind measurement

5.2.1.1. Image Mode (SM-IW-EW)

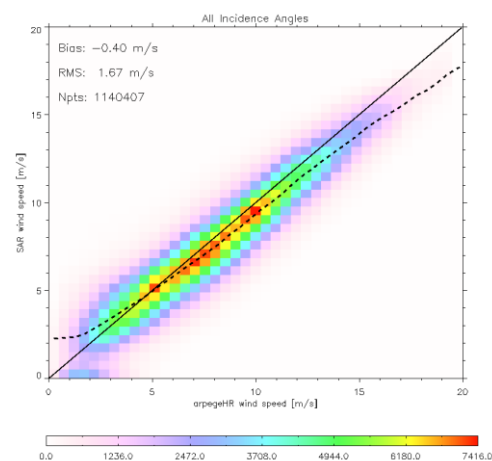
The SAR wind measurement is strongly dependant of the product calibration accuracy. It takes benefit from the efforts made on the SAR Level1 products to improve the calibration constant and align the gamma profile as the function of the elevation angle over Rain Forest. These improvements impact the wind measurements, making it appearing more consistent all along the subswath and also subswath by subswath.

Statement of the wind measurements accuracy:

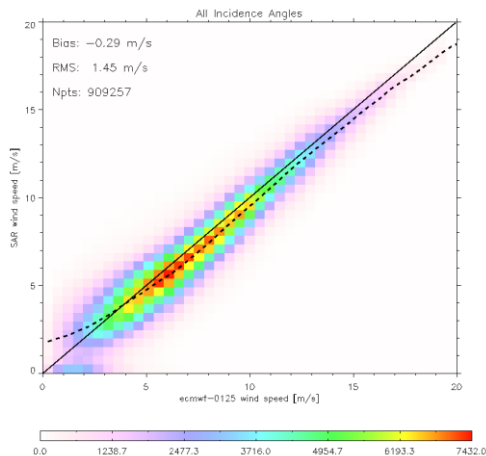
The strategy to assess the accuracy of the wind retrieval is to compare it with an auxiliary wind source which is used as a reference. This source could be in-situ data from buoy, other satellite data (ex: scatterometer) or atmospheric model outputs. Here, the strategy is to multiply the types and the number of the data used as reference, to overcome some lacks on the reference data due to their coverage, resolution or possible bias. In this scope, Ifremer has performed systematic collocations with such data (model: ECMWF (global), Arome, Arpege (European), hundreds of buoys, Metop scatterometers ASCAT- A/B, altimeters ex Cryosat, radiometer ex SMAP etc.) with L2 products generated by the ESA-IPF by PDGS.



a) Arome



b) Arpege HR



c) ECMWF

	bias	Rms
Arome	-0.55	1.79
Arpege	-0.40	1.64
ECMWF	-0.29	1.45

Figure 37: SAR Wind speed compared with reference wind speed for IW mode VV polarisation.

The S1A wind performance has been stable during 2017. Indeed, no large improvements have been introduced in the OWI module, except the change of coding language, with IPF 2.84. It had no impact on the performances but had allowed to increase the processing rate (number of products processed up to L2 OCN). Figure 37 presents the performance achieved on December 2017 for IW mode in VV polarisation of the retrieved wind compared to model references (Arome, Arpege and ECMWF). It can be noticed the strong correlation of the SAR-derived wind speeds with the wind references. The bias and the RMS are less important for ECMWF re-analysis since the wind inversion is based on the ECMWF forecast as an a priori wind input.

A nominal RMS of 1.5m/s to 2m/s is observed; which is better than the S1 wind product specification/requirement (RMSE<2m/s). A bias of around -0.3 to -0.7 m/s depending on the wind reference is present, even at moderate wind speed. As expected, at low wind speeds, the NESZ impacts the SAR wind measurement (overestimation). The bias is wind speed dependant. At high wind speeds, the SAR tends to under-estimate the wind speed. These biases are related to the choice of the current geophysical model function (GMF- function allowing the prediction of the sea surface backscattering as a function to sensor-scene-view and sea-surface-wind parameters) used for the wind retrieval from the co-polarized channel in the inversion scheme. Indeed, the currently-used GMF (Cmod-lfr2, Quilfen *et al.*, 2004) does not well predict the saturation of VV NRCS for high wind speed (above 15m/s). In addition, for moderate wind speeds (5 to 10m/s), its response gives higher Normalised Cross Section than more recent GMF (ex: Cmod5n/Cmod7) currently used for scatterometers (as for example ASCAT). In these moderate-wind value ranges, Cmod-if2 behavior is close to Cmod5, shown as biased in Hersbach *et al* 2008, which explains the overall negative bias. In addition, at low wind speed and low incidence angle, its response is high, and it tends to overestimate the number of 0-wind speed values on the inversion. Then, it has been decided to investigate during 2018 on a possible use of another GMF. Same kind of performances is achieved on EW VV.

At HH polarisation, the bias introduced by the GMF choice looks less important on the global statistics, due to the cumulative impact with NESZ, which introduces a positive bias especially on large incidence angle.

Indeed, a noticeable impact of the noise can be observed especially on HH polarization and high incidence angles (over estimation, beam shaped profile), and even visible in VV polarization, when assessing the performance as the function of SAR elevation angle (beam shaped patterns can clearly be noticed) cf Figure 38.

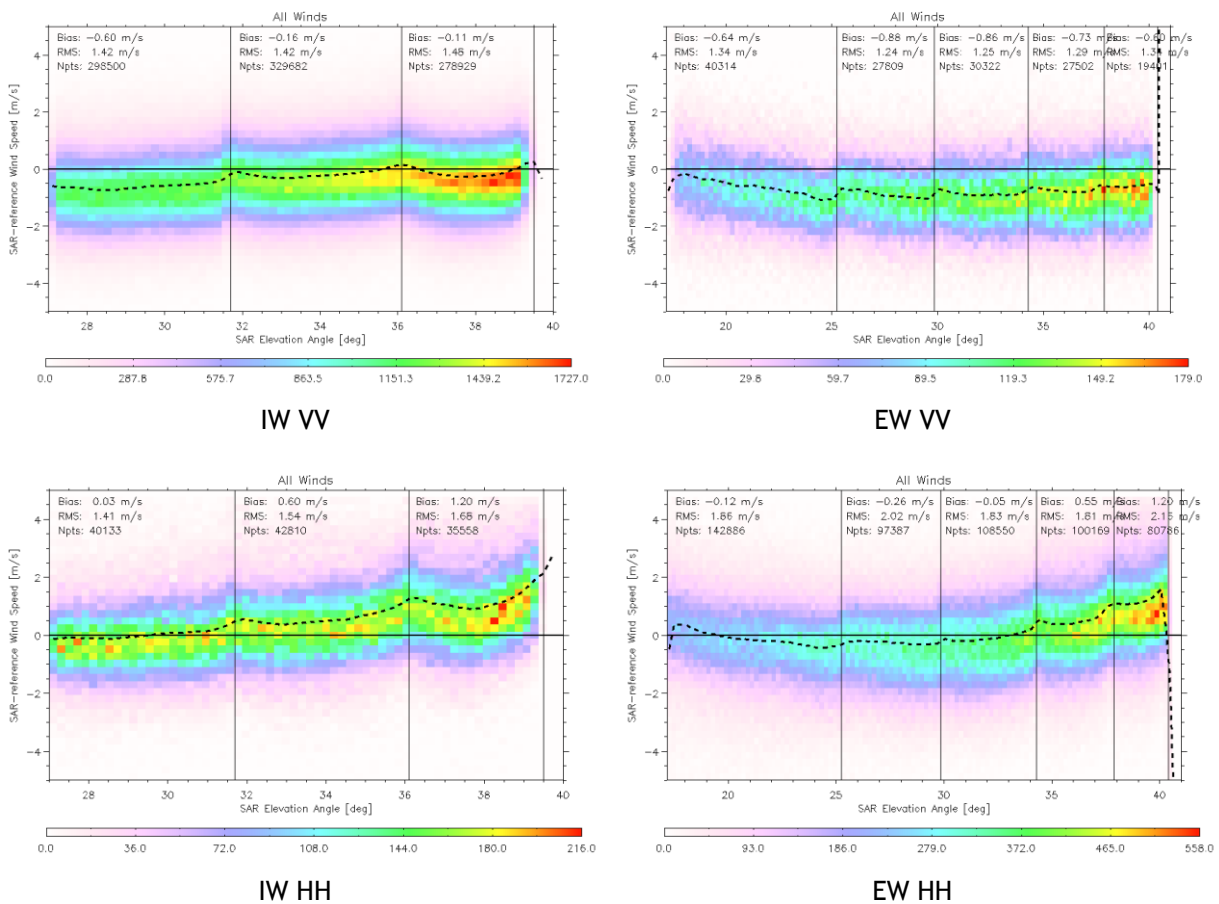


Figure 38: S1A OWI wind speed performance as the function of the elevation angle demonstrating visible NESZ impact on the wind measurement

Improvement performed during 2017:

The main changes are related to IPF upgrades. Please refer to section 3. Please notice the correction of the issue related to ice mask with IPF 2.84 (described in the previous annual report of 2017 [S1-RD-013])

Planned Improvements:

1. Export of cross-Pol information

With the next version of the processor IPF 2.90, the format of L2 data will be extended in order to include additional information on cross-polarization (NRCS, NRCS corrected and NESZ annotation on the OWI grid) for the dual pol acquisition as a new dimension. This is a good opportunity for the community working on very strong wind-speed conditions (extreme wind phenomena: ex hurricanes...).

2. GMF change

GMF is the empirical function to relate an ocean surface wind situation (speed and direction) and the radar configuration (incidence angle, antenna look direction, polarization and frequency) to the sea-surface-backscattered level. SAR wind performances validation has outlined some deficiencies in the current GMF (Cmod-Ifr2, Quilfen et al., 2004). An activity on the assessment of the performances of several candidate GMFs of the Cmod family will be performed.



3. Possible issue on Bright target removal

The aim of the Pbright algorithm is to remove bright targets (such as the ships, oil rigs, offshore wind farms for example) from the averaging of the scattering level (normalized radar cross section) on the cell where the wind retrieval is performed to avoid their contribution. A first quantitative inspection indicated that the results of the Pbright algorithm are not optimal and tend to over-estimate the number of bright targets in the wind cell. It means that it reduces the number of points for the averaging, and then could result in a less-confident and underestimated SAR-retrieved wind speed. Since the processing parameters used in the Pbright algorithm have not been re-adjusted after Sentinel-1 launch, the action of a quantitative estimation of the algorithm performances have been already identified last year. This has been postponed to 2018 and it will be performed for the different acquisition modes and processing levels and adjustments will be proposed if necessary.

4. Activation of the noise removal

The activation of the noise removal will allow to reduce the impact of the NESZ on the wind measurements especially for low-to-moderate wind speed and for wind measurements performed at high incidence angle, resulting on an over-estimation of the SAR derived wind speed and possible modulation of the measured wind speed profiles by the antenna lobe (Figure 38 for S1A, Figure 82 for S1B). The noise vectors of the L1 product will be updated on 2018 (with next version of the processor IPF 2.90), to be more accurate. Once this activity and after performance assessment, it could be decided to activate the noise removal for wind retrieval production.

5.2.1.2. Wave Mode

2017 is the second complete year with a nominal use of the wave mode for Sentinel-1 A. Following the acquisition plan, wave mode is acquired at global scale in VV polarization over the oceans. It leads to about 48000 acquisitions every month (~20000 collocations with WW3 numerical model for WV1 and ~20000 for WV2 each month). Please note that during 2017, with IPF 2.84, the variables `oswLandFlag` and `oswLandCoverage` are not correctly filled. The amount of data enables to investigate the stability of the Level-2 products performances with respect to time. Results are focused on VV in this report. The performances of HH polarization will be discussed in a future report.

Figure 39 shows the monthly performances for ocean surface wind speed with respect to time during 2017 for (a) WV1 and (b) WV2. Top panel presents the bias and the standard deviation for the wind speed. Bottom panel presents the number of acquisitions used for validation. The bias is computed by comparing the wind speed from Sentinel-1 and the wind speed from ECMWF analysis (3 hours and 0.125 degrees). An example for December 2017 is shown on Figure 41.

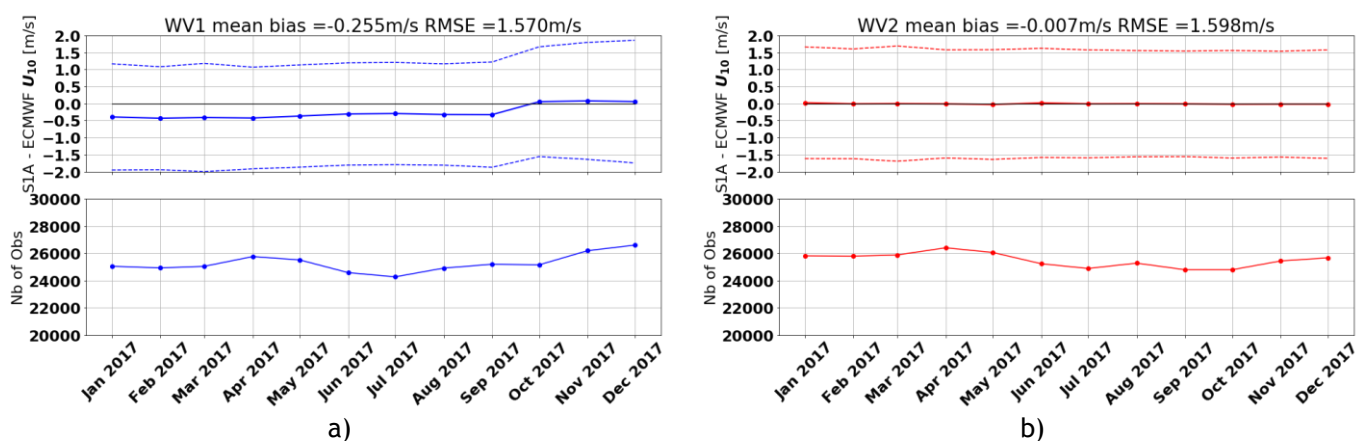


Figure 39: Ocean surface wind monthly performances for WV1 (a) and WV2 (b) and number of acquisitions co-located to reference data for validation for WV1 (bottom-left) and WV2 (bottom-right). For top panels, coloured thick solid lines stand for the mean difference between



Sentinel-1 and ECMWF model wind speeds. Coloured thin solid lines are associated standard deviation.

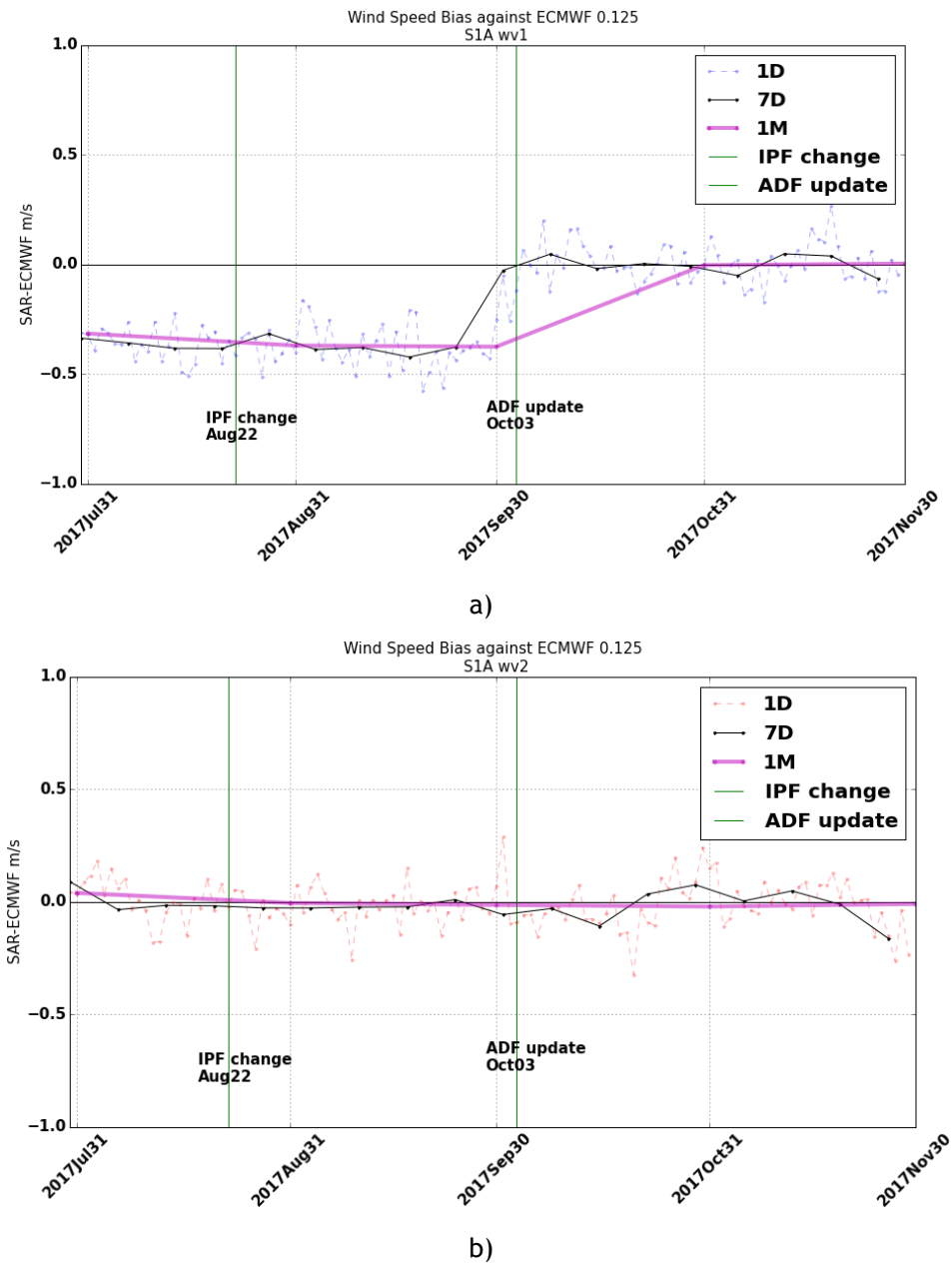


Figure 40: Focus on ocean surface wind monthly performances for WV1 (a) and WV2 (b). Colored thick solid lines stand for the 7-days mean difference between Sentinel-1 and ECMWF model wind speeds.

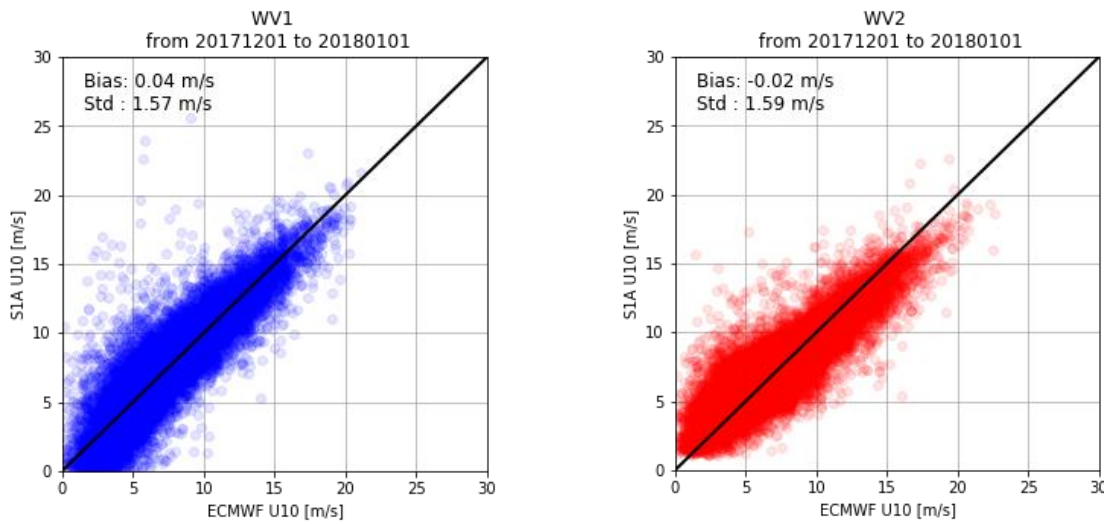


Figure 41: scatter plot of wind speed from S-1A WV1 versus ECMWF Dec 2017 (left WV1 and right WV2).

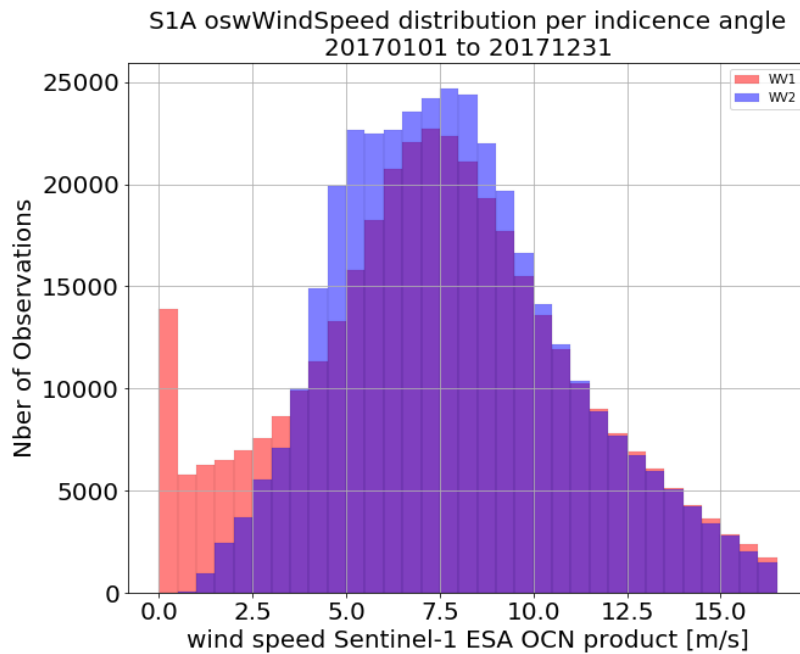


Figure 42: S-1A oswWindSpeed distribution per incidence angle. Red bars are WV1 and blue ones are WV2.

Here ocean surface wind speed from ECMWF model outputs are used as reference and SAR wind speed equal to zero are not considered. This approach is considered valid from a statistical point of view because the analysis is global, monthly and performed in open-ocean. Figure 39 shows that S1A WV1 has a significant change in the wind speed performances in 2017. Figure 40 is a focus on the performance analysis obtained in 2017 when the changes happened.

- S1A WV1 wind measurements had a bias of negative 0.4 m/s (i.e. underestimation of the SAR) visible on the first 8 months. This bias has been reduced in October. This improvement is due to the update of AUX_PP1 files aiming at changing the calibration gain of WV.



- For S1A WV2 wind measurements, bias is stable around 0m/s the small correction on AUX_PP1 (3rdOctober2017) has no visible impact on WV2 wind speed performances.

Note that there is not exactly the same number of observations used for WV1 and WV2 because of the filter applied on the dataset. More specifically, we are filtering all the points where the variable `oswWindSpeed` is equal to 0 m/s. And as it is shown on Figure 42 it occurred more frequently for WV1. Indeed, for this mode, too many WV1 data have values of `oswWindSpeed` equal to zero. This is obvious when comparing the wind speed PDF from WV1 with ECMWF model wind speed or with `oswWindSpeed` from WV2.

Conclusion

For 2017 WV1 wind speed bias with respect to ECMWF 0.175° is about -0.26 m/s with a RMSE of about 1.57 m/s (resp. 1.60m/s for WV2) which is better than the Sentinel-1 mission requirements for ocean surface WV wind speed (RMSE<2m/s).

In 2017 there was no modification of the wind inversion, a change of calibration occurred in October 2017 (via AUX_PP1 update) and improved the calibration especially for WV1. The 2 major limitations observed in the ocean surface wind speed (`oswWindSpeed`) measurements from ESA Sentinel-1 A Level-2 Ocean products are:

1. Wind speed performances are wind speed dependent for both WV1 and WV2.
2. The presence of null wind speed obtained with WV1. This is due to the use of CMOD IFR2 for the wind inversion. (The fact that a filter on null wind speed is applied on the figures showing the wind speed performances explains why we have less WV1 than WV2 observations.)

These two issues are related to the Wave Mode calibration and the choice of the Geophysical Model Function in the inversion scheme.

5.2.2. Swell Measurement

5.2.2.1. Wave Mode

2017 is the second complete year with a nominal use of the wave mode for Sentinel-1 A. Following the acquisition plan, wave mode is acquired at global scale in VV polarization over the oceans. It leads to about 48000 acquisitions every month (~20000 collocations with WW3 numerical model for WV1 and ~20000 for WV2 each month). This enables to investigate the stability of the Level-2 products performances with respect to time. Results are focused on VV in this report.

The waves performances are estimated by comparison between the significant wave height of the long waves as measured by Sentinel-1 and produced by Wave Watch 3 model (WW3). WW3 is run to produce a 2D ocean wave spectrum for each Sentinel-1 acquisition. On a statistical basis and over open-ocean, WW3 is used as the reference. For both S-1A and WW3, the significant wave height of the long waves is estimated by integration of the 2D ocean wave spectra up to the cut-off values (above this value, the inversion is not expected to work). This is why this parameter is called the effective significant wave height. It is directly computed from the ocean swell spectrum (`oswPolSpec`) and the 2D cut-off (`oswSpecRes`). The use of this variable aims at filtering the spectral domain that is considered as valid after ocean swell inversion) variables included in the L2 OCN products. Figure 43 shows an example of comparison between Sentinel-1 A and WW3 effective significant wave height, respectively for WV1 and WV2 obtained in December 2017. Very similar performances are visible for the two incidence angles.

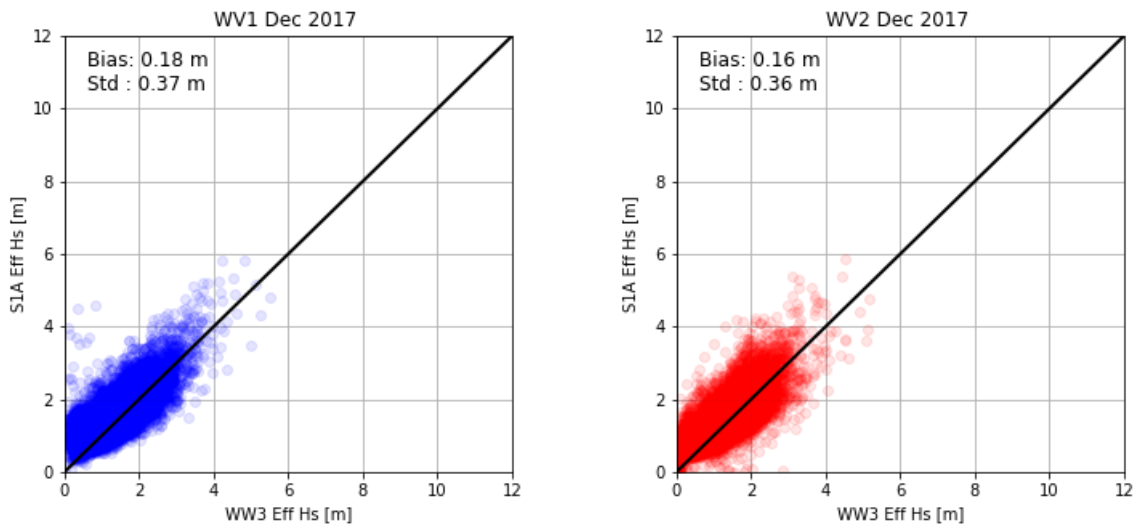


Figure 43: scatter plot of effective significant wave height from S-1A WV1 versus WW3 significant wave height Dec 2017. The model outputs are considered as reference here. This is only valid from a statistical point of view

Figure 44 shows performances for the effective significant wave height with respect to time. We observed very stable performances for S-1A on both WV1 and WV2 along the whole year. A constant overestimation of 0.2 m is observed. Standard deviation values are lower than 0.5 m for both WV1 and WV2. These results are within the specifications. The standard deviation of the effective significant wave height remains constant through 2017.

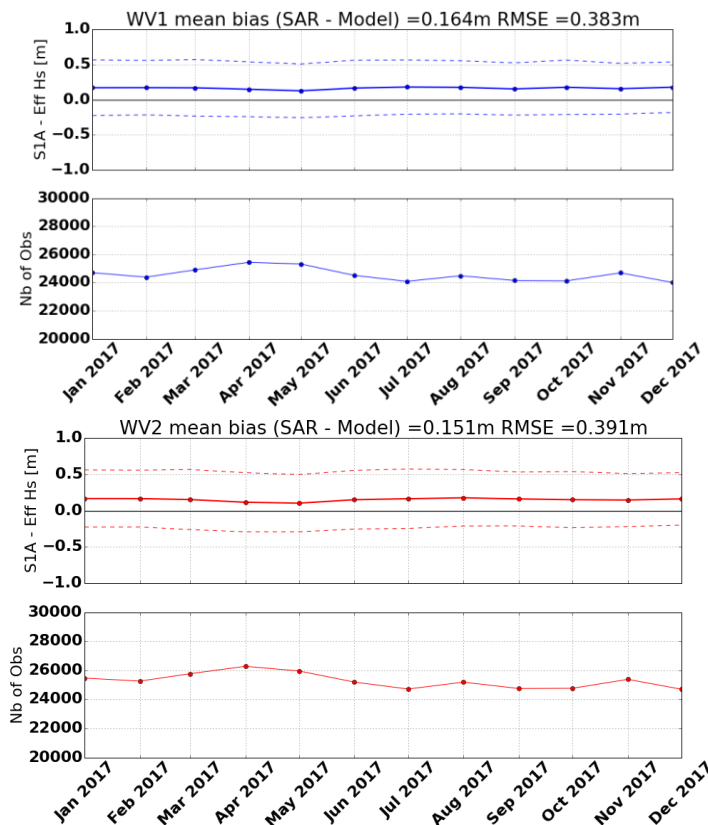


Figure 44: S-1A WV1 and WV2 Ocean Swell monthly performances as function of time.



For top panels, coloured thick solid lines stand for the mean difference between effective significant wave height from Sentinel-1 and from WW3 model. Coloured thin solid lines are for standard deviation.

Conclusion:

This report only gives performances regarding the significant wave height (period and wave direction will be discussed later).

For effective significant wave height derived from ESA Sentinel-1A level-2 Ocean products, the key elements for 2017 are:

- The absence of update in the swell inversion: With respect to year 2016, during which several updates in the wave inversion algorithm have impacted the stability of the wave parameter performances, no change on the wave retrieval performances were observed during year 2017. This performance stability is illustrated in Figure 44.
- The update of the processing gains coefficients (via AUX_PP1 in October 2017). This mostly impacts performances on ocean surface wind speed (oswWindSpeed, see Figure 39). Indeed, although the wind speed is used as input to estimate the non-linear part of the cross-spectrum, the small change in the wind speed performances (<0.4m/s) is negligible regarding the waves parameters performances.

Significant wave height performances with respect to WW3 numerical model forecasts are better than the mission requirements for the RMSE (specifications: <0.5m) but not for the bias (specifications: <0.1m).

We estimated:

- a mean bias of about 0.16m for WV1, 0.15m for WV2
- a RMSE about 0.38m for WV1 and 0.39 for WV2.

Those values are stable during the year 2017

5.2.3. Radial Velocity Measurement

5.2.3.1. Wave Mode

2017 is the second complete year with a nominal use of the wave mode for Sentinel-1 A. Following the acquisition plan, wave mode is acquired at global scale in VV polarization over the oceans. It leads to about 48000 acquisitions every month (~20000 collocations with WW3 numerical model for WV1 and ~20000 for WV2 each month). This enables to investigate the stability of the Level-2 products performances with respect to time. Results are strictly based on VV in this report.

The radial velocity measurement is derived from the Geophysical Doppler anomaly. In the S-1 IPF, this geophysical Doppler is estimated by:

$$F_{dc_{ocean}} = F_{dc_{SAR}} - F_{dc_{attitude}} - F_{dc_{antenna}}$$

where:

- FdcSAR is estimated from the SAR data
- FdcOcean is the component related to the ocean radial velocities.
- FdcAttitude is estimated from the geometry knowledge (quaternion based)
- Fdcantenna is the antenna contribution related to TRM drifts, failures, misalignments, etc

At global scale, in open-ocean and at medium resolution (20km), the expected relationship between the geophysical Doppler and the sea state (or at first order the ocean surface wind vector) is well known since Envisat/ASAR. The performances of the geophysical Doppler are assessed by estimating the bias between the expected Doppler given the sea state conditions (provided by ECMWF ocean surface wind speed projected along the antenna pointing direction) and the geophysical Doppler as derived from the variables included in the Level 2 products.



Statement of the ocean surface radial velocities measurements accuracy:

Figure 45 shows the geophysical Doppler as computed from the Level 2 products as a function of radial wind speed (wind speed projected in the line of sight of the radar). The colour code indicates the latitude. As observed, the Doppler and the radial wind speed are strongly correlated for both WV1 and WV2. However, the color code indicates a clear and non-geophysical dependence to the latitude. In addition, Doppler is not 0 Hz (whereas it should be. Here, we obtain rather 60 Hz) when the radial wind speed is 0 m/s for WV1 and WV2. This shows that the geophysical Doppler shift deduced from the Level-2 products using the different Doppler components included in the Level-2 products is not only related to ocean surface radial velocities. This prevents for getting any quantitative geophysical signature such as ocean surface currents in the product. Both, the scatter and the bias illustrate the issue regarding the poor accuracy on the attitude orbit control system of the platform along its orbit.

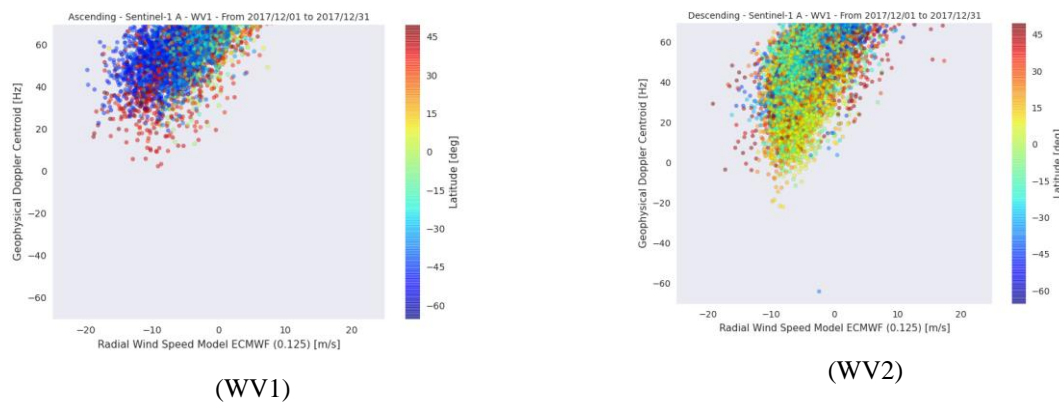


Figure 45: Geophysical Doppler as included in the Level 2 products as a function of radial wind speed (wind speed projected in the line of sight of the radar) for WV1 and WV2. The colour code indicates the latitude.

The monitoring of the Geophysical Doppler bias and of the scattering in the relationship between the Geophysical Doppler and the sea state are monitored by estimating the mean and standard deviation of the Geophysical Doppler obtained for radial wind speed values around 0 m/s +/- 2 m/s. Figure 46 shows the temporal evolution of these 2 parameters. As observed the mean bias varies between 40 Hz and 110 Hz. WV1 and WV2 exhibit the same variations with respect to time.

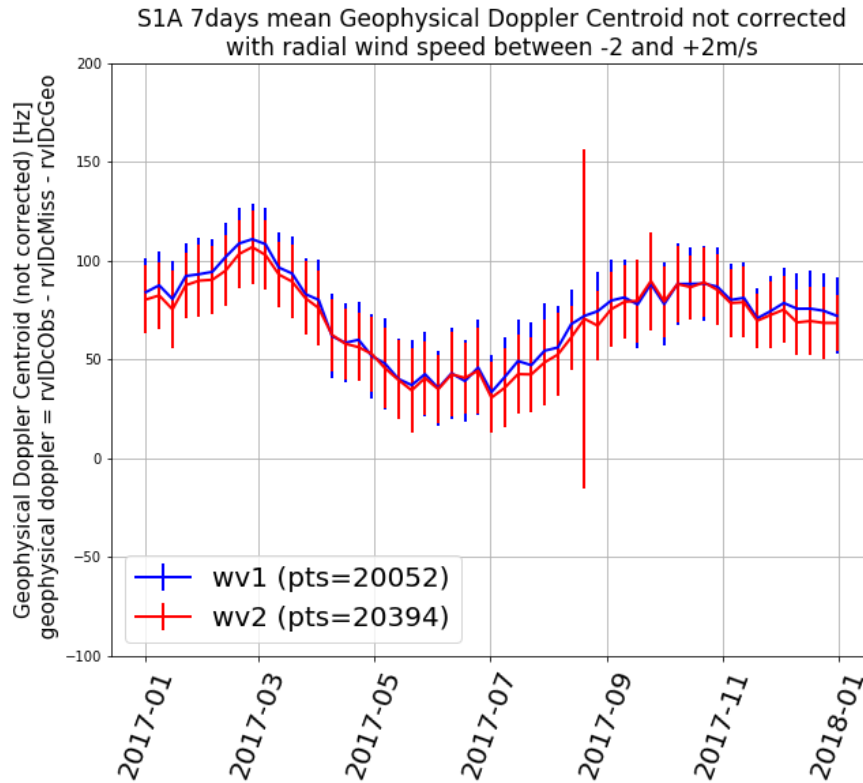


Figure 46: Evolution of the Geophysical Doppler Centroid during the year 2017. The blue curve is the 7 days averaged Geophysical Doppler Centroid computed from Level2 RVL products for WV1 and red for WV2. Only measurements corresponding to ECMWF radial wind speed forecast is between -2 m/s and 2m/s are taken into account.

The various S1 WV OCN Doppler components (i.e. the data DC, the EM DC bias, the geometricDC) for one month of S-1A WV are shown in next figures. Note that the geometric DC is always close to zero Hz.

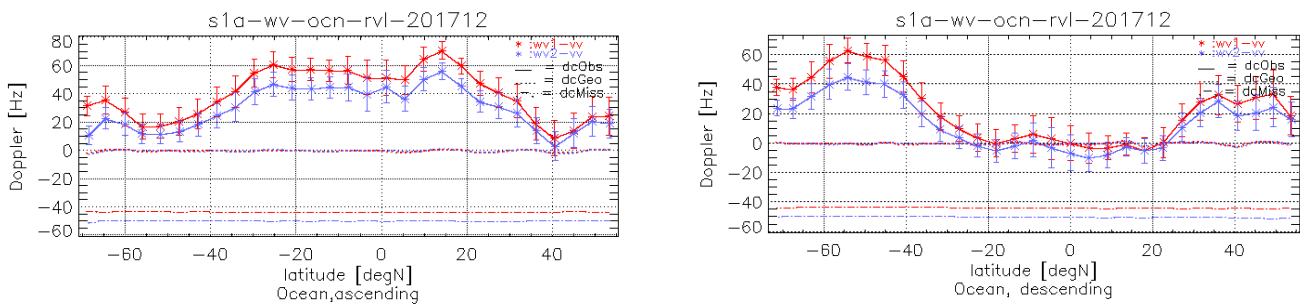


Figure 47: S-1A WV OCN Doppler components from December 2017. The vertical bars are the spread in measured DC over the period. Note that the geometric DC is around zero and the EM DC bias is around -40Hz for S-1A.

Improvement performed during 2017:

No improvements in the S1A WV OCN Doppler during 2017.

Coming improvement for 2018:

An improvement of the attitude control will be uploaded to S-1A in mid-February 2018. This is similar to what was performed on S-1B during late November 2017 (see Section 7.1.8.2 & 7.2.3.1 on S-1B)



Furthermore, efforts are undertaken to develop and demonstrate a way to fully calibrate the S1 OCN Doppler by using the restituted attitude data in combination with a data driven model to assess the residual geometric Dc. This activity will also include a monitoring of the antenna electronic miss pointing DC bias.

5.2.3.2. TOPS Mode

Statement of the ocean surface radial velocities measurements accuracy:

As for Wave Mode, the contamination of the geophysical Doppler by the geometry knowledge (quaternion based) and the antenna contribution prevents us for getting any quantitative geophysical signature such as ocean surface currents in the product. Nevertheless, in cases where land areas are present in the image an ad-hoc calibration is performed by merging the DC over the swaths and computing a mean DC range profile over the land areas. An example is shown in Figure 48 taken from the Sentinel Hurricane Observation Campaign (SHOC) data set.

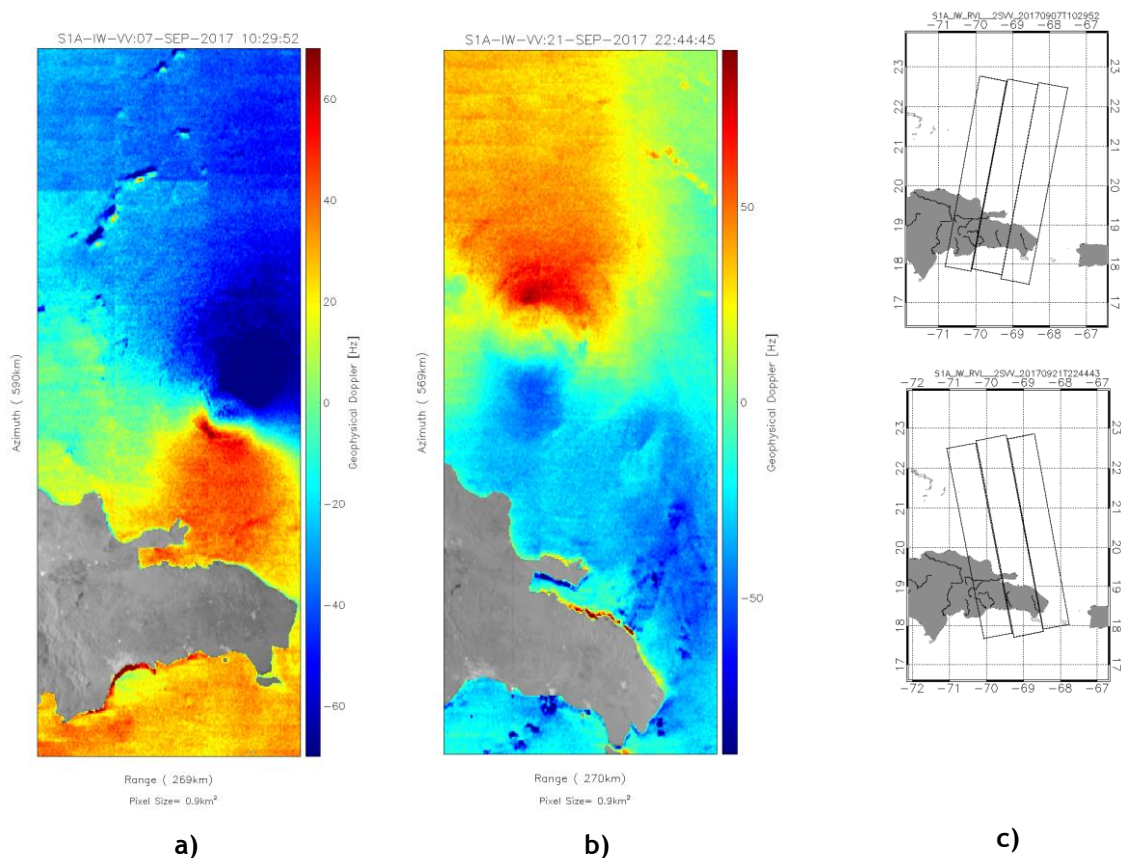


Figure 48: (a,b) Doppler anomaly field from Sentinel 1A IW RVL product acquired over tropical cyclones in Caribbean. Here land areas are used to calibrate the Doppler anomaly. c) Acquisition areas.

Improvement performed during 2017:

Efforts were undertaken to better predict and compensate the measured Doppler for the electromagnetic (EM) Doppler bias introduced by the skewness of the antenna elevation pattern. A new version of the antenna model parameters has been ingested into the Level 2 processor and the EM Doppler bias over EW swaths is compared with the data driven Doppler estimated over rain forest areas (see Figure 49).



Although the relative trends over swaths are predicted well, a significant Doppler bias is observed between the model and data. Compared to previous results, the model and data are better aligned and the jumps between swaths are better predicted.

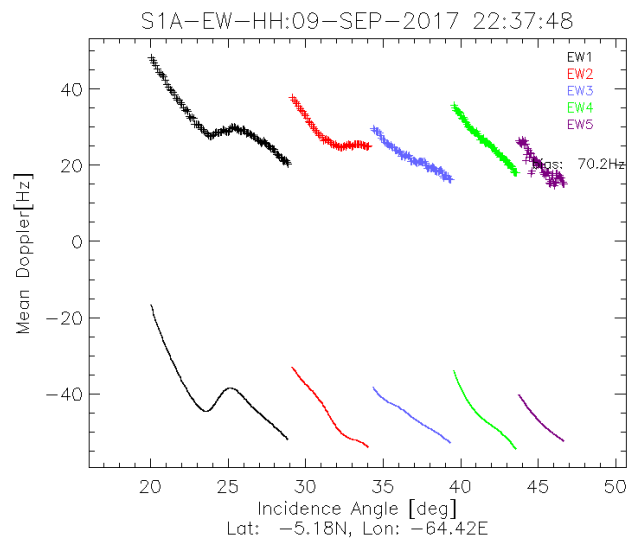


Figure 49: S-1A HH EM DC offset computed from antenna model (full line) with error matrix corresponding to the day of acquisition and estimated from rain forest data using the Level 2 processor.

Coming Improvements for 2018:

A further refinement of the de-scalloping will be implemented without increasing the processing time.



5.2.4. Geophysical Calibration

5.2.4.1. Wave Mode

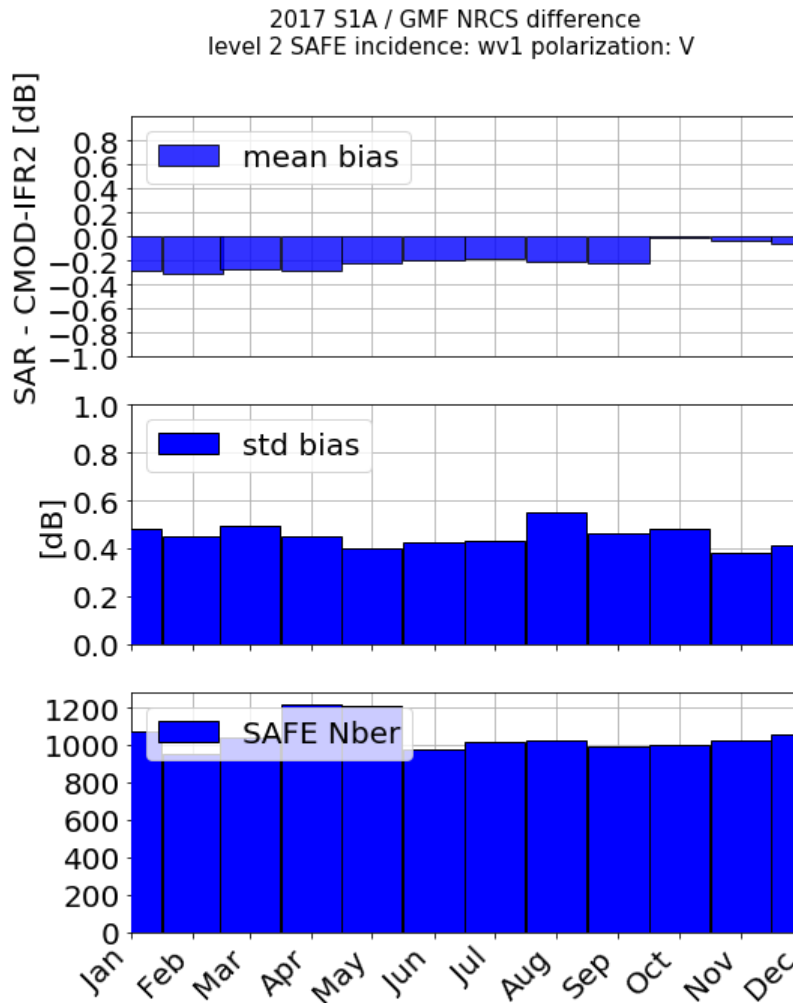


Figure 50: Sentinel-1A geophysical relative RCS computed using CMOD-IFRv2+ECMWF for WV1 VV polarisation between 50° and -50° latitude. Panel 1 shows the mean bias between ECMWF and Sentinel-1A. Panel 2 shows the bias standard deviation. Panel 3 shows the number of SAFE used to perform the analysis.

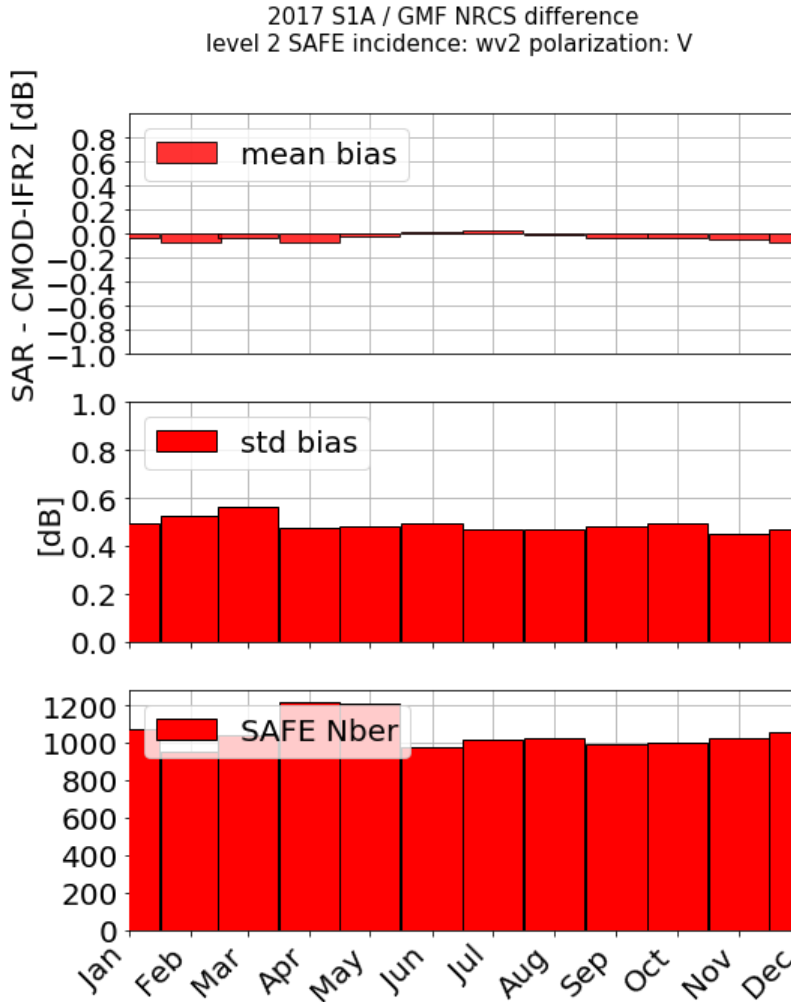


Figure 51: Sentinel-A geophysical relative RCS computed using CMOD-IFRv2+ECMWF for WV2 VV polarisation between 50° and -50° latitude. Panel 1 shows the mean bias between ECMWF and Sentinel-1A. Panel 2 shows the bias standard deviation. Panel 3 shows the number of SAFE used to perform the analysis.

As shown in Figure 50 WV1 sigma0 values are underestimated of -0.25 dB on the 10 first months of 2017. WV2 is also stable and close to zero dB. After the calibration gain change applied in October, the Sentinel-1A sigma0 (Level2 *oswNrcs* variable) the difference with the GMF are reduced for both WV1 and WV2. The standard deviation is stable about 0.4 dB for WV1 and 0.5 dB for WV2. It is consistent with S-1B.

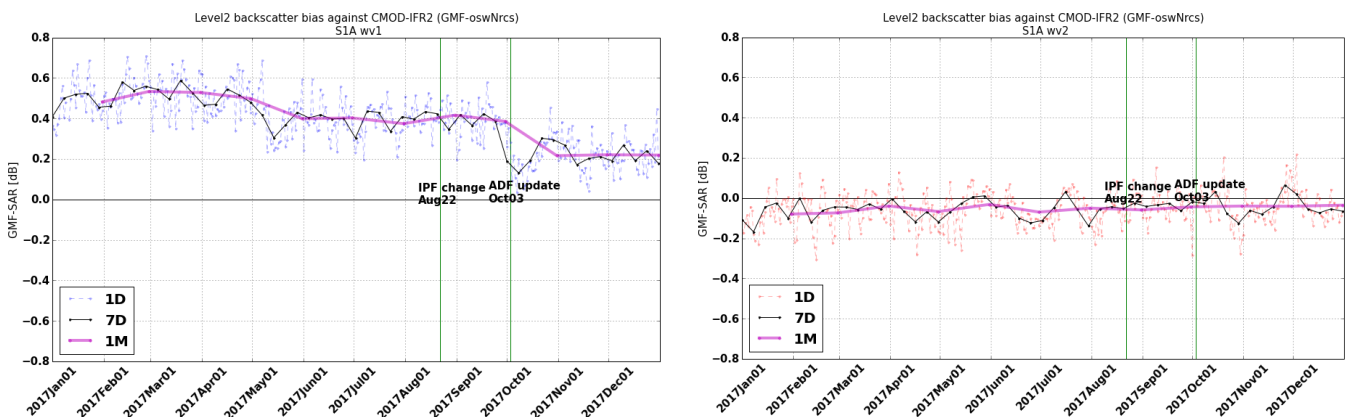




Figure 52: External Geophysical calibration evolution for 2017. WV1 (left) and WV2 (right) curves are showing the evolution of the bias between the level2 sigma0 and the sigma0 that CMOD-IFR2 model is giving. Green vertical lines are showing the date of AUX_PP1 update and IPF 2.84 deployment.

On Figure 52 we can see in detail the evolution of the difference between the L2 sentinel-1 NRCS values and the model CMOD-IFR2. The effect of the modification in the AUX_PP1 file to change in the calibration gain is clearly visible



6. S-1B Instrument Status

Hereafter, the status of the S-1B instrument during 2017:

6.1. S-1B Antenna Status

The Antenna status is routinely monitored using the dedicated RFC calibration mode. The RFC products are processed, in order to generate the Antenna Error Matrix from which it is possible to retrieve the failure and drift of each TRM.

The Figure below shows the antenna Transmit/Receive Module (TRM) status at the end of 2017. Seven (7) failures are counted in total among TX-RX and H-V. On the 16th January 2017 the RX H TRM #8 of tile 5 failed. The element is indicated with a red arrow in the image. This was the only S-1B antenna related event of the whole 2017. All the failed TRMs are connected to a single Electronic Front End (each EFE includes 8 TRMs), which probably failed during the S-1B launch. A full list of all TRM failures during 2017 is given in Appendix F -.

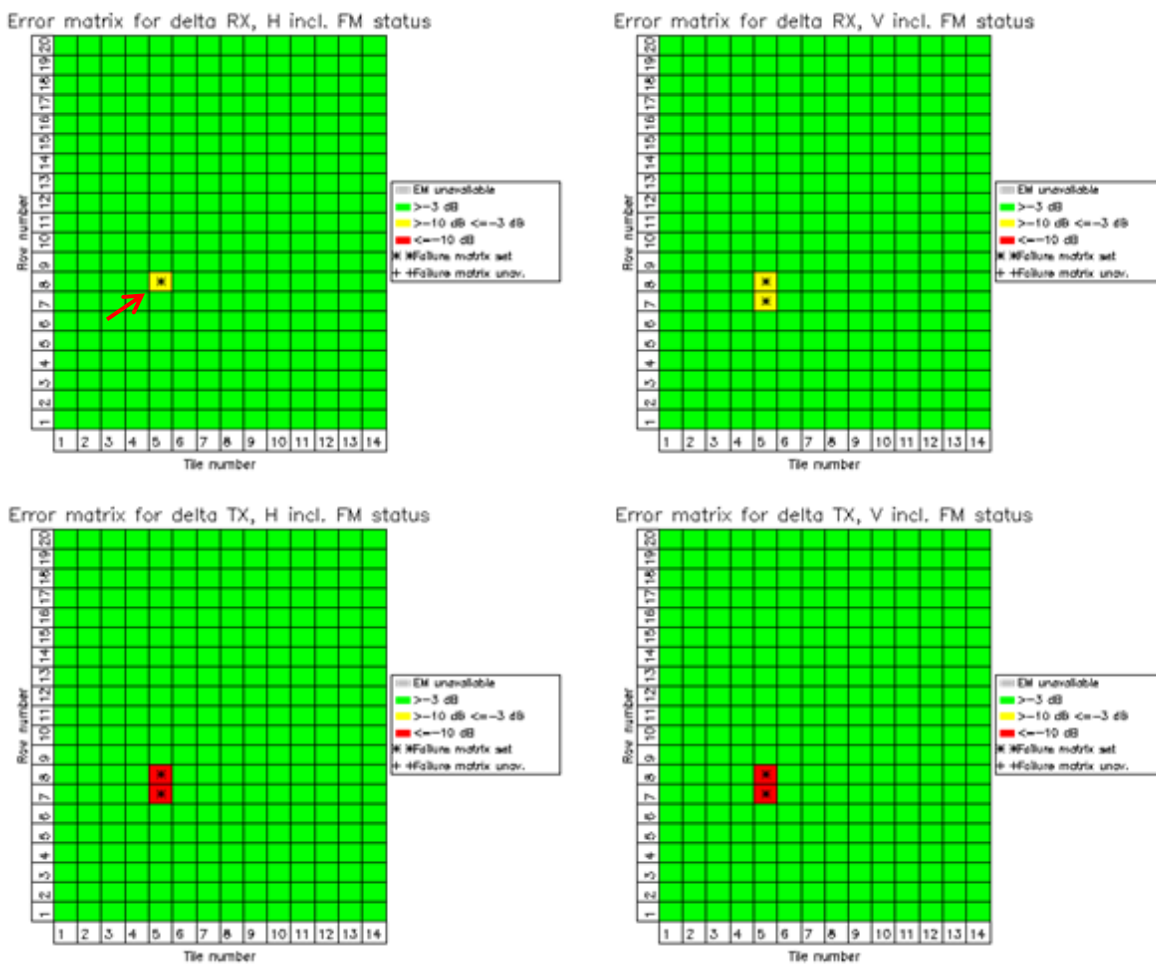


Figure 53: S-1B antenna status on 31/12/2016. The top charts refer to RX elements and the bottom charts refer to TX elements

The following figures show the TX and RX excitation coefficients (averaged per tile) during the 2017. The overall antenna behaviour is very stable. Only tile 5 TX V gain shows small jumps which



have been observed since the S-1B Commissioning Phase. The tile 5 behaviour is currently under investigation but no issues on SAR performances are introduced by the observed jumps.

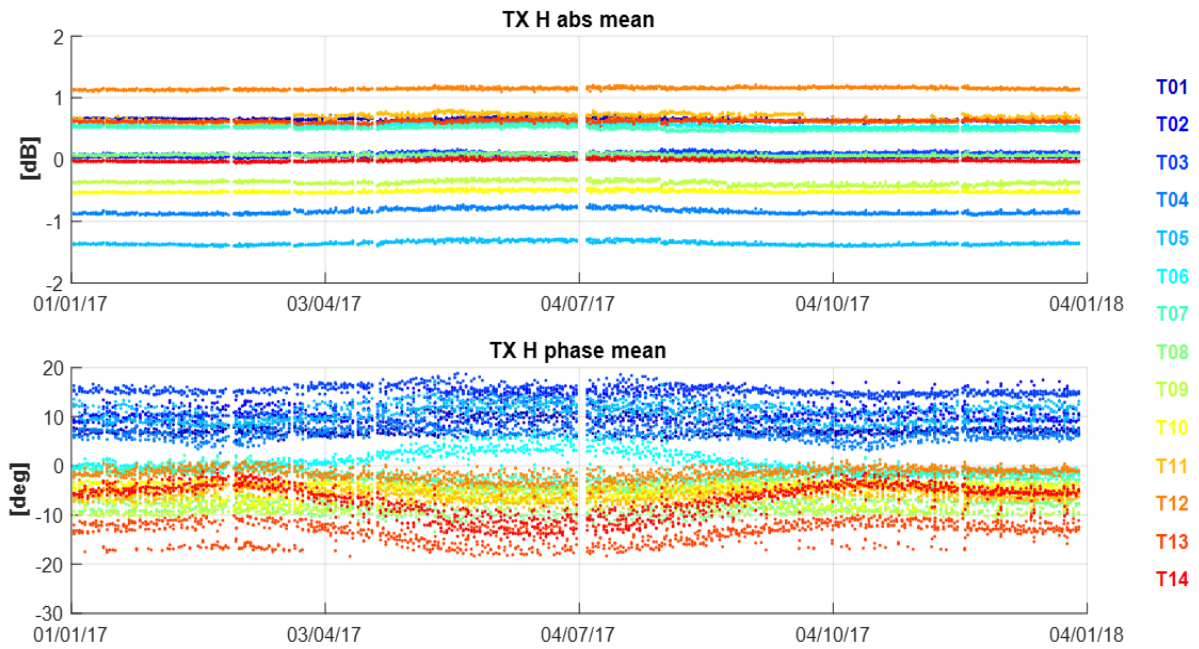


Figure 54: Gain (top) and phase (bottom) stability of the SAR antenna tiles (average of the RFC coefficients in TX H over rows).

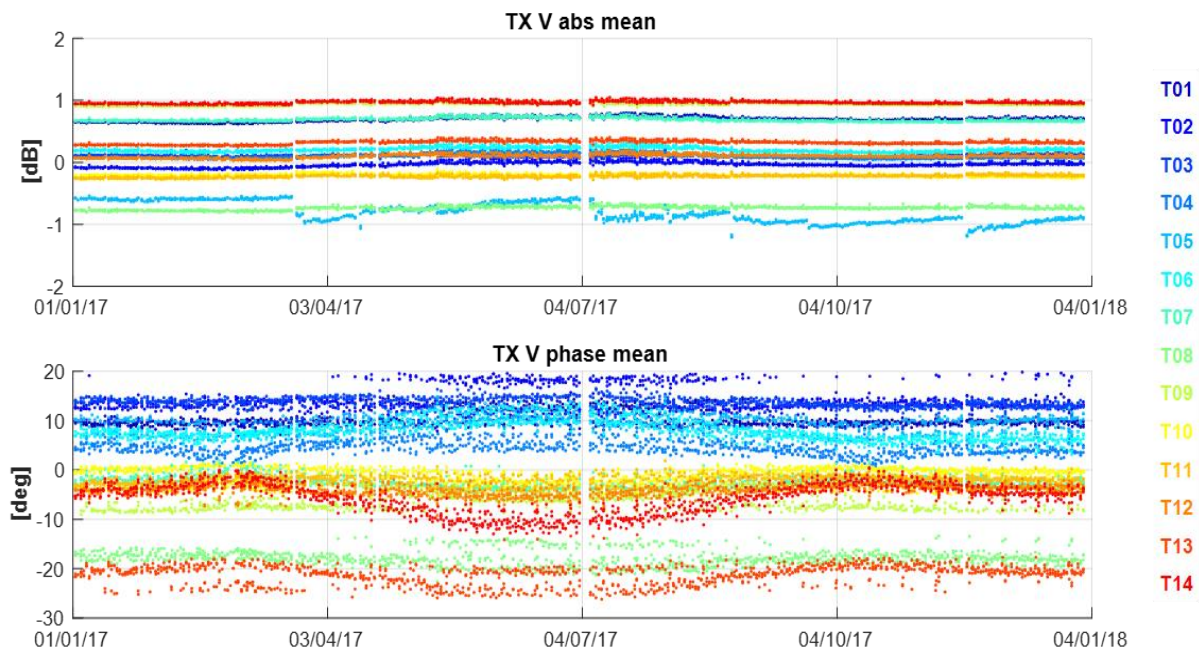


Figure 55: Gain (top) and phase (bottom) stability of the SAR antenna tiles (average of the RFC coefficients in TX V over rows).

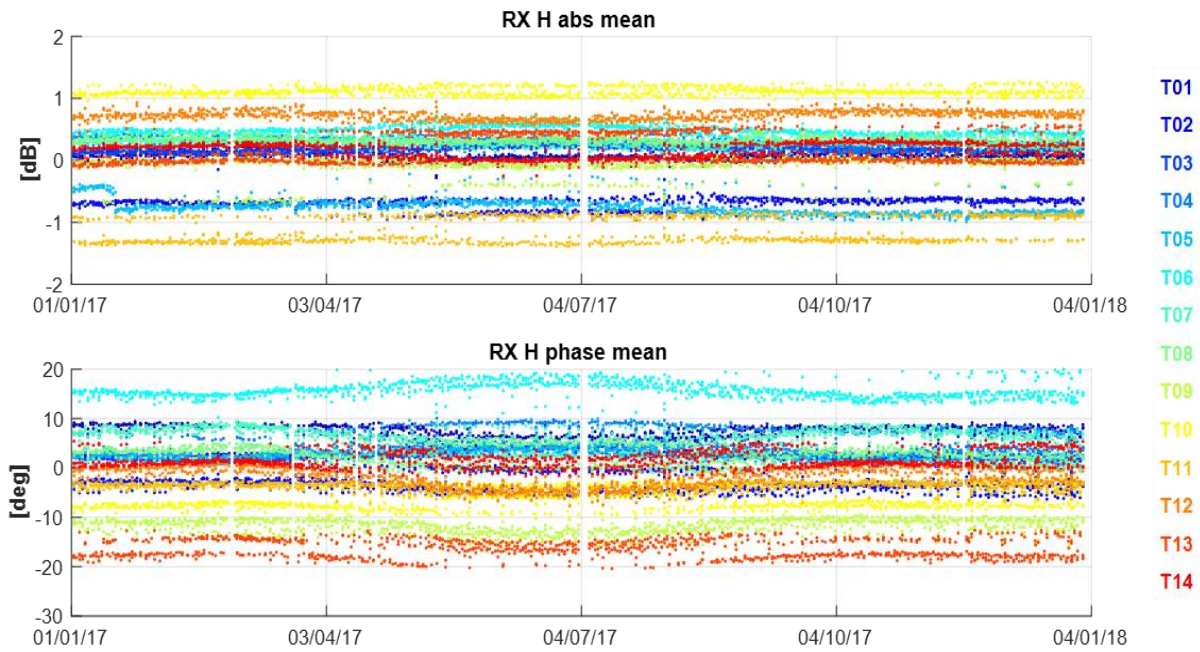


Figure 56: Gain (top) and phase (bottom) stability of the SAR antenna tiles (average of the RFC coefficients in RX H over rows).

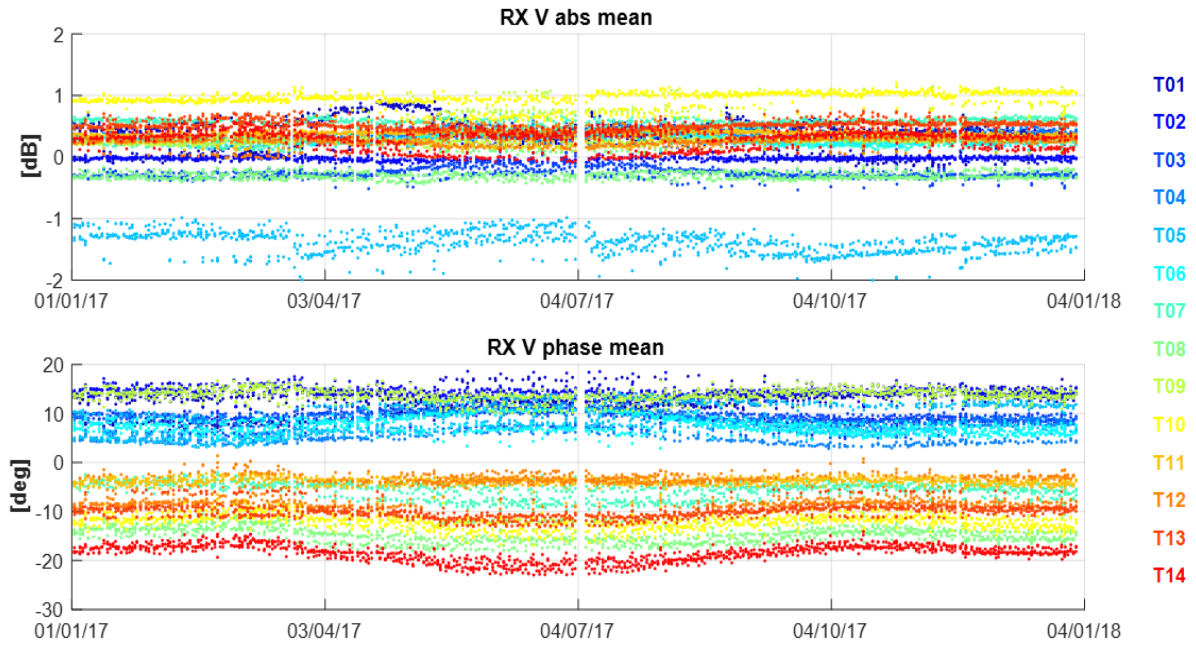


Figure 57: Gain (top) and phase (bottom) stability of the SAR antenna tiles (average of the RFC coefficients in RX V over rows).

6.2. S-1B Instrument Unavailability

A list of S-1B instrument unavailabilities during 2017 is given in Appendix C - .



6.3. S-1B Radar Data Base Updates

There were no S-1B Radar Data Base (RDB) updates during 2017.

6.4. S-1B Internal Calibration

The instrument stability over time is monitored through the internal calibration signals. The plot in Figure 58 shows the main parameters monitored: PG gain and phase. The colour in the plot represents the different sub-swaths.

The PG gain is quite stable in the reporting period. Unlike S-1A, no polarization related difference in the PG gain levels can be observed for S-1B.

The observed PG phase jumps are expected. They occur at every instrument switch off due to a different initialization of the ADC. They are not an issue since they only provide a phase constant in the SAR data.

Figure 59 and Figure 60 show in detail the PG gain evolution for EW DH and IW DV acquisitions. A decrease of the PG gain of about 0.2 dB can be noticed between March and April 2017 for all modes and polarizations. After such gain drop, only small fluctuations of the PG gain can be observed with a peak to peak variation lower than 0.1 dB. The origin of the PG gain drop is not clear and should be investigated at instrument level. In any case, the stability of the S-1B radiometry (see Section 7.1.2) suggests that the instrument gain reduction is well captured by the internal calibration.

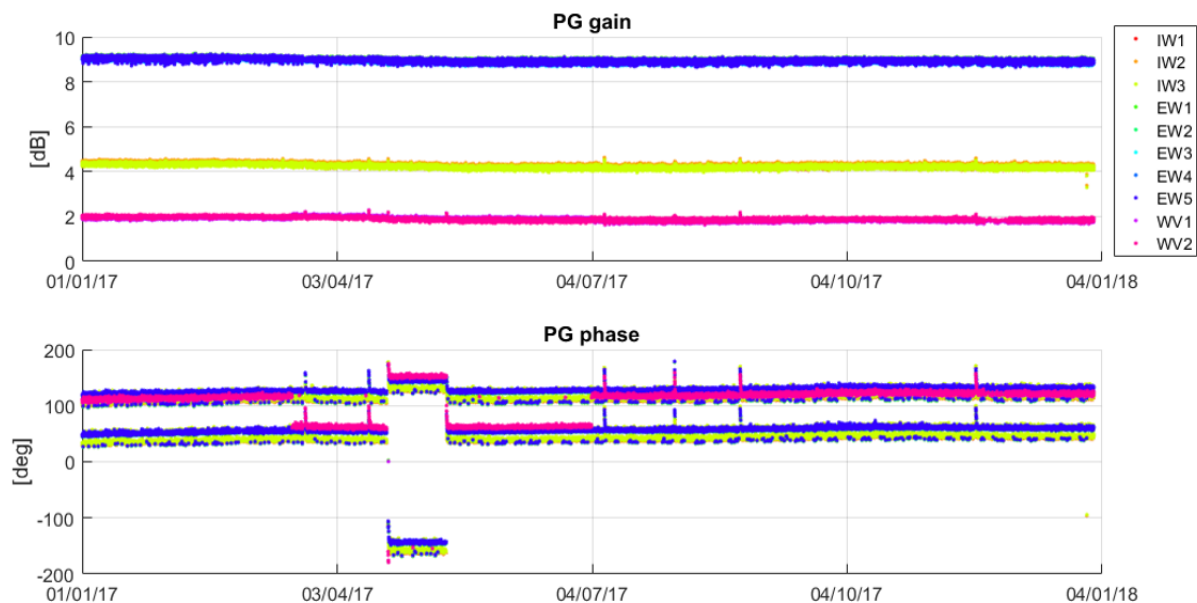


Figure 58: Internal calibration parameters over time. The colour represents the sub-swath.

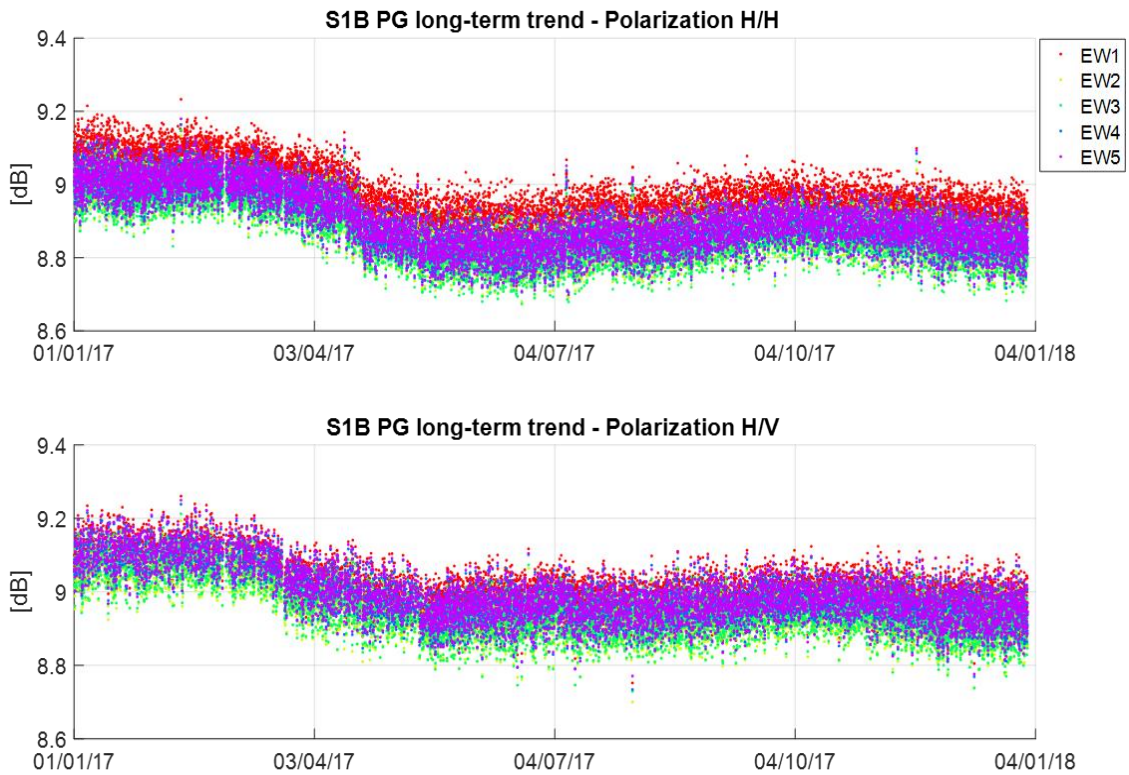


Figure 59: EW HH (left) and HV (right) PG gain divided by sub-swath.

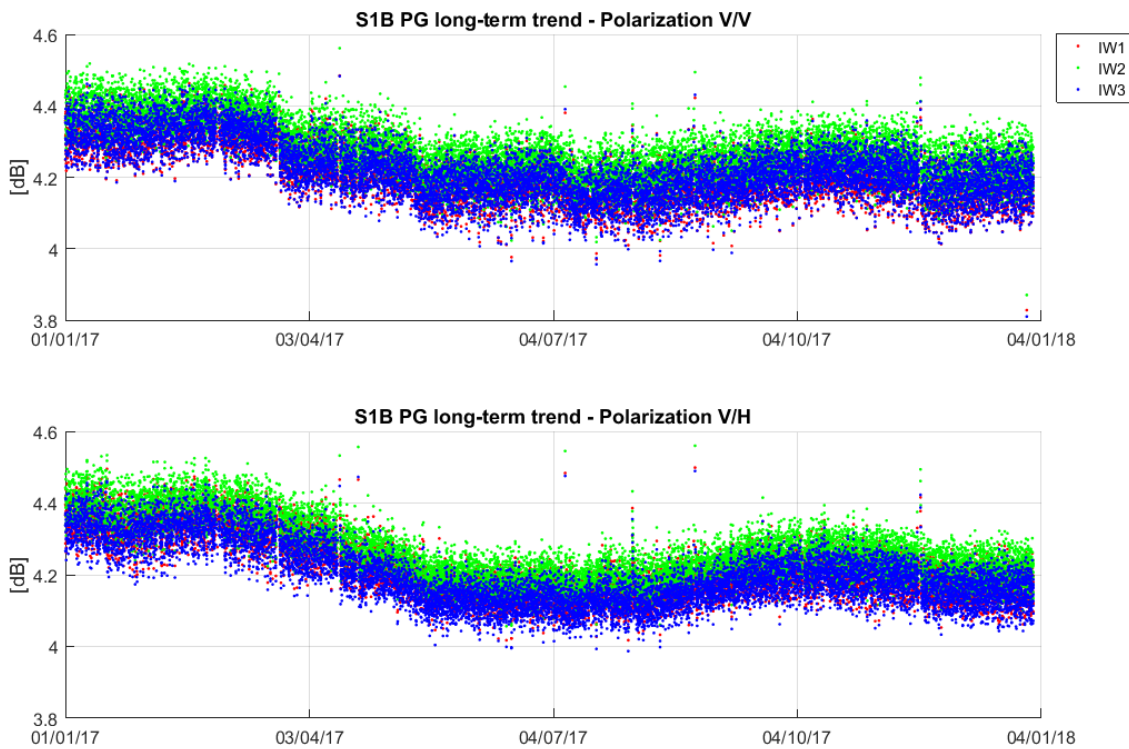


Figure 60: IW VV (left) and VH (right) PG gain divided by sub-swath.



6.5. S-1B Noise Power

The noise power is monitored through the dedicated RX-only pulses embedded at the start/stop of each data-take. Figure 61 shows the noise power versus time during 2017. Overall, the noise power has a good stability, with a standard deviation of approximately 1 dB in the short term. Table below reports the noise power stability (3σ) averaged over the full reporting period. The number in the parenthesis represents the number of products considered. Note that in the period from March to July WV data were acquired in HH polarization resulting in a slightly lower noise power in that period (as visible in the plot).

Acquisition mode	Noise power stability [dB]
SM	HH: 6.2 ± 1.1 (363) VV: 5.7 ± 0.9 (1454) HV: 6.2 ± 1.14 (364) VH: 5.6 ± 1 (1456)
IW	HH: 7.7 ± 1.1 (8811) VV: 7.8 ± 1.3 (75564) HV: 7.7 ± 1 (3771) VH: 7.75 ± 1.6 (71807)
EW	HH: 6.4 ± 1.2 (99680) VV: 6.25 ± 1 (3728) HV: 6.5 ± 0.9 (75982) VH: 6.05 ± 1.3 (3510)
WV	HH: 6.8 ± 0.75 (14062) VV: 7.0 ± 0.7 (35492)

Table 19: Noise power stability (3-sigma): period JAN 2017 - DEC 2017

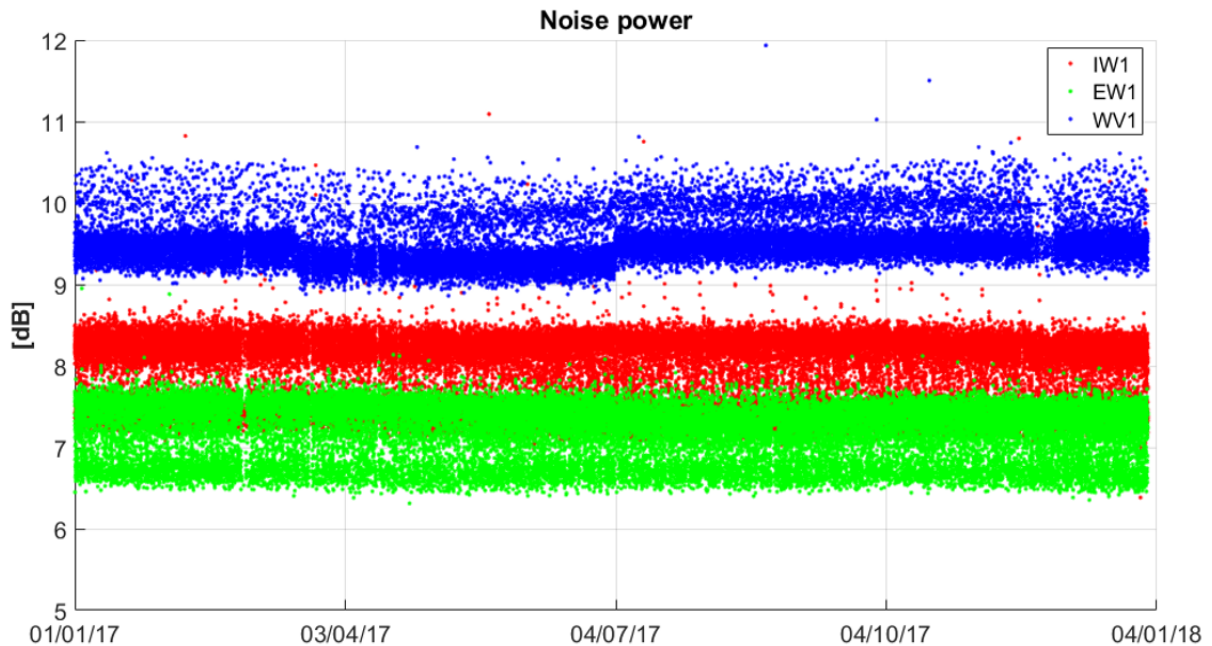


Figure 61: Noise power versus time. The colour represents the different beams.



7. S-1B Products Status

Hereafter, the status of the S-1B products during 2017:

7.1. S-1B Level 1 Products

A general summary of status of S-1B Level 1 products was presented at several conferences and workshops (see [S1-RD-01], [S1-RD-02], [S1-RD-03] and [S1-RD-04]).

7.1.1. Level 1 Basic Image Quality Parameters

The DLR Transponders & Corner Reflectors, the BAE Corner Reflector and the Australian Corner Reflector array have been used to assess various impulse response function parameters as described below. The products analysed were acquired during 2017 and processed with the Sentinel-1 IPF v2.7.2, v2.8.2 and v2.8.4.

7.1.1.1. Spatial Resolution

The Figures and Tables below give the azimuth and range spatial resolutions derived from SM, IW and EW SLC data. The numbers in brackets indicate the number of measurements.

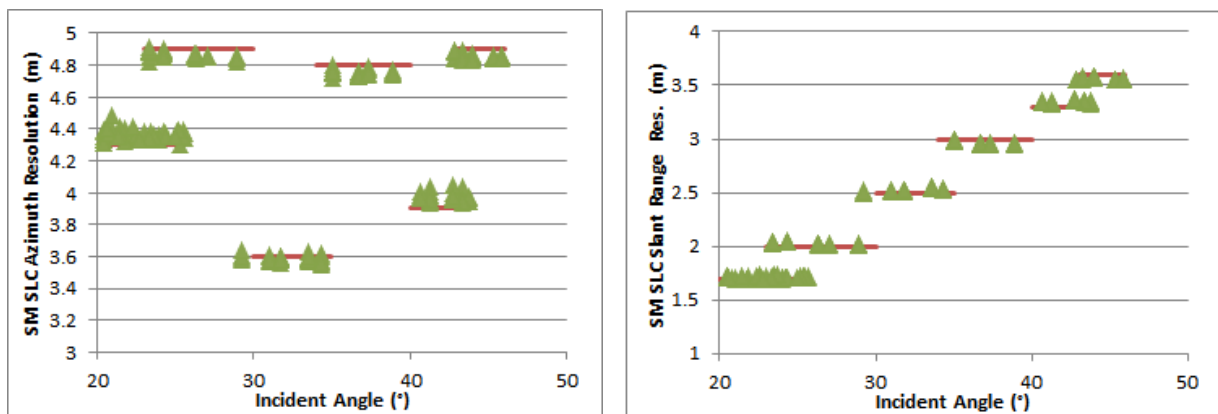


Figure 62: SM Azimuth and Slant Range Spatial Resolutions

Mode/Swath	Azimuth Spatial Resolution (m)	Slant Range Spatial Resolution (m)
S1	4.36±0.03 (69)	1.72±0.01 (69)
S2	4.86±0.02 (35)	2.03±0.01 (35)
S3	3.59±0.02 (35)	2.53±0.02 (35)
S4	4.75±0.02 (30)	2.97±0.02 (30)
S5	3.98±0.03 (38)	3.35±0.01 (38)
S6	4.85±0.02 (40)	3.57±0.01 (40)

Table 20: SM Azimuth and Slant Range Spatial Resolutions

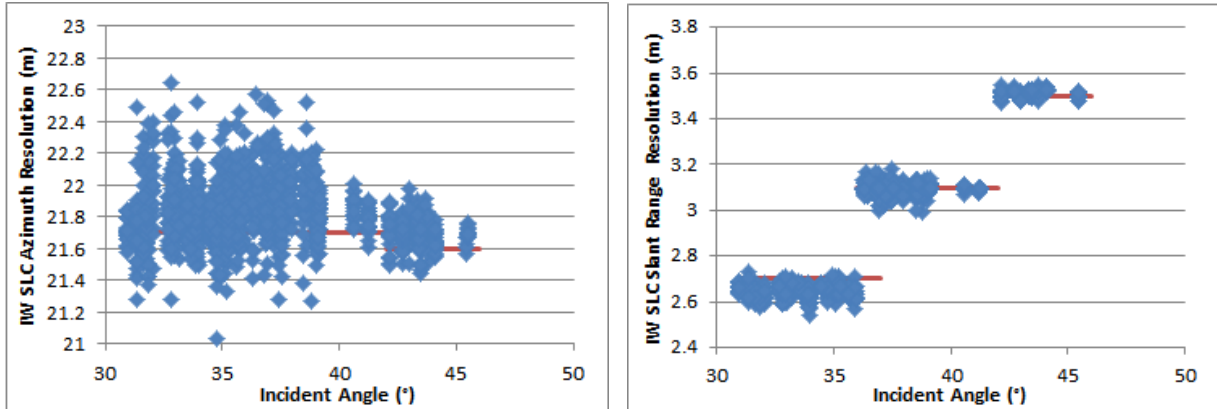


Figure 63: IW Azimuth and Slant Range Spatial Resolutions

Mode/Swath	Azimuth Spatial Resolution (m)	Slant Range Spatial Resolution (m)
IW1	21.82±0.20 (710)	2.65±0.02 (710)
IW2	21.89±0.19 (449)	3.09±0.02 (449)
IW3	21.70±0.09 (240)	3.51±0.01 (240)

Table 21: IW Azimuth and Slant Range Spatial Resolutions

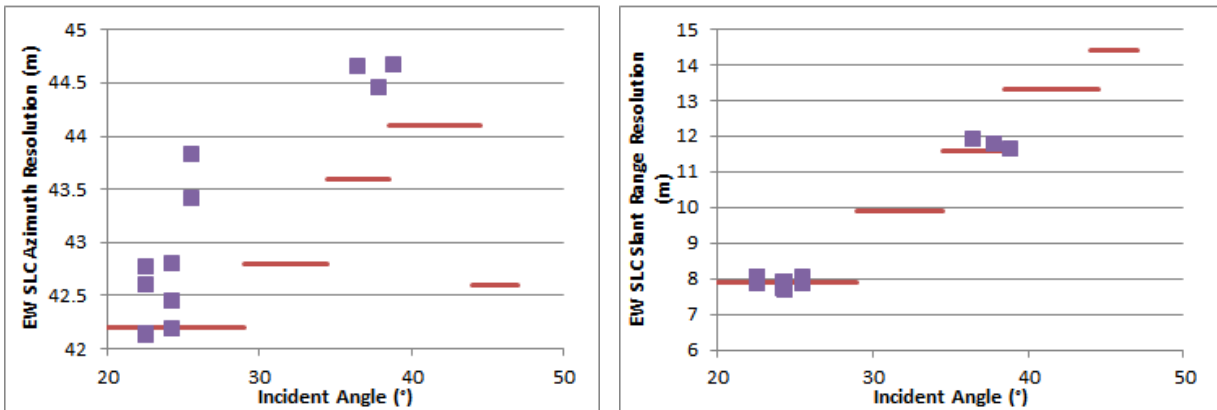


Figure 64: EW Azimuth and Slant Range Spatial Resolutions

Mode/Swath	Azimuth Spatial Resolution (m)	Slant Range Spatial Resolution (m)
EW1	42.35±0.73 (13)	7.89±0.12 (13)
EW3	44.59±0.12 (3)	11.76±0.14 (3)

Table 22: EW Azimuth and Slant Range Spatial Resolutions

The measured spatial resolutions match the predicted resolutions as indicated by the red horizontal lines.



7.1.1.2. Sidelobe Ratios

The table below gives the measured impulse response function sidelobe ratios derived from SM, IW and EW SLC data - these indicate acceptable values.

Mode/Swath	Integrated Sidelobe Ratio (dB)	Range ISLR (dB)	Azimuth ISLR (dB)	Peak Sidelobe Ratio (dB)	Spurious Sidelobe Ratio (dB)
SM	-13.31±1.04	-15.85±0.55	-17.09±1.00	-20.50±0.71	-26.59±1.33
IW	-11.56±3.08	-15.81±1.25	-16.71±1.59	-19.85±1.26	-23.42±3.38
EW	-12.96±2.20	-16.92±3.30	-17.13±2.78	-19.21±3.23	-19.41±2.76

Table 23: SM & IW Sidelobe Ratios

7.1.1.3. ENL and Radiometric Resolution

Large uniform distributed targets are used to measure the equivalent number of looks (ENL) and radiometric resolution (RR) in imagery as given in Table 24 to Table 7 below. For each swath/sub-swath and product type, the first number is the ENL while the second is the RR in dB.

	IW1	IW2	IW3
GRDH	4.66, 1.65	4.60, 1.66	4.48, 1.68

Table 24: IW ENL & RR Measurements

	EW1	EW2	EW3	EW4	EW5
GRDH	2.33, 2.19	2.40, 2.16	2.52, 2.12	2.56, 2.11	2.61, 2.09

Table 25: EW ENL & RR Measurements

7.1.1.4. Ambiguity Analysis

7.1.1.4.1. Azimuth Ambiguities

The table below gives mean azimuth ambiguity ratio for DLR transponder targets acquired in IW mode.

	IW
Early Azimuth Ambiguity Ratio (dB)	-27.86±2.35
Late Azimuth Ambiguity Ratio (dB)	-27.85±3.00

Table 26: Azimuth Ambiguity Ratios

7.1.1.4.2. Range Ambiguities

No imagery suitable for range ambiguity measurements were identified during 2017.



7.1.2. Radiometric Calibration

The DLR Transponders & Corner Reflectors, the BAE Corner Reflector and the Australian Corner Reflector array have been used to assess various impulse response function parameters as described below. The products analysed were acquired during 2017 and processed with the Sentinel-1 IPF v2.7.2, v2.8.2 and v2.8.4.

7.1.2.1. Absolute Radiometric Calibration

DLR Transponders have been used to calculate the relative radar cross-section for SM and IW modes during 2017 (there were no EW mode acquisitions over the DLR sites). The results per mode are shown in Table 27 where mean (radiometric accuracy) and standard deviation (radiometric stability) of the relative radar cross-section in dB are given. The number of measurements is given in brackets. The majority of the transponder measurements are for IW mode reflecting the S1-B planning over land. The radiometric accuracies are close to zero and good stabilities.

SM	IW
-0.19±0.38 (160)	-0.12±0.23 (428)

Table 27: SLC Relative Radar Cross-Section for the DLR transponders (dB)

The following results are also for the DLR transponders but are separated by polarisation. Figure 65 and Table 28 give the results for SM mode - the relative radar cross-sections indicate a reasonable radiometric calibration.

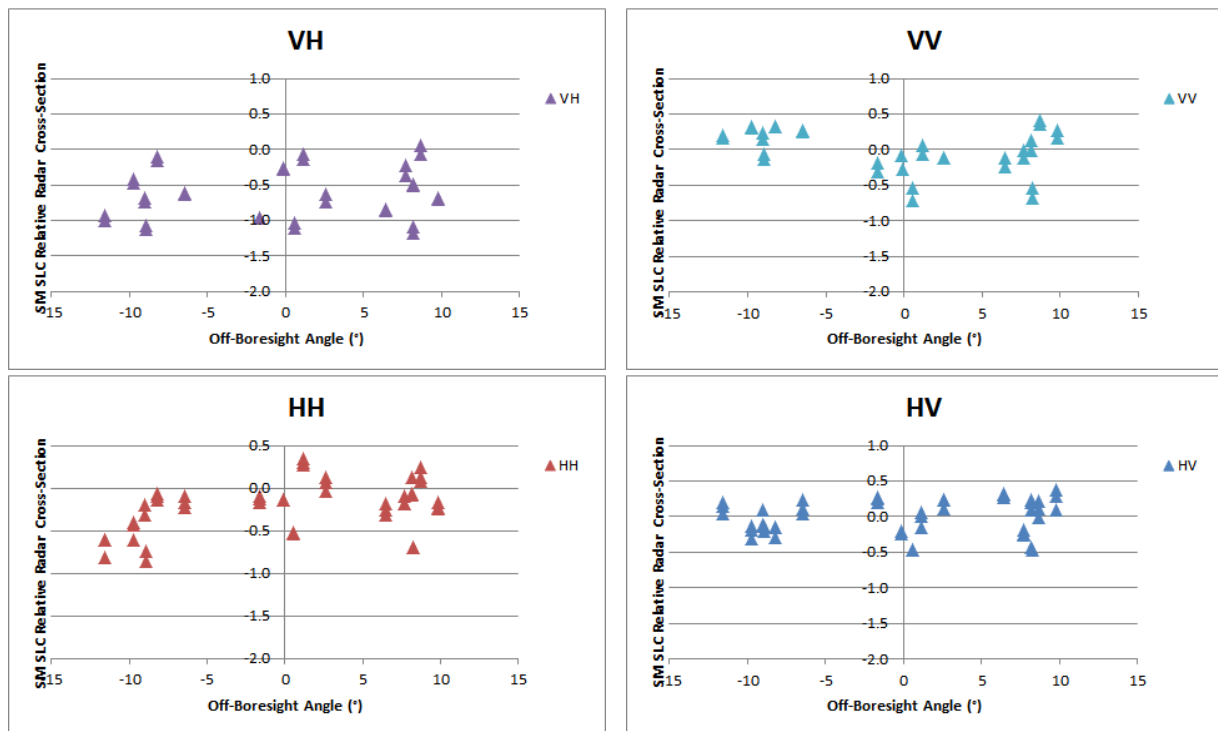


Figure 65: SM SLC Relative Radar Cross-Section for the DLR transponders

	VH	VV	HH	HV
S1	-0.83±0.31 (6)	0.13±0.19 (6)	-0.63±0.17 (8)	-0.07±0.18 (8)
S2	-0.49±0.28 (6)	0.26±0.07 (6)	-0.16±0.08 (8)	-0.03±0.18 (8)



S3	-0.77±0.39 (6)	-0.35±0.24 (6)	-0.25±0.20 (7)	-0.09±0.33 (7)
S4	-0.39±0.34 (4)	-0.06±0.08 (4)	0.18±0.15 (6)	0.08±0.15 (6)
S5	-0.76±0.38 (6)	-0.28±0.26 (6)	-0.32±0.24 (8)	-0.08±0.33 (8)
S6	-0.40±0.32 (6)	0.22±0.16 (6)	-0.02±0.17 (9)	0.18±0.12 (9)

Table 28: SM SLC Relative Radar Cross-Section for the DLR transponders (dB)

The IW results below indicate a good radiometric calibration with many mean relative radar cross-section values close to zero (the radiometric accuracy) and a standard deviation of typically 0.3dB (the radiometric stability). The differences between polarisations are also small (see also Section 7.1.4.1).

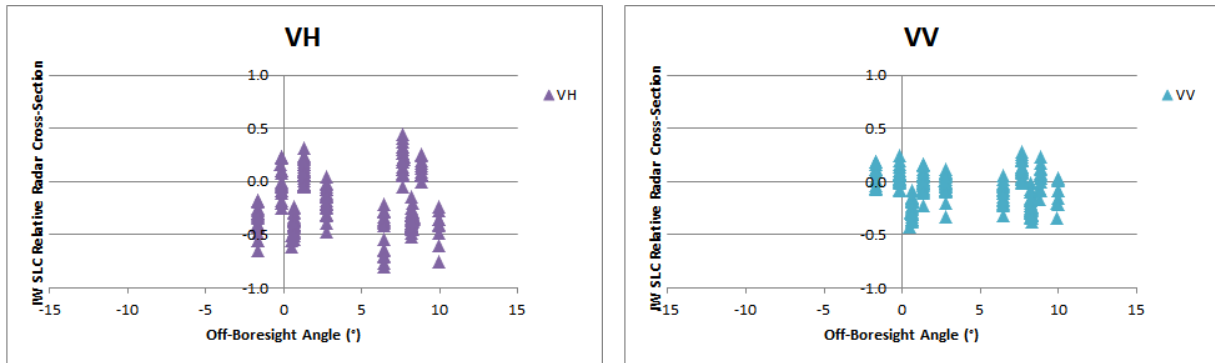


Figure 66: IW SLC Relative Radar Cross-Section for the DLR transponders

	VH	VV	HH	HV
IW	-0.19±0.27 (214)	-0.06±0.16 (214)	No measurements	No measurements

Table 29: IW SLC Relative Radar Cross-Section for the DLR transponders (dB)

	IW1	IW2	IW3
VH	-0.18±0.25 (95)	-0.31±0.22 (40)	-0.14±0.29 (79)
VV	-0.04±0.16 (95)	-0.06±0.22 (40)	-0.08±0.18 (79)

Table 30: IW SLC Relative Radar Cross-Section for the DLR transponders (dB)

The radiometric calibration results using the DLR Transponders and the BAE Corner Reflector for IW SLC products are shown in Figure 67 from imagery acquired during 2017. The derived relative radar cross-section for the DLR transponders during the same period is -0.12±0.23dB while from the BAE corner reflector is -0.26±0.17dB.

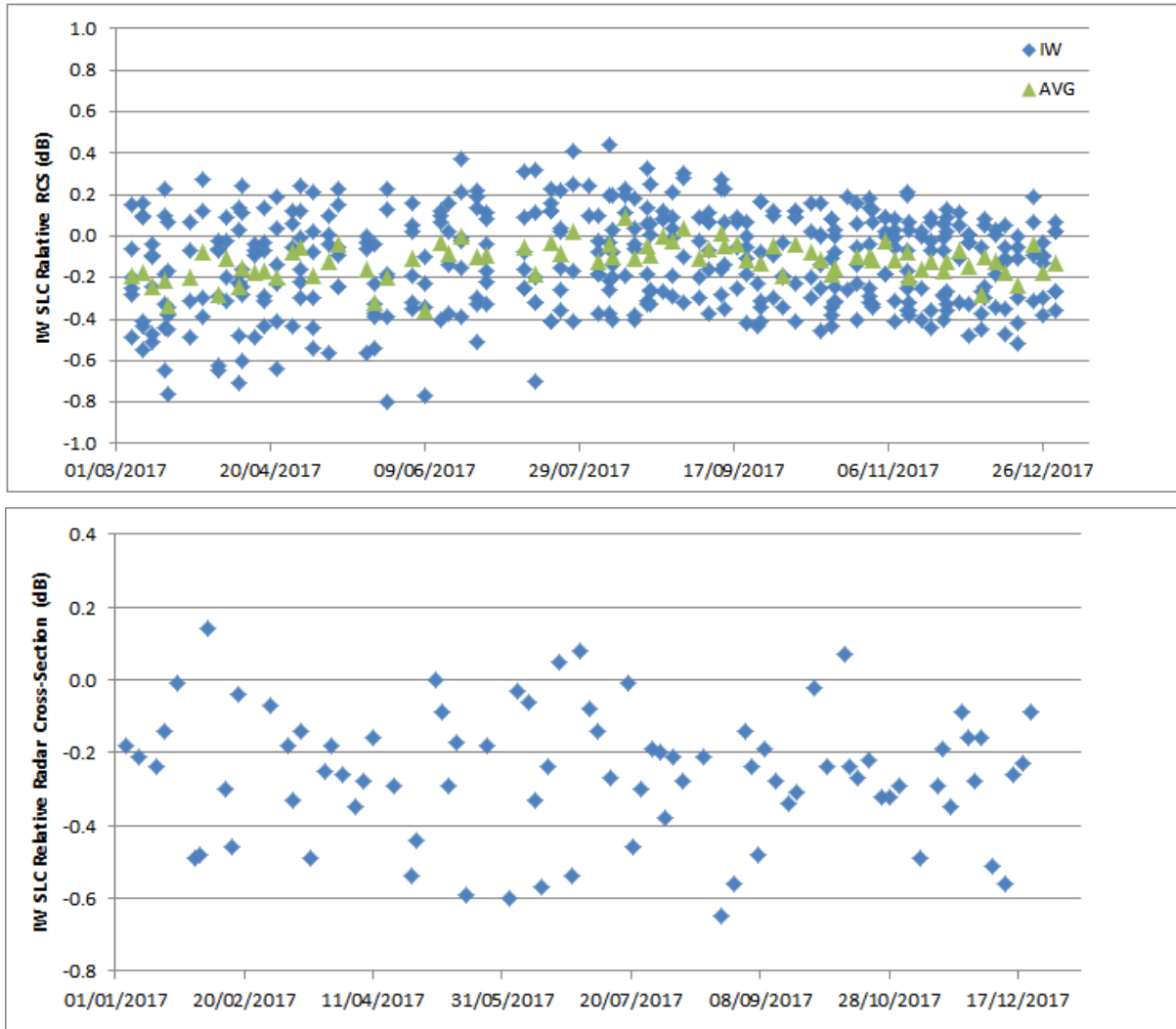


Figure 67: IW SLC Relative Radar Cross-Section for the DLR Transponders and the BAE Corner Reflector

An array of 40 corner reflectors has been deployed near Brisbane, Australia as a component of the Australian Geophysical Observing System (AGOS) - see [S1-RD-04] for further details. The CRs are size 1.5m (34), 2.0m (3) and 2.5m (3) with fixed orientations. Given that these corner reflectors have a fixed elevation and azimuth orientation they will not be pointing directly at S-1B. However, for IW acquisitions the reduction in radar cross-section compared to the case of a perfect orientation is small at less than 0.05dB. Table 31 gives the radiometric accuracy and stability for all corner reflector measurements during 2017 together with results for IW1 and IW2 sub-swaths and for HH polarisation (there were no VV acquisitions). The numbers in brackets refer to the number of measurements. The results indicate an accuracy close to zero, while the stability is less than 0.5dB.

All	IW1	IW2	IW1 HH	IW2 HH
0.09±0.47 (690)	0.16±0.42 (413)	-0.01±0.51 (277)	0.16±0.42 (413)	-0.01±0.51 (277)

Table 31: IW SLC Relative Radar Cross-Section for the Australian Corner Reflectors (dB)



7.1.2.2. Permanent Scatter Calibration

The following figure shows a recent S-1B IW VV Permanent Scatter Calibration series over Paris. The series covers the period from September 2016 (end of the Commissioning Phase) to the end of 2017. The S-1B PS calibration constant time series is stable during the whole monitored period.

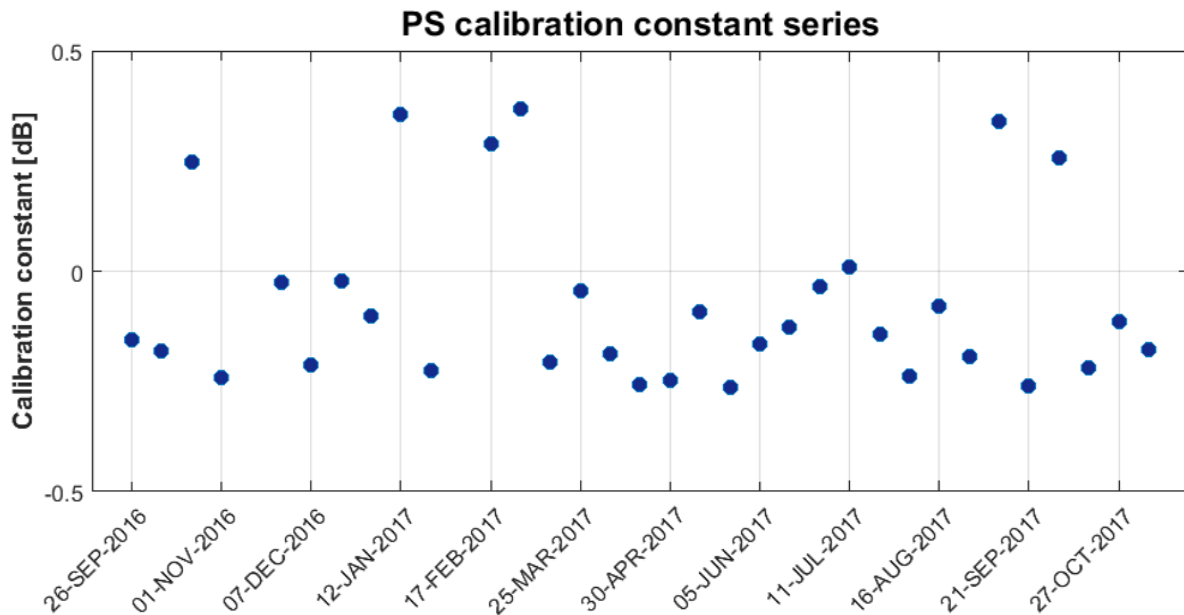


Figure 68: S-1B Permanent Scatter Calibration time series for TopSAR IW over Paris.

7.1.3. Geometric Validation

S-1B geolocation quality was monitored regularly throughout 2017 using IW SLC products. However, SM and EW SLC products acquired during 2016 S-1B commissioning campaign were re-analysed after correction for significant, new timing biases were implemented in post-processing. The trihedral corner reflectors (CRs) whose positions had been installed and surveyed with cm-level accuracy at the Swiss test sites *Torny-le-Grand* and *Dübendorf* during S1-B commissioning continued to serve as reference targets in 2017.

Geolocation estimates were made according to the steps described in section 5.1.3. In particular, the burst-dependent range bias (for TOPS products) and updated bulk bistatic corrections represented the most important post-processing improvements in 2017.

The geolocation and post-processing steps described for S-1A in section 5.1.3 were run separately for S-1B, with the results shown in Figure 69. As a time series dating back to the S-1B launch is available, all the data are shown, and separated by year. The ALE plots in Figure 69 indicate that given bias compensations, the localisation performance was much better than the original requirements (according to sections 5.5.2.1 and 5.5.2.2 in [S1-RD-09]). A method for integrating azimuth bias compensation annotations in the IPF is under study.

Figure 70 contrasts the previous and current best ALE estimates for SM, IW and EW mode SLC products. Some indication of beam-specific grouping can be seen in the previous-best SM SLC plot shown in Figure 70(a); this grouping has been eliminated in (b), which shows the current SM SLC ALE plot. Although the mean range offset is small (-2.4 cm), it is not exactly zero even though the official SWST bias was applied during geolocation estimation. This is partly due to improvements made to the atmospheric path delay model *after* the original SWST bias estimate had been incorporated into the IPF. As a result, the slant range estimates for the targets in Figure 70(b) products changed, corresponding to an updated range ALE. Two distinct azimuth outliers remain; it is not known if these represent real anomalies or a true (possibly intermittent) processor or post-processing effect, especially as relatively few SM acquisitions were available.



Affecting both IW and EW products, the clear sub-swath grouping (visible in (c) and (e)) was the most significant improvement in 2017. The previous and current S-1B IW SLC plots are shown in Figure 70(c) and (d). A similar comparison may be seen in Figure 70(e) and (f) for EW SLC products. Although the measurement noise was higher and fewer products exist than for IW mode, a clear improvement was observed here as well.

The ALE plots in Figure 70 indicate that given bias compensations, the localisation performance was much better than the original requirements (according to sections 5.5.2.1 and 5.5.2.2 in [S1-RD-09]).

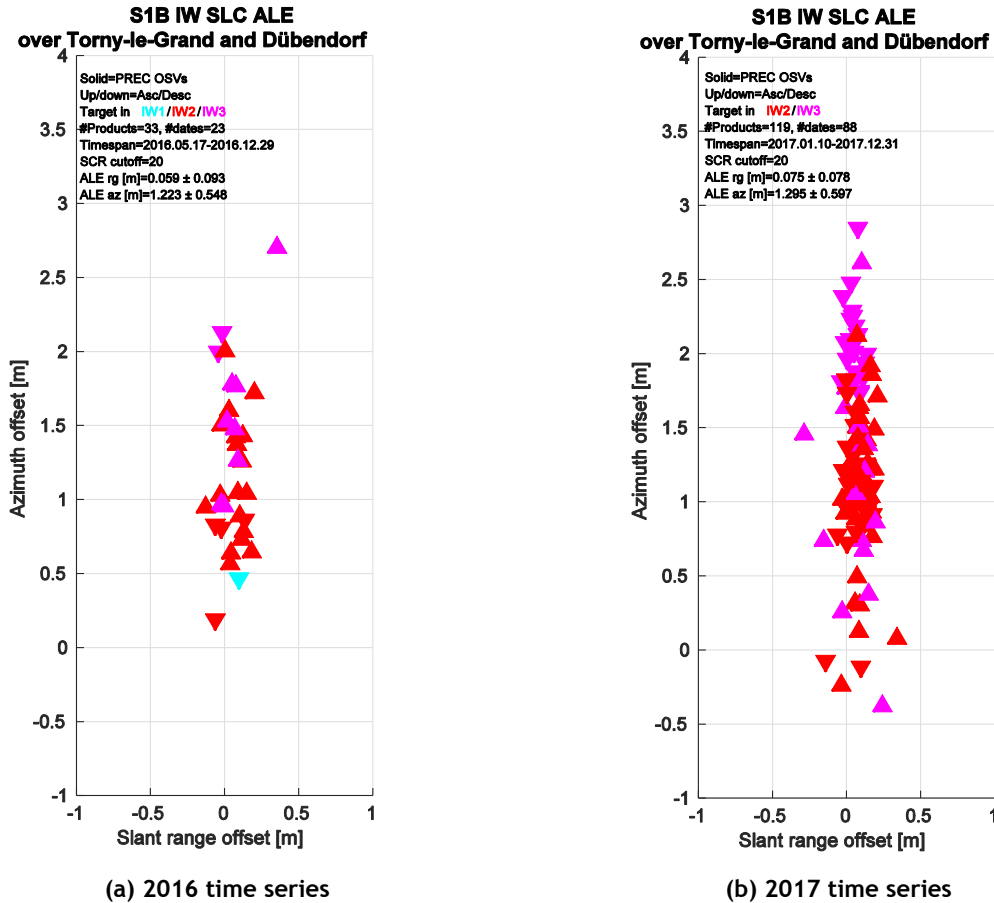
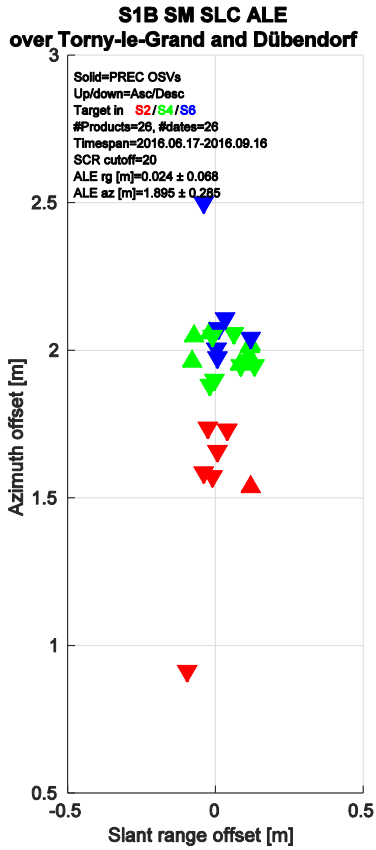
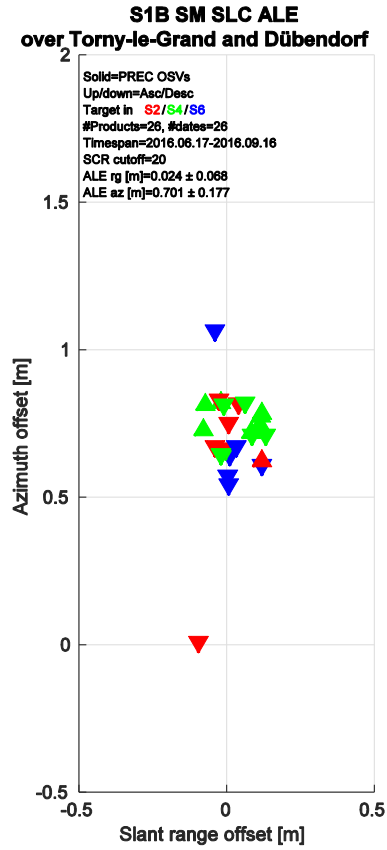


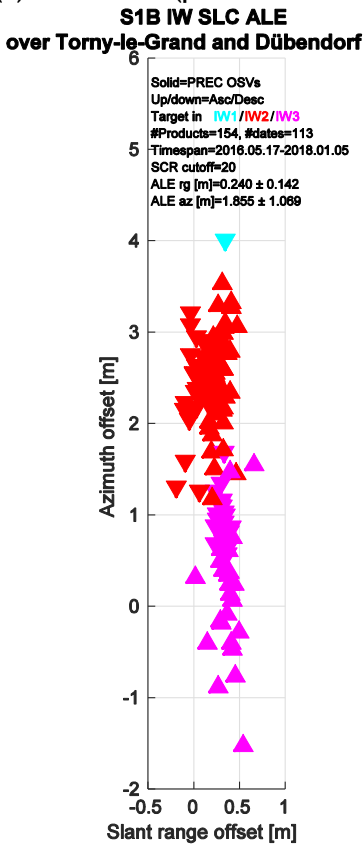
Figure 69: ALE estimates for S-1B IW SLC product time series acquired over the Swiss test sites using precise state vectors (AUX_POEORB). (a) products acquired in 2016; (b) products acquired in 2017. Product date ranges are shown in the figure inset. Point colours represent beam/subswath.



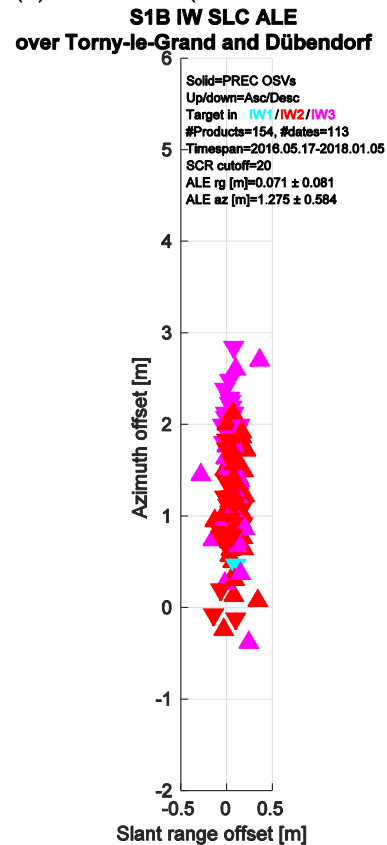
(a) S-1B SM SLC (previous ALE scatter)



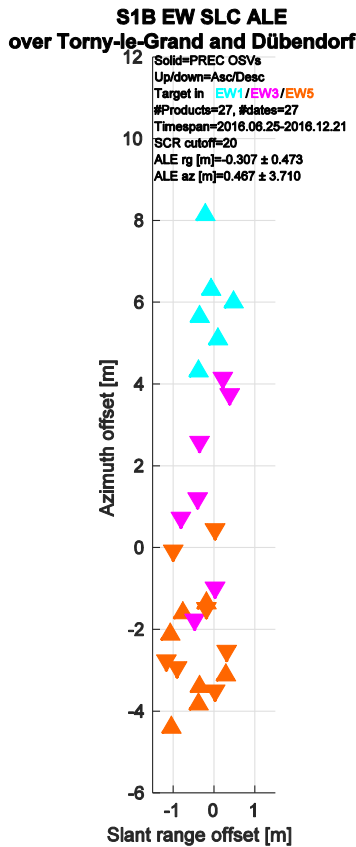
(b) S-1BSM SLC (current ALE scatter)



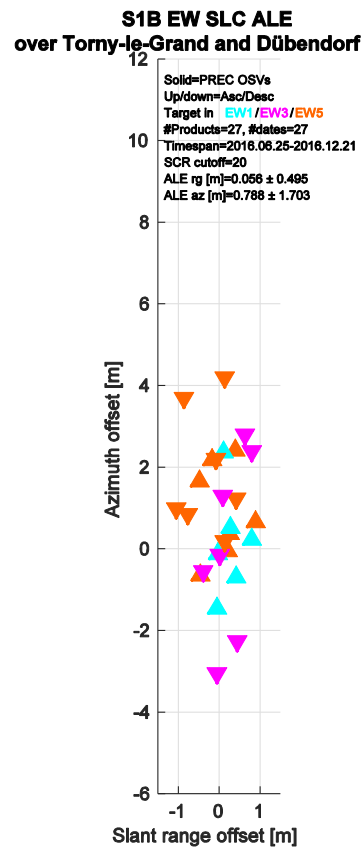
(c) S-1BIW SLC (previous ALE scatter)



(d) S-1B IW SLC (current ALE scatter)



(e) S-1B EW SLC (previous ALE scatter)



(f) S-1BEW SLC (current ALE scatter)

Figure 70: ALE estimates for S-1B StripMap (SM), IW and EW SLC product time series acquired over the Swiss test sites using precise state vectors (AUX_POEORB). The left column shows ALE using previous post-processing methods; the right column shows more recent results after improved post-processing. Product date ranges are annotated in the figure inset text (N.B. no new S-1B SM or EW acquisitions were made over Switzerland in 2017; they are shown here to highlight the improved post-processing). Point colours represent beam/subswath. The S-1B SWST (range) bias (output of the respective commissioning and calibration phases) was applied in all cases.

7.1.4. Polarimetric Calibration

7.1.4.1. Gain Imbalance

The DLR transponders and acquisitions during 2017 have been used to calculate the gain imbalance (the difference in radar cross-section between the two polarisations of dual polarisation products). Table 32 give a summary of the gain imbalance for the SM and IW modes.

	Gain Imbalance (dB)
SM	-0.38±0.36 (80)
IW	-0.13±0.20 (214)

Table 32: Gain Imbalance using the DLR transponders



The following results show the gain imbalance split between the two possible polarisations of VH/VV and HH/HV. Figure 71 and Table 33 give the gain imbalance for SM & IW modes.

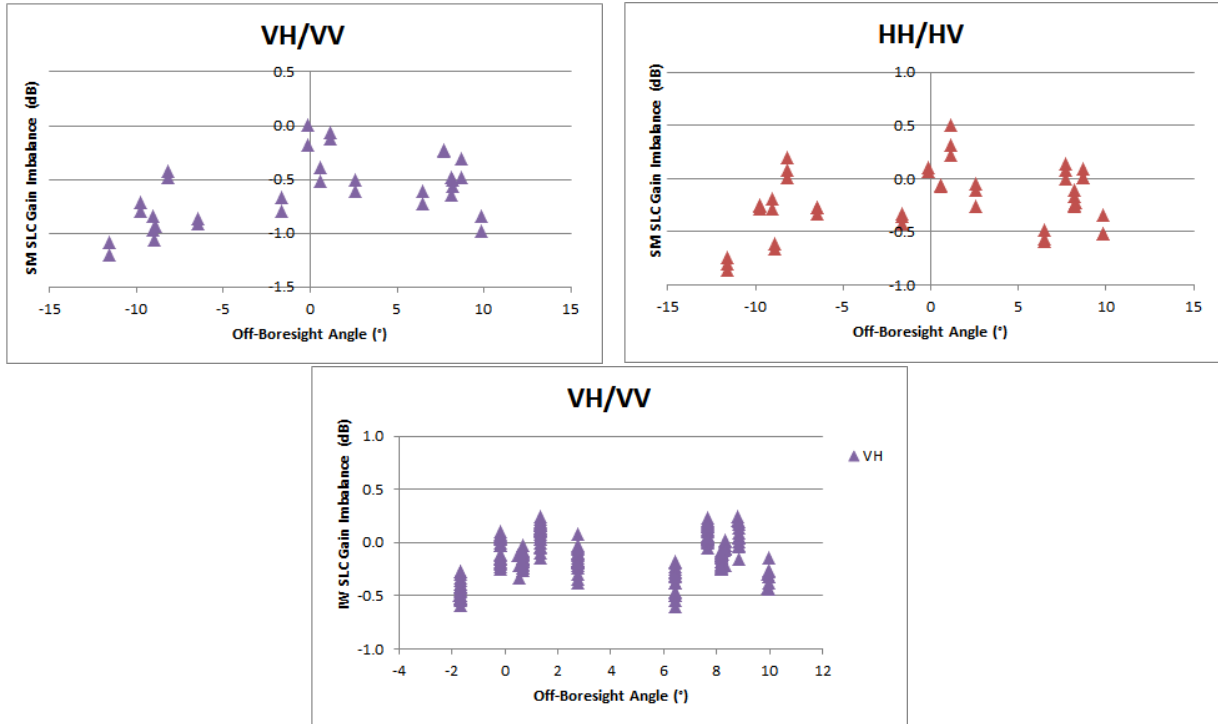


Figure 71: Gain Imbalance using the DLR transponders.

	VH/VV	HV/HH
SM	-0.61±0.31 (34)	-0.21±0.30 (46)
IW	-0.13±0.20 (214)	

Table 33: Gain Imbalance using the DLR transponders

7.1.4.2. Phase Imbalance

The DLR transponders have been used to calculate the phase imbalance (the difference in peak phase between the two polarisations of dual polarisation products). Figure 72 and Table 34 give the gain imbalance for SM, IW and EW for acquisitions start of the routine phase in September 2016. As expected the phase difference is close to zero.

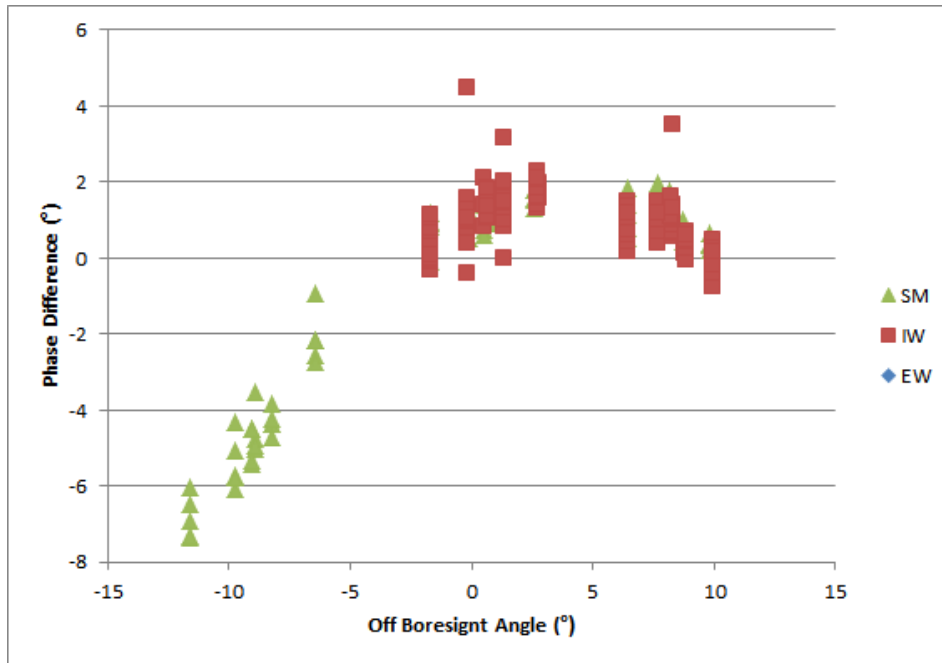


Figure 72: Phase Imbalance using the DLR transponders.

	Phase Difference (°)
SM	-0.95±2.93 (80)
IW	1.03±0.66 (214)

Table 34: Phase Imbalance using the DLR transponders

7.1.4.3. Coregistration

The DLR transponders both provide an impulse response in both polarisations of dual polarisation imagery which enables coregistration to be performed between the two polarisation images. Table 16 below shows that the average measured polarimetric co-registration derived from SLC products acquired during 2017 is very small (the IRF peak position is measured to a 1/8 of a pixel).

Mode/Swath	Range Co-registration Accuracy (m)	Azimuth Co-registration Accuracy (m)	Number of Measurements
SM	0.01±0.06	0.02±0.09	160
IW	0.00±0.03	0.11±0.42	428

Table 35: SLC Polarimetric Co-registration

7.1.4.4. Cross-talk

The DLR corner reflectors enable the S1-A cross-talk to be measured since they provide an impulse response in only one polarisation (HH or VV) of dual polarisation imagery. Table 15 gives the IW cross-talk derived using SLC products - the measured cross-talk is acceptably low.

Corner Reflector Cross-talk (dB)	Number of Measurements
-40.4±3.5	8



Table 36: Cross-talk Measurements

7.1.5. Elevation Antenna Patterns

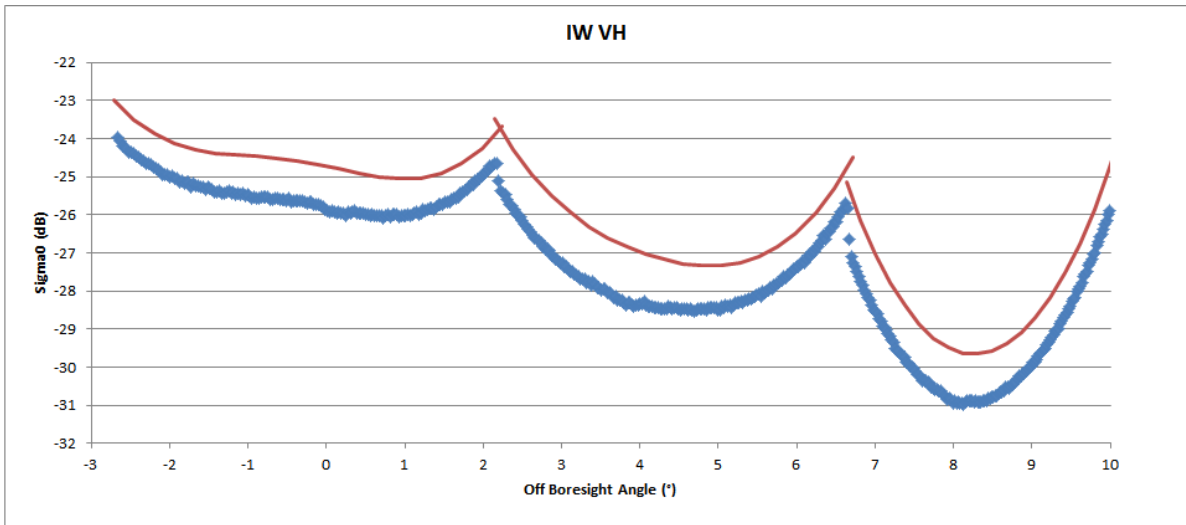
No new S-1B elevation antenna patterns were derived during 2017.

7.1.6. Azimuth Antenna Patterns

There were no updates to the S-1B azimuth antenna patterns during 2017.

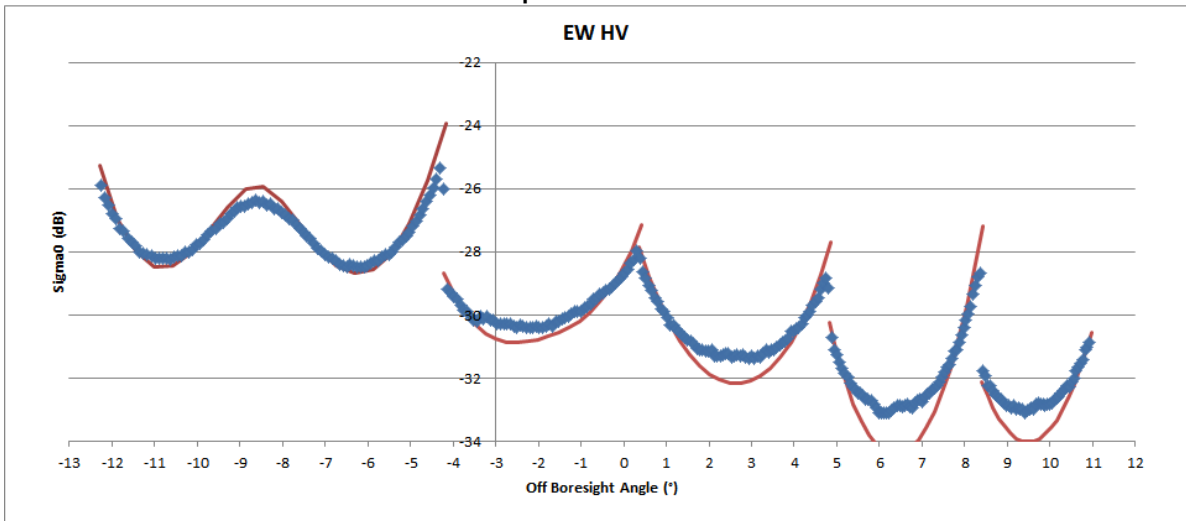
7.1.7. Noise Equivalent Radar Cross-section

S-1B imagery with low ocean backscatter can be used to estimate the Noise Equivalent Radar Cross-section (NESZ). In Figure 73 and Figure 74 show example NESZ measurements for IW and EW mode derived from data acquired in 2017. The requirement that the NESZ should be below -22 dB is met at all sub-swaths. For IW the measurements are slightly better than the prediction (red curves) while for EW the measurements are slightly worse than the prediction.



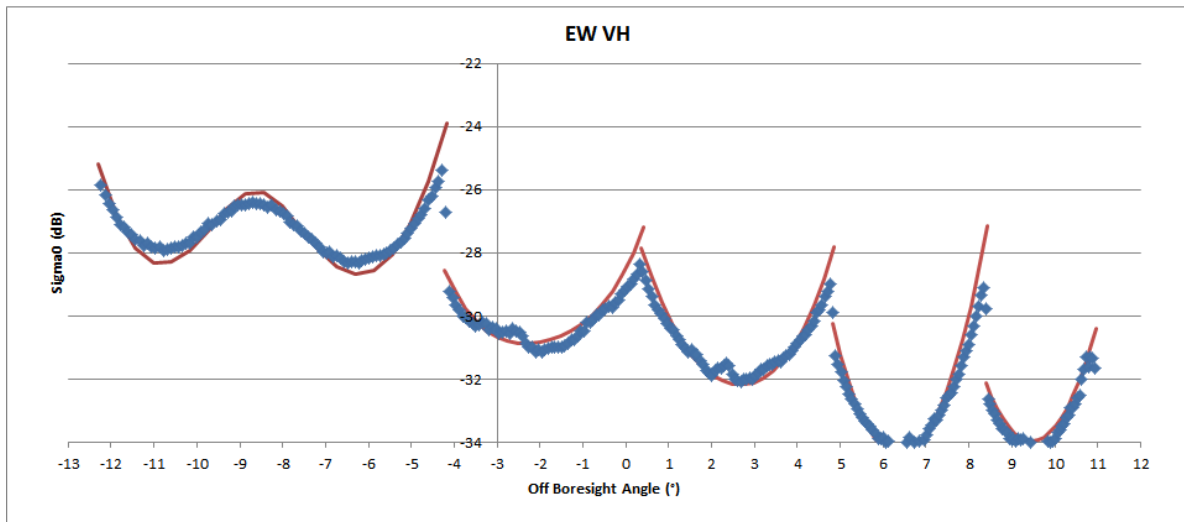
S1B_IW_GRDH_1SDV_20170515T005135_20170515T005200_005602_009D01_605D.SAFE

Figure 73: NESZ measures for IW. Blue is the measured NESZ and the red lines are the predicted NESZ.





S1B_EW_GRDH_1SDH_20170819T005101_20170819T005205_007002_00C560_59FF.SAFE



S1B_EW_GRDH_1SDV_20170608T005106_20170608T005210_005952_00A716_2B30.SAFE

Figure 74: NESZ measures for EW. Blue is the measured NESZ and the red lines are the predicted NESZ.

7.1.8. Interferometric performances

The interferometric performances, and in particular the coherence level of an interferogram between two S-1 images, depend on several factors including:

- Stability of the imaged scene (temporal coherence)
- Thermal noise level of the considered acquisitions (see section 5.1.7)
- Volumetric decorrelation due to different acquisition geometry (orbit baseline)
- Stability of the sensor pointing to ensure Doppler spectrum overlap
- Synchronization of the acquisitions (for TOPSAR modes only)

The S-1B performances related to the last three points are reported in the next sections.

7.1.8.1. S-1B Orbit Baseline

Repeat pass interferometry requires that acquisitions at different times are performed with a similar orbit to ensure high coherence interferograms. The “distance” between the orbits of a pair of interferometric acquisition is called interferometric baseline. The interferometric baseline is continuously monitored by the PDGS OBS tool, which compares the S-1B orbits with an arbitrary selected reference cycle (for S-1B it's cycle number 39, 16- 28 May 2017).

Figure 75 shows the three interferometric baseline components (Parallel on top, Normal in the mid and Along-Track on the bottom) evolution during 2017. The hot colours represent the maximum baseline value and the cold colours represent the minimum baseline value measured for each orbit. The different colours represent the track number evolving for each cycle from 1 to 175.

The most critical baseline component for the interferometric coherence is the normal one, which shall be lower than a certain threshold named critical baseline (about 5 km for S-1 and depending on the considered swath). The measured normal baseline (mid plot) shows that the worst case coherence loss due to the interferometric baseline is always well below 5%.

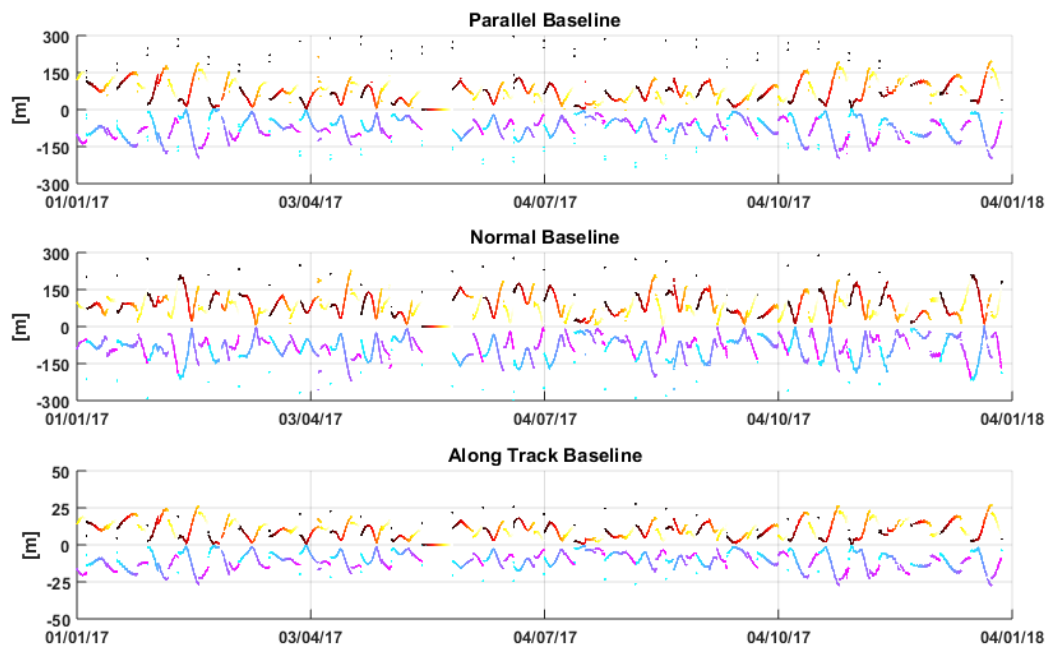


Figure 75: Parallel (top) Normal (mid) and Along-Track (bottom) interferometric baseline during 2017. The hot colours represent the maximum value and the cold colours represent the minimum value for each orbit. The colours represent the track number.

7.1.8.2. Instrument Pointing

The instrument pointing is continuously monitored exploiting the attitude quaternions annotated in the SAR packets and the DC estimates from the data. The annotated attitude shows very small deviations w.r.t. the nominal attitude (Total Zero Doppler + Roll Steering) and does not allow predicting the short term fluctuations of the DC estimates from the data as required for some L2 applications. This is related to the working of the on-board attitude control system (AOCS). An optimization of AOCS has been performed for S-1B during 2017 (details are reported below).

Figure 76 shows the average S-1B Doppler Centroid evolution during 2017 on a slice basis (dots) and on a daily basis (red line). The reported values are in line with expected S-1B pointing performances. The dashed vertical line represents the STTs configuration changes occurred in the reporting period.

During 2017 a few STTs characterization campaign (purple dashed vertical lines) were performed. During such campaigns STTs configuration are alternated, in order to better characterize STTs working. The final goal of the campaigns was the implementation of a couple of attitude patches to improve the S-1B pointing. In particular, the patches were aimed at reducing the difference between the DC estimated from the data and the DC estimated exploiting geometric information annotated in the SAR packets.

The applied patches were:

- Enabling of the on-board correction of the relativistic aberration correction to remove orbital trends in DC and roll pointing. The patch was applied on the 16th November (1st green dashed vertical line)
- Improvement of the on-board AOCS filter gains used for real time attitude estimation and correction. The patch was applied on the 28th November (2nd green dashed vertical line)



Figure 77 shows on the left a comparison between the data DC estimates vs. ANX time during three different periods: the blue dots refer to September 2017 before attitude patches application, the red dots refer to the period after the relativistic aberration patch application and the yellow dots refer to the period after new AOCs filter gains application. The DC values refer to STT 1+2 configuration but similar results have been obtained for the remaining configurations. Table 37 lists the results of the data DC analysis during patches application. A clear reduction of the DC standard deviation can be observed. The attitude patches will be applied to S-1A during 2018.

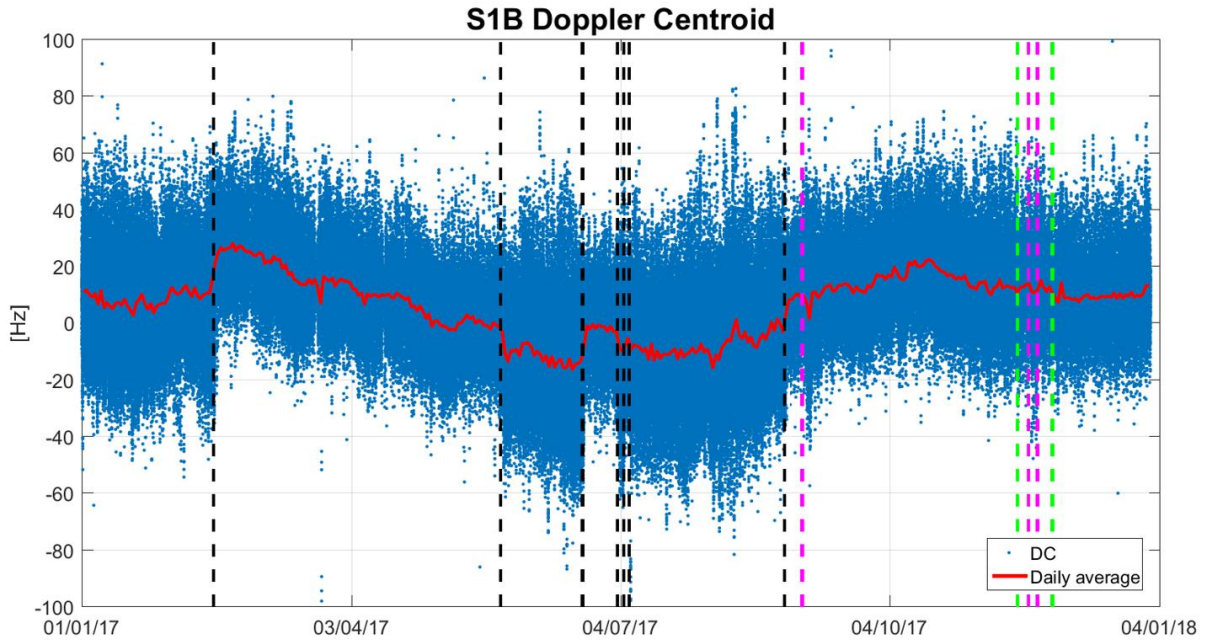


Figure 76: Doppler Centroid versus time. Average on a data-take basis (dots) and daily average (red line). The star-trackers reconfigurations events are marked by the vertical black lines.

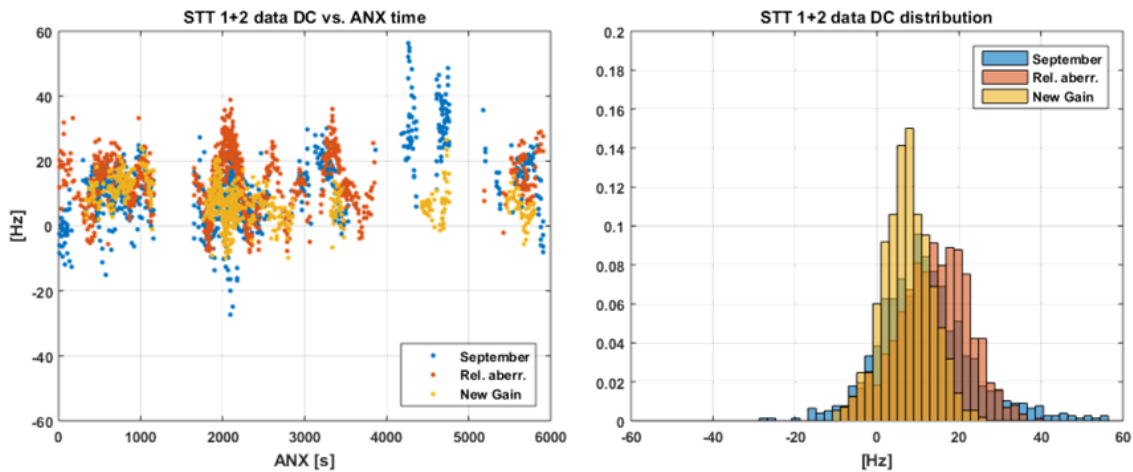


Figure 77: (Left) Doppler Centroid versus ANX time during three different periods: blue before attitude patches application, red after relativistic aberration patch application and yellow after new AOCs filter gains application. (Right) Histogram of the DC estimates (same colour code).



	Start (UTC)	Stop (UTC)	# slices	μ [Hz]	σ [Hz]
September	4 th Sept. 09:36	5 th Sept. 15:07	783	11.8	11.5
Patch #1	20 th Nov. 08:59	21 st Nov. 09:40	877	13.8	8.7
Patch #2	28 th Nov. 11:16	29 th Nov. 08:38	566	7.4	6.0

Table 37: Results of data DC analysis after attitude patches application.

7.1.8.3. S-1B Burst synchronization

The burst synchronization between repeat pass interferometric acquisitions is relevant for the TOPSAR modes (IW and EW), to provide an indication of the quality of the interferometric phase that can be expected. The SAR acquisition start time is planned over a discrete set of points round orbit with precision down to milliseconds. The performance of the synchronization is monitored by the PDGS OBS tool.

Figure 78 shows the burst synchronization error over time for IW and EW mode, considering as reference cycle number 39 (16- 28 May 2017). The reference cycle has been updated during 2017 to maximize the number of ground control points. The colour of the dots represents the number of repeat pass acquisitions falling in a certain temporal and burst synchronization interval (light blue meaning few points and purple meaning many points).

The daily average synchronization is reported with a continuous black line. It can be noticed that the average synchronization is always very good with a small seasonal trend (less than 5 ms peak to peak). A similar trend can be observed also for S-1A burst synchronization (see Figure 28 section 5.1.8.2) suggesting a common origin due to some long-term orbit perturbation.

The black dashed lines represent the S-1 synchronization requirement (about ± 7 ms). This value is obtained starting from the timing requirement for single acquisitions (5 ms) and multiplying it by $\sqrt{2}$ due to the fact that all the values in the image are obtained by combining the timing error two independent acquisitions. The synchronization performance is quite good with 98.3% of IW acquisitions and 97.1% of EW acquisitions being better than the timing requirement.

A strange pattern can be observed in the S-1B burst synchronization, which seems to be better in the period between March and September. The reason of this behaviour is currently under investigation.

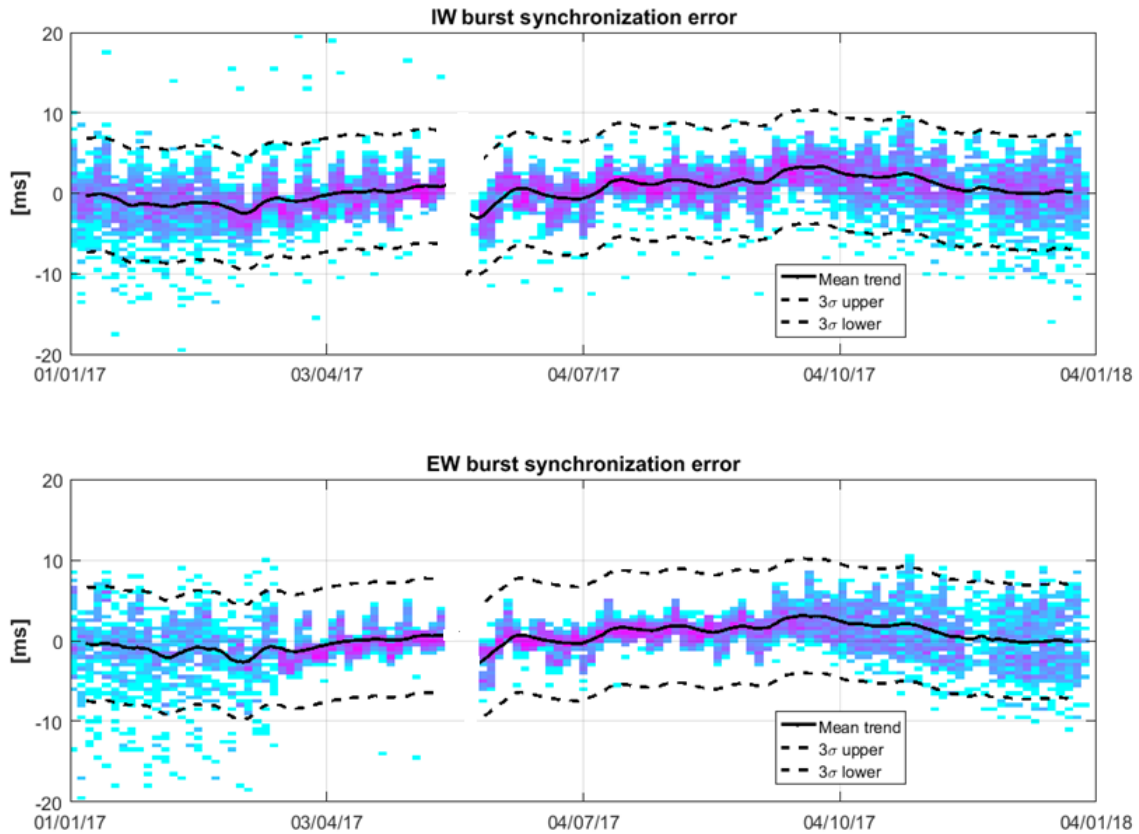
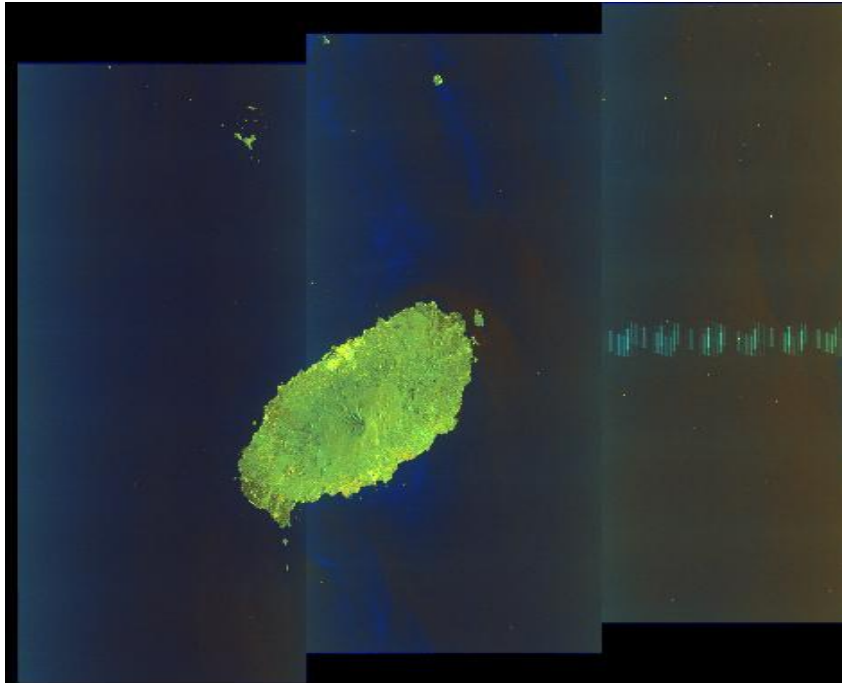


Figure 78: S-1B burst synchronization during 2017.

7.1.9. Summary of Anomalies

7.1.9.1. Radio Frequency Interference

As observed for S-1A, a small percentage of S-1B imagery is affected by the presence of Radio Frequency Interference from the ground. An example is shown below from just south of South Korea. Usually RFI only affects a few range lines of raw data.



S1B_IW_SLC__1SDV_20170829T213231_20170829T213252_007160_00C9E7_51A5.SAFE

Figure 79: An example of Radio Frequency Interference

7.1.9.2. Radarsat-2/Sentinel1-A Mutual Interference

Also as observed for S-1A, a small percentage of S-1B imagery is affected by mutual interference between S-1B and Radarsat-2. One further example of such mutual interference occurred during 2017 as indicated in Table 38 and shown in Figure 32. More details and examples could be also found in a specific technical note on Sentinel-1 RadarSat-2 mutual interference (link is provided in Appendix B -)

Satellite	Orbit	Relative Orbit	Acquisition Date	Start Time (UT)	End Time (UT)	Approx. Latitude	Approx. Location
S1-B	5432	156*	3rd May 2017	10:00	10:01	20° S	Bolivia

* Descending Pass

Table 38: S-1B/Radarsat-2 Mutual Interference during 2017

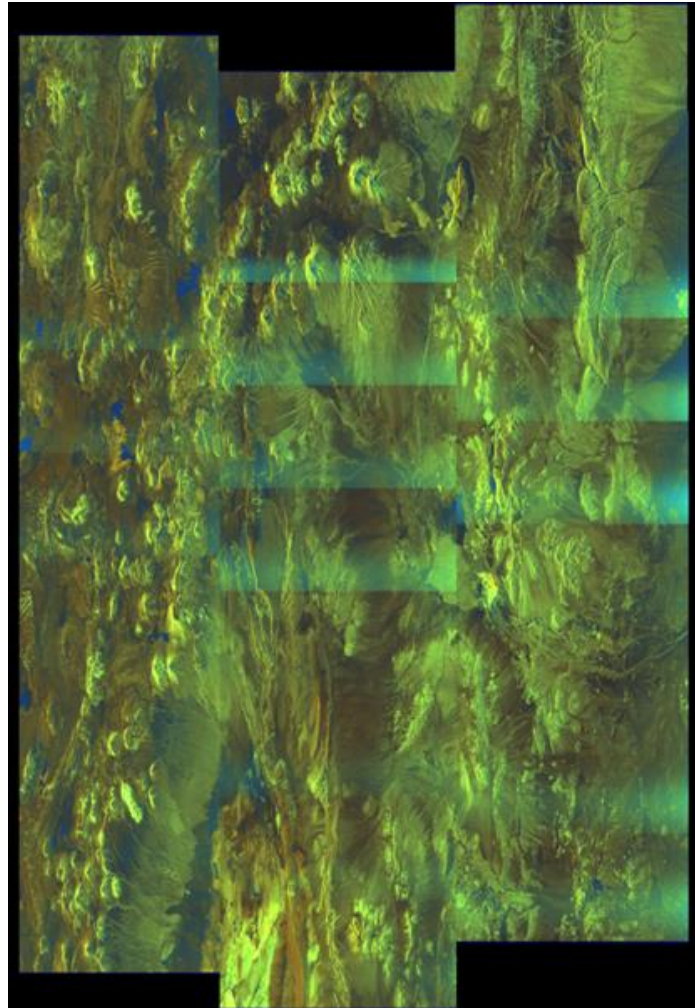


Figure 80: An example of Radarsat-2/Sentinel1-B Interference (3rd May 2017)

7.1.10. Quality Disclaimers

Quality disclaimers issued during 2017 are given in Appendix D -.

7.2. S-1B Level 2 products

7.2.1. Wind measurement

7.2.1.1. Image Mode (SM-IW-EW)

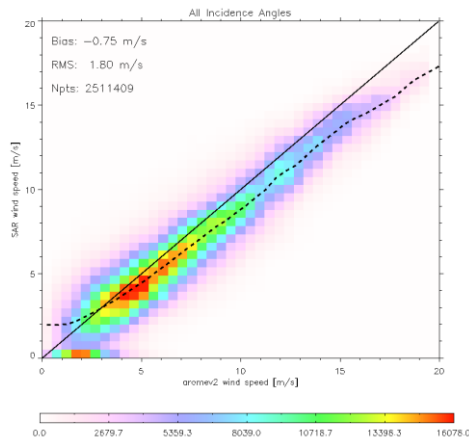
The SAR wind measurement is strongly dependant of the product calibration accuracy. Before the products delivery to the end user, the L1 processing parameters has been optimized in order to improve beam to beam of set, EAP ... It takes benefit from the efforts made on the SAR Level1 products to improve the calibration constant and align the gamma profile as the function of the elevation angle over Rain Forest.

Statement of the wind measurements accuracy:

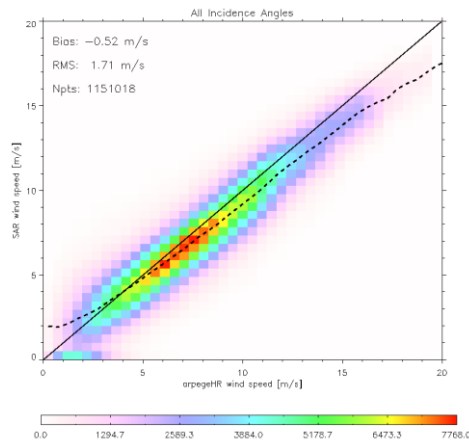
The strategy to assess the accuracy of the wind retrieval is the same as S-1A, consisting in comparing it with an auxiliary wind source (buoys, scaterrometers, atmospherical model...) which is used as a reference.



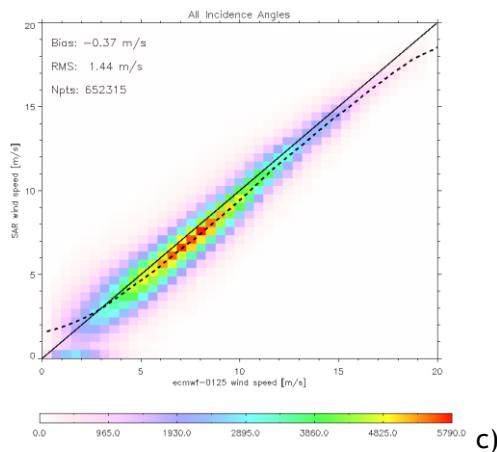
Figure 81 presents the performances achieved on the 3 last months of 2017(October, November, December) for IW mode in VV polarisation of the retrieved wind compared to model references (Arome, Arpege and ECMWF). The statistics are close to the ones observed on S-1A. It can be noticed the strong correlation of the SAR-derived wind speeds with the wind references. The bias and the RMS are less important for ECMWF re-analysis since the wind inversion is based on the ECMWF forecast as an a priori wind input. A nominal RMS of 1.5m/s to 2m/s is observed, which is better than the S1 wind product specification/requirements [AD-02]. A negative bias same is observed due to the choice of the current geophysical model function (GMF) used for the wind retrieval, as mentioned in the S1A paragraph. Same as S1-A, it also appears an over estimation of the number of 0-speed values. The use of another GMF will be investigated in 2018.



a) Arome



b) Arpege HR



c) ECMWF

	bias	Rms
Arome	-0.75	1.80
Arpege	-0.52	1.71
ECMWF	-0.37	1.44

Figure 81: SAR Wind speed compared with reference wind speed for IW mode VV polarisation.

As for S1A, the bias introduced by the GMF seems less important due to NESZ impact (artificially increasing the backscatter, thus the wind retrieval), at high angle of incidence or in HH polarization. Please ref Figure 82

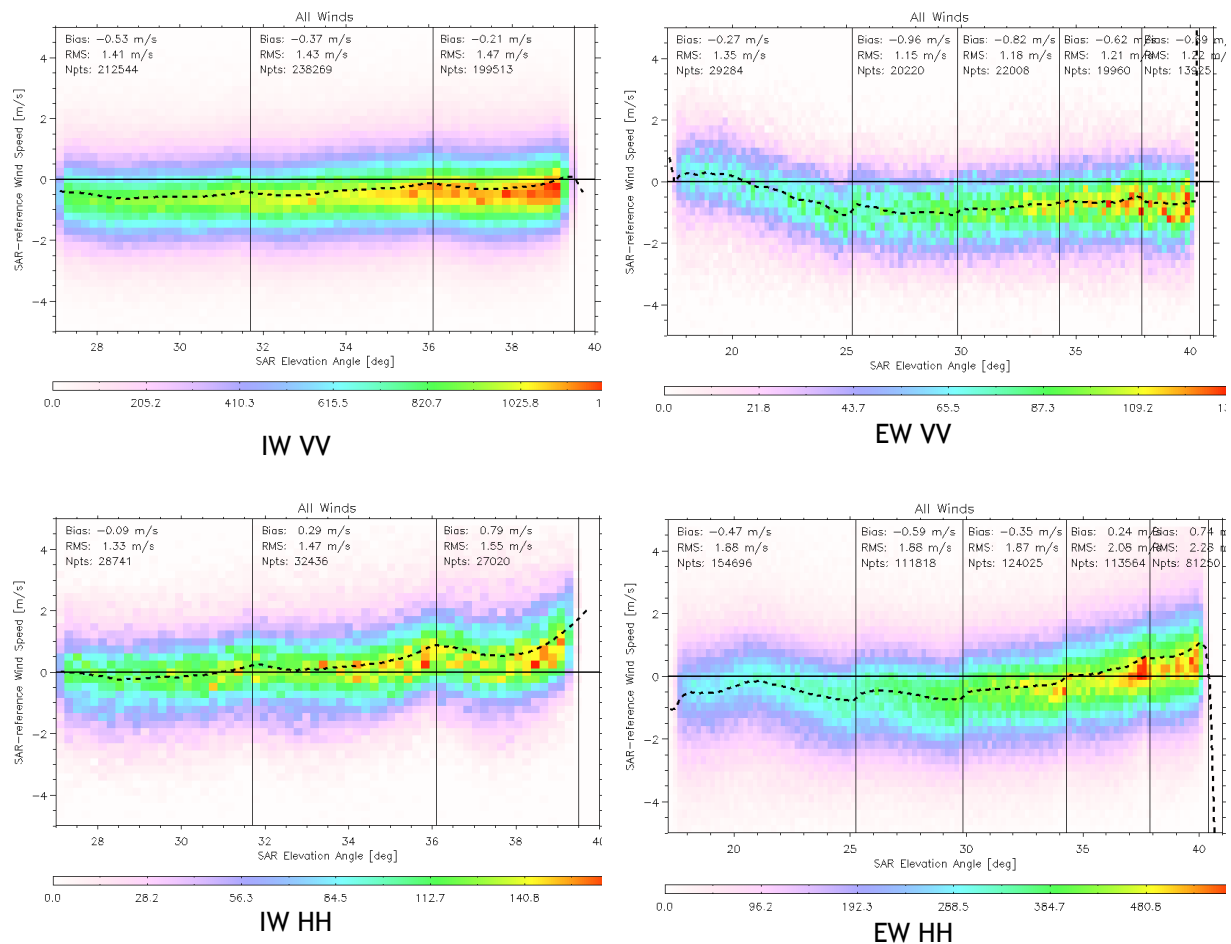


Figure 82: S1B OWI wind speed performance: bias as the function of the elevation angle (noticeable impact of the NESZ at high incidence angle: beam shaped profile)

Improvement performed during 2017:

No changes specific to S-1B have been performed during 2017. The changes, described on the paragraph on the S-1A Wind-measurement assessment, are related to the processor and then are applied on S-1B as well.

Planned Improvements:

No changes specific to S-1B are currently planned. The changes, described on the paragraph on S-1A Wind-measurement improvements, are related to the processor and then will be applied on S-1B as well. Please refer to this section 5.2.1.1 for more details.

7.2.1.2. Wave Mode

In 2017, Sentinel-1B acquisitions in wave mode have been performed at global scale over the oceans in a routine configuration during the whole year. It leads to about 480000 acquisitions (between ~20000 and ~20000 for both WV1 and WV2 each month) of acquisitions every cycle. Please note that during 2017, with IPF 2.84, the variables `oswLandFlag` and `oswLandCoverage` are not correctly filled. A period of 3 months (20/03/2017 to 03/07/2017) has been dedicated to acquisitions in HH polarization. This report focuses only on VV polarisation which is the nominal acquisition mode. The performances obtained for HH polarization will be assessed in a future report.

For level-2 products as measured by Sentinel-1B, the major changes are:



- Update of the processing gains coefficients in October. This mostly impacts performances on ocean surface wind speed (oswWindSpeed), see Figure 84
- Attitude correction STT Aberration Correction and an AOCs Fine Attitude Tuning (proper to S1B): November/December 2017 ; and which has no impact on the product calibration, thus on wind measurement performance (expected impact on RVL, please ref paragraph 7.2.3.1)

Figure 83 shows the monthly performances with respect to time in 2017 for WV1 (left) and WV2 (right). Top panel presents the bias and the standard deviation for the wind speed. Bottom panel presents the number of acquisitions used for this validation. The bias is computed by comparing the wind speed from Sentinel-1 and the wind speed from ECMWF analysis (3 hours and 0.125 degrees). An example for December 2017 is shown on Figure 85. The period with HH measurements is not to consider here. As for Sentinel-1A, significant changes occur in Sept/Oct 2017. The Figure 84 allows seeing in details the impact of IPF upgrade and AUX configuration file change on the wind performances.

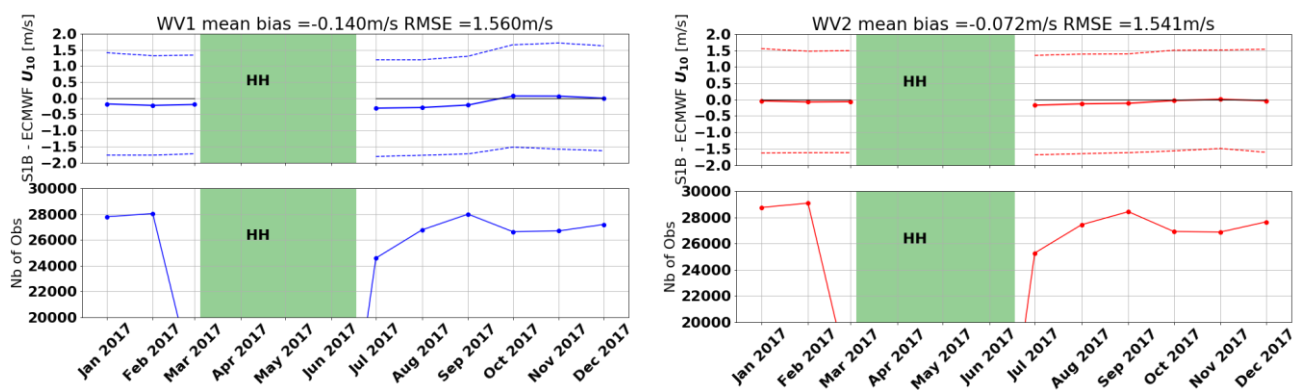


Figure 83: S-1B WV1 and WV2 wind speed performances as function of time. Ocean surface wind monthly performances for WV1 (top-left) and WV2 (top-right) and number of acquisitions co-located to reference data for validation for WV1 (bottom-left) and WV2 (bottom-right). For top panels, coloured thick solid lines stand for the mean difference between Sentinel-1 and ECMWF model wind speeds. Coloured thin solid lines are for standard deviation.

The performances of wind speed for WV1 and WV2 are comparable at the end of 2017, with a consistency with S-1A thanks to ADF upgrade (PP1 in 3rd October 2017)

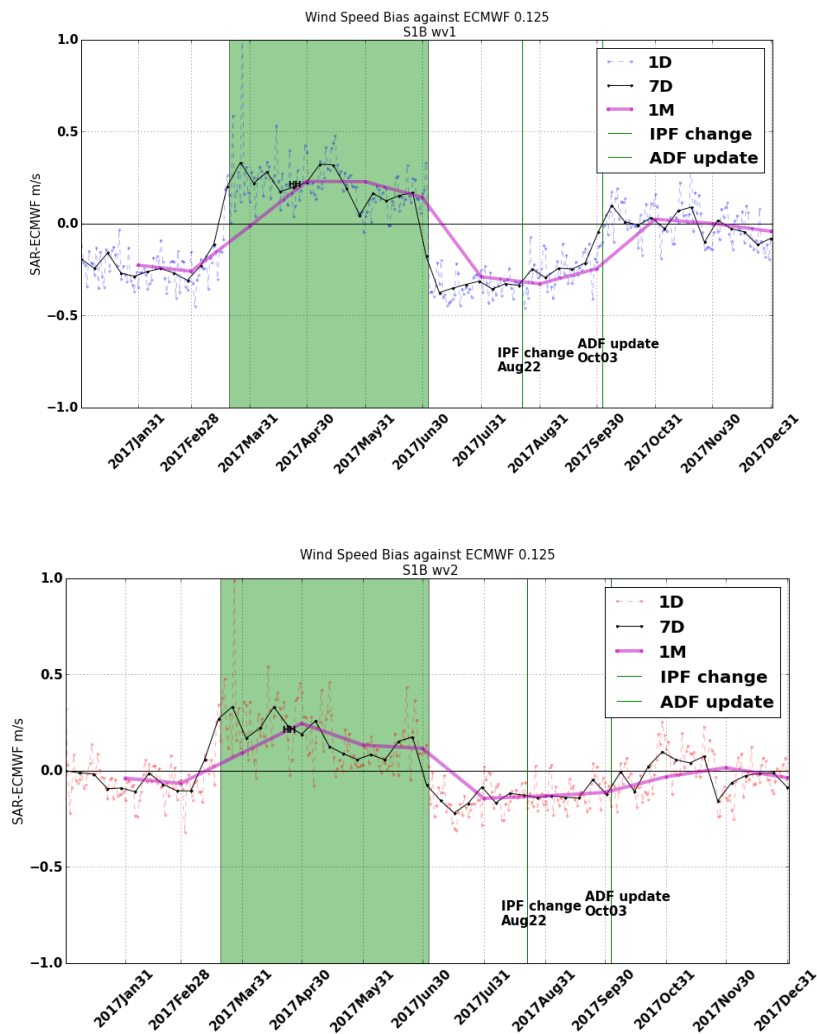


Figure 84: S-1 Wind speed bias evolution for year 2017. Top panel represents WV1 measurements and resp. WV2 on bottom panel. Reference wind speed is ECMWF with a 0.125° resolution and 3-hourly temporal resolution. Dash line is the mean daily bias of OCN WV acquisitions. Black plain line is the 7-day mean and magenta line is the 30-day mean bias. The green vertical lines indicate technical facts linked to performance changes on WV. Green area delineates the period of HH acquisitions.

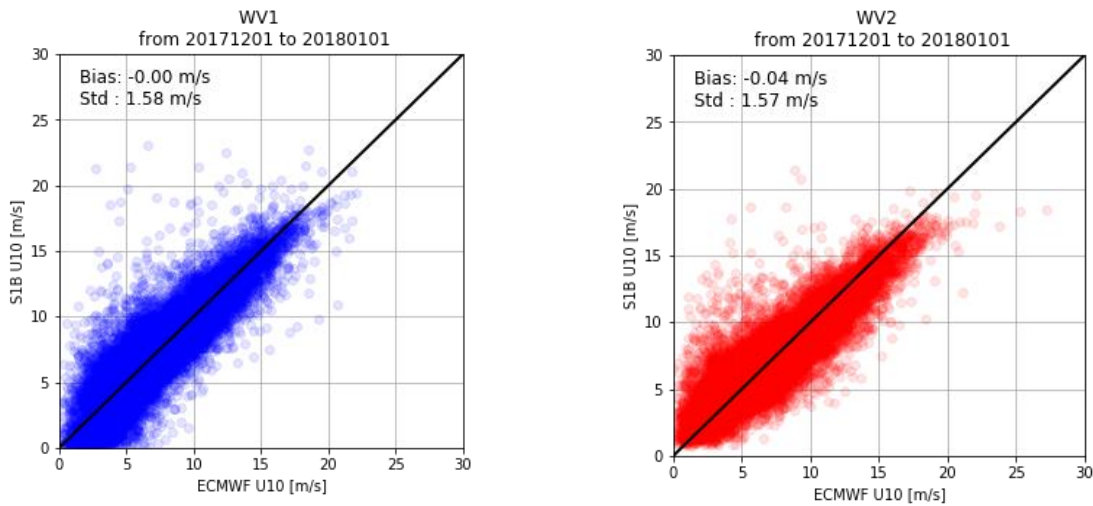


Figure 85: Scatter plot of wind speed from S-1B WV1 versus ECMWF Dec 2017. The model outputs are considered as reference here. This is only valid from a statistical point of view.

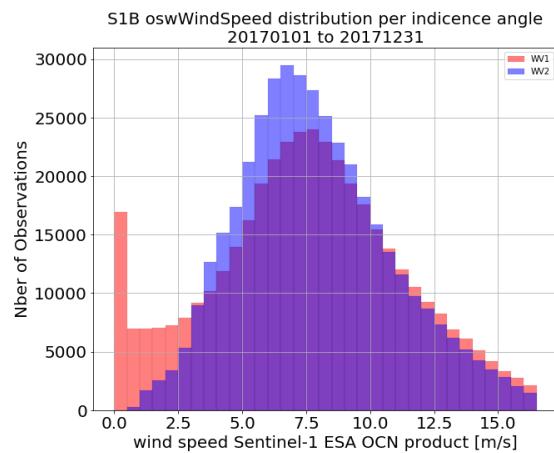


Figure 86: Sentinel-1 oswWindSpeed distribution per incidence angle. Red bars are WV1 and blue ones are WV2.

As shown for S-1A, we observe in Figure 86 the same difference of distribution between WV1 and WV2 at low wind speed. In particular, this figure shows two issues on WV1 distribution, one regarding values of wind speed set to zero and another one with unexpectedly low wind speed between 0 m/s and 2.5 m/s.

Conclusion:

2017 was the first complete year for routine acquisition in Wave mode with Sentinel-1B. However, from 20/03/2017 to 03/07/2017, acquisition have not been done in VV polarization (default acquisition mode), but in HH for scientific purposes (algorithm development). This annual report only deals with the default acquisition mode. The conclusions obtained for VV polarization are the same than for S-1A. For 2017 Sentinel-1B WV1 and WV2 wind speed bias with respect to ECMWF 0.175° are about -0.14 and -0.07 m/s with mean RMSE of about 1.56m/s and 1.54m/s, respectively. Those performances are better than the Sentinel-1 mission requirements for ocean surface wind speed (RMSE<2m/s). In line with Sentinel-1A, there was no modification of the wind inversion in 2017. The 2 major limitations observed in the ocean surface wind speed



(oswWindSpeed) measurements performances of Sentinel-1 B ESA Level-2 Ocean products are the same than with Sentinel-1 A. They are:

1. Wind speed performances are wind speed dependent for both WV1 and WV2.
2. The presence of null wind speed obtained with WV1. This is due to the use of CMOD IFR2 for the wind inversion.

These two issues are related to the Wave Mode calibration and the choice of the Geophysical Model Function in the inversion scheme.

7.2.2. Swell Measurement

7.2.2.1. Wave Mode

In 2017, Sentinel-1 acquisitions in wave mode have been performed at global scale over the oceans in a routine configuration during the whole year. It leads to about 480000 acquisitions (between ~20000 and ~20000 for both WV1 and WV2 each month) of acquisitions every cycle. A period of 3 months (20/03/2017 to 03/07/2017) has been dedicated to acquisitions in HH polarization. This report focuses only on VV which is the nominal acquisition mode. The performances obtained for HH polarization will be assessed in a future report.

As for Sentinel-1 A, the waves performances are estimated by comparison between the significant wave heights of the long waves as measured by Sentinel-1 and produced by Wave Watch 3 model (WW3). WW3 is used to produce a 2D ocean wave spectrum for each Sentinel-1 acquisition. On a statistical basis and over open-ocean, WW3 is used as the reference. For both S-1A and WW3, the significant wave height of the long waves is estimated by integration of the 2D ocean wave spectra up to the cut-off values (above this value, the inversion is not expected to work). This is why this parameter is called the effective significant wave height. It is directly computed from the ocean swell spectrum (oswPolSpec) and the 2D cut-off (oswSpecRes. The use of this variable aims at filtering the spectral domain that is considered as valid after ocean swell inversion) variables included in the L2 OCN products. Figure 87 shows an example of comparison between Sentinel-1 B and WW3, respectively for WV1 and WV2 as obtained in December 2017. Very similar performances are obtained for the two incidence angles.

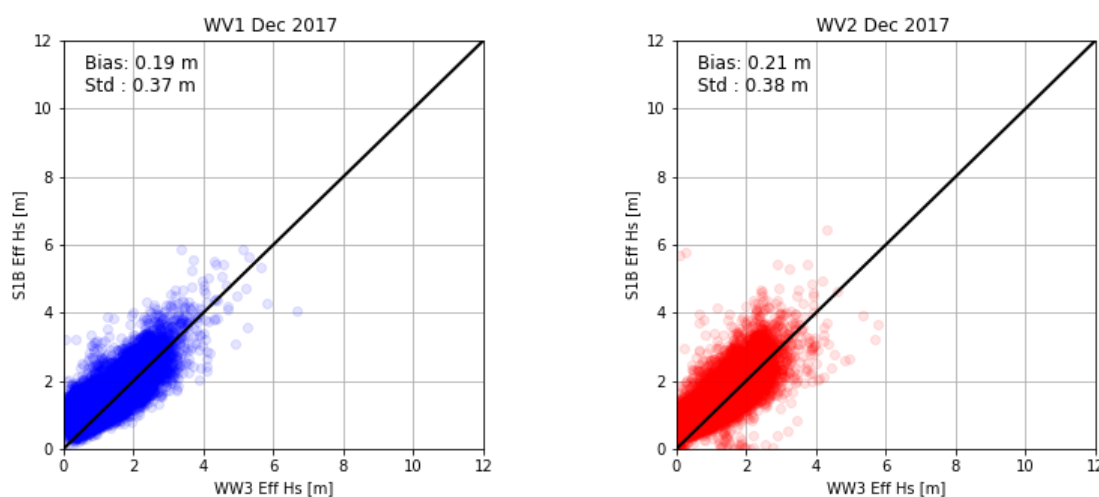


Figure 87: Significant wave height for the long waves performances for December 2017 in Wave Mode 1. The model outputs from WW3 are considered as reference here. This is only valid from a statistical point of view.

Figure 88 shows performances for the effective significant wave height with respect to time. We observed very stable performances of S-1B on both WV1 and WV2 along year 2017. An overestimation of 0.2 m is observed. Standard deviation values are lower than 0.5 m for both WV1



and WV2. These results are within the specifications. The standard deviation of the effective significant wave height remains constant through 2017. Note that, when the acquisitions are in HH polarization, the performances are changing. This will be investigated in the future.

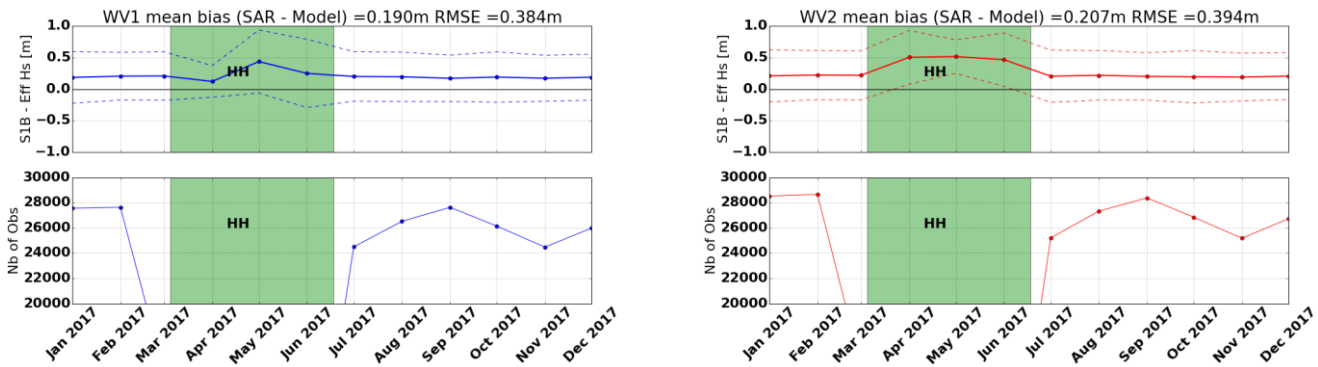


Figure 88: S-1B WV1 Ocean Swell monthly performances as function of time. For top panels, coloured thick solid lines stand for the mean difference between effective significant wave height from Sentinel-1 and from WW3 model. Coloured thin solid lines are for standard deviation.

Conclusion

Sentinel-1B significant wave height performances with respect to WW3 numerical model forecasts are better than the mission requirements regarding the bias but not for the RMSE (specifications are $RMSE < 0.5m$ and $bias < 0.1m$).

We estimated:

- a mean bias of about 0.19m for WV1 and 0.21m for WV2
- a RMSE about 0.38m for WV1 and 0.39m for WV2

Except the period of HH polarization acquisition (not evaluated in this report), those values are stable during the year 2017.

7.2.3. Radial Velocity Measurement

7.2.3.1. Wave Mode

In 2017, Sentinel-1 acquisitions in wave mode have been performed at global scale over the oceans in a routine configuration during the whole year. It leads to about 480000 acquisitions (between ~20000 and ~20000 for both WV1 and WV2 each month) of acquisitions every cycle. A period of 3 months (20/03/2017 to 03/07/2017) has been dedicated to acquisitions in HH polarization. This report focuses only on VV polarisation which is the nominal acquisition mode. The performances obtained for HH polarization will be assessed in a future report.

The radial velocity measurement is derived from the Geophysical Doppler anomaly. In the S-1 IPF, this geophysical Doppler is estimated by:

$$F_{dc_{Ocean}} = F_{dc_{SAR}} - F_{dc_{attitude}} - F_{dc_{antenna}}$$

where:

- $F_{dc_{SAR}}$ is estimated from the SAR data
- $F_{dc_{Ocean}}$ is the component related to the ocean radial velocities.
- $F_{dc_{attitude}}$ is estimated from the geometry knowledge (quaternion based)
- $F_{dc_{antenna}}$ is the antenna contribution related to TRM drifts, failures, misalignments, etc



At global scale, the expected relationship between the geophysical Doppler and the sea state (or ocean surface wind vector) is well known since Envisat/ASAR. The performances of the geophysical Doppler are assessed by estimating the bias between the expected Doppler given the sea state conditions (provided by ECMWF) and the geophysical Doppler as included in the Level 2 products.

Statement of the ocean surface radial velocities measurements accuracy:

As shown for Sentinel-1A, (see section 5.2.3), the same issues (bias (see Figure 89 and Figure 90 and variability along an orbit) with the geophysical Doppler shift as derived from the different Doppler components included in the Level-2 products have been observed with Sentinel-1 B during its commissioning phase. However, although not satisfying, it must be noted that the geophysical Doppler as obtained with S-1B exhibits less non-geophysical variability than what is observed with S-1A (see Figure 90 compared to Figure 43).

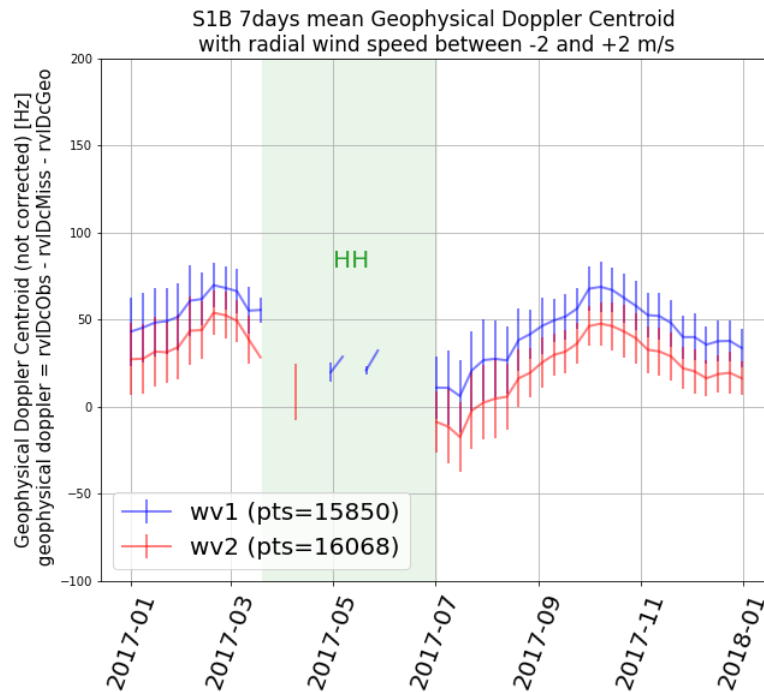


Figure 89: Geophysical Doppler Centroid evolution. Light green area delineates the HH period of acquisition.

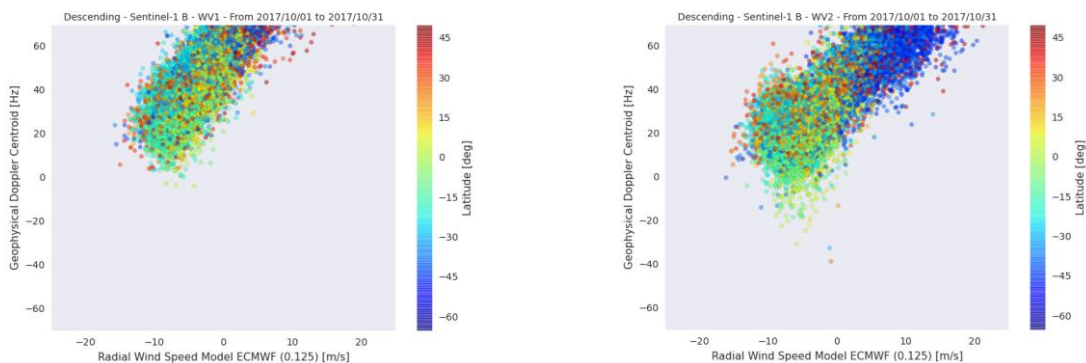


Figure 90: S-1B Geophysical Doppler as included in the Level 2 products as a function of radial wind speed (wind speed projected in the line of sight of the radar) for WV1 and WV2. The colour code indicates the latitude.



The various S1 WV OCN Doppler components (i.e. the data DC, the EM DC bias, the geometricDC) for one month of S-1B WV are shown in next figures. Note that the geometric DC is always close to zero Hz.

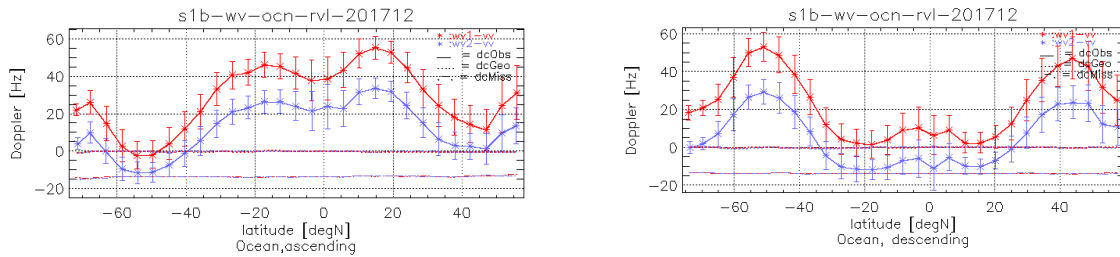
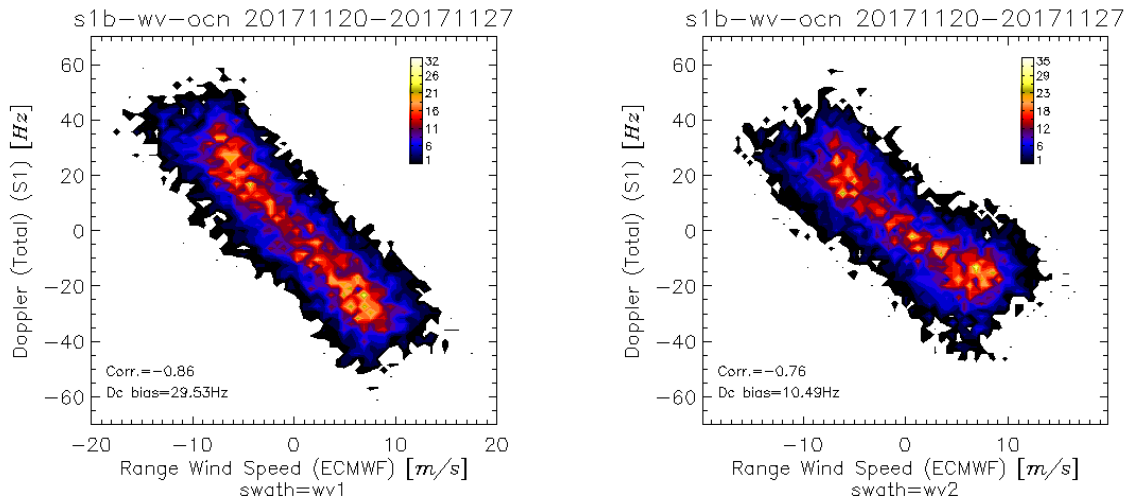


Figure 91: S-1B WV OCN Doppler components from December 2018.The vertical bars are the spread in measured DC over the period. Note that the geometric DC is around zero and the EM DC bias is around -15Hz for S-1B.

Improvement performed during 2017:

In late November 2017 ESA performed a STT Aberration Correction and an AOCs Fine Attitude Tuning on Sentinel-1B. A positive impact was observed on the S-1B OCN Doppler product, as shown in **Figure 92**. A significant increase in correlation between S-1B OCN Doppler and radial wind speed is observed after the corrections.



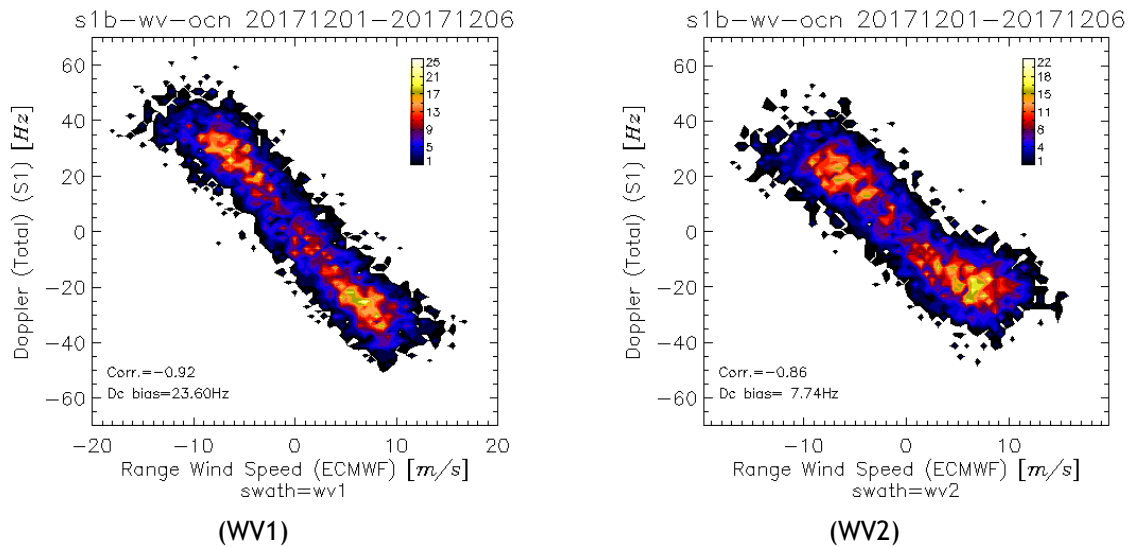


Figure 92: S-1B WV OCN Doppler versus range wind speed before (upper plots) and after (lower plots) attitude correction.

Coming improvement for 2018:

Furthermore, efforts are undertaken to develop and demonstrate a way to fully calibrate the S1 OCN Doppler by using the restituted attitude data in combination with a data driven model to assess the residual geometric Dc. This activity will also include a monitoring of the antenna electronic miss pointing DC bias.

7.2.3.2. TOPS Mode

Statement of the ocean surface radial velocities measurements accuracy:

As for Wave Mode, the contamination of the geophysical Doppler by the geometry knowledge (quaternion based) and the antenna contribution prevents us for getting any quantitative geophysical signature such as ocean surface currents in the product.

Azimuth scalloping in the DC over the bursts are also observed in S-1B. This is similar to what is observed in S-1A IW and EW modes. The scalloping is quantified to be around ± 5 Hz amplitude as shown in Figure 93.

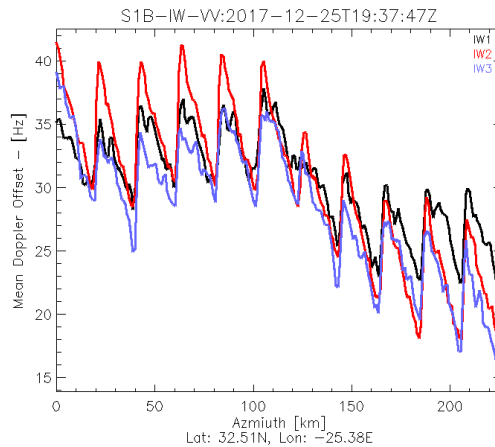


Figure 93: S-1B IW OCN RVL mean DC bias as function of azimuth pixel. Data acquired over ocean areas.



Improvement performed during 2017:

Efforts were undertaken to better predict and compensate the measured Doppler for the electromagnetic (EM) Doppler bias introduced by the skewness of the antenna elevation pattern. A new version of the antenna model parameters has been ingested into the Level 2 processor and the EM Doppler bias over EW swaths is compared with the data driven Doppler estimated over rain forest areas (see Figure 94).

Although the relative trends over swaths are predicted well, a significant Doppler bias is observed between the model and data. Compared to previous results, the model and data are better aligned and the jumps between swaths are better predicted.

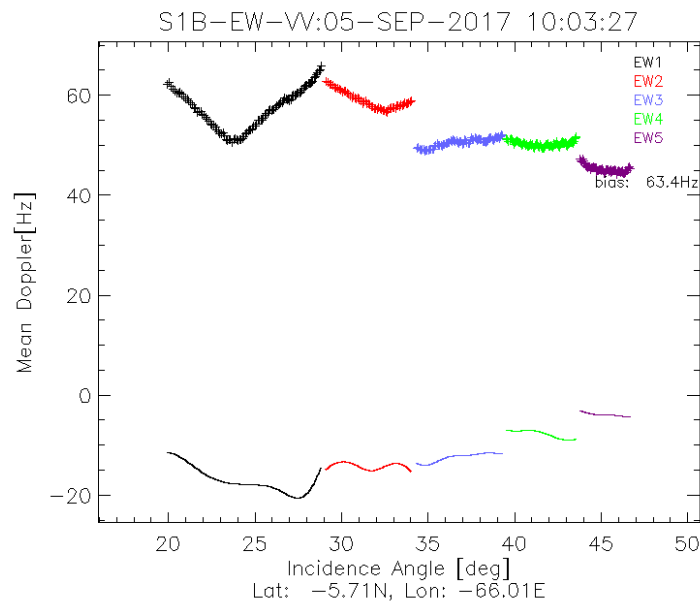


Figure 94: S-1 B VV EM DC offset computed from antenna model (full line) with error matrix corresponding to the day of acquisition, and estimated from rain forest data using the Level 2 processor.

Coming Improvements for 2018:

A further refinement of the de-scalloping will be implemented without increasing the processing time.



7.2.4. Geophysical Calibration

7.2.4.1. Wave Mode

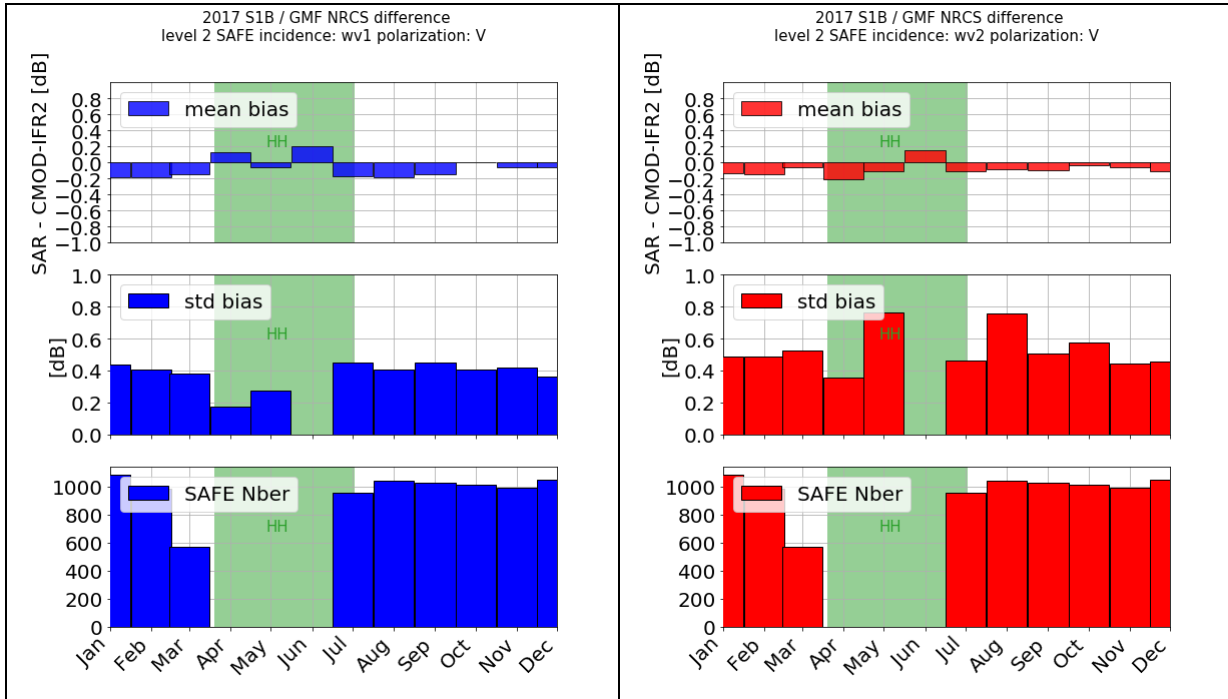


Figure 95: Sentinel-1B geophysical relative RCS computed using CMOD-IFRv2+ECMWF for WV1 VV polarisation between 50° and -50° latitude. Panel 1 shows the mean bias between ECMWF and Sentinel-1B. Panel 2 shows the bias standard deviation. Panel 3 shows the number of SAFE used to perform the analysis.

As shown in Figure 95, S-1B WV1 calibration oscillated around -0.1dB during the 10 first month. The change of calibration gain at the beginning of October reduced this underestimation to values close to zero dB. Same behaviour has been observed for WV2 except that the HH period of acquisition introduced a negative shift of 0.5dB (as shown in Figure 96) degrading the expected sigma0 compare to the empirical C-band model (CMOD-IFR2). Standard deviation is stable around 0.5dB and consistent with S-1A.

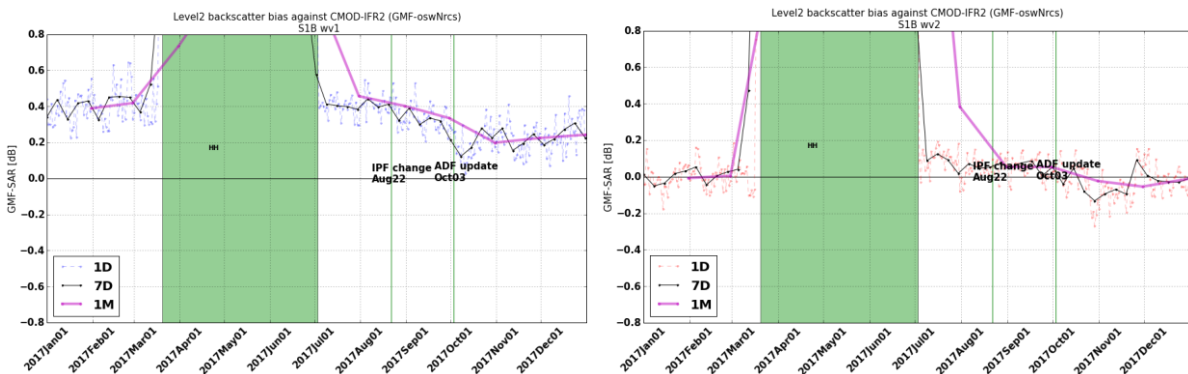


Figure 96: External Geophysical calibration bias. WV1 (left) and WV2 (right) 7-days mean of sigma0 difference with a GMF are displayed. Green vertical line indicates the date of the AUX_PP1 calibration update and IPF 2.84 deployment.



8. S-1A and S-1B Cross-comparison

8.1. Radiometric Calibration

8.1.1. Absolute Radiometric Calibration

As explained in Sections 5.1.2.1 and 7.1.2.1, the BAE corner reflector has been used for absolute calibration. Figure 97 shows the relative RCS of the corner reflector during 2017 for both S1-A and S1-B. There is a good radiometric correspondence between the two satellites.

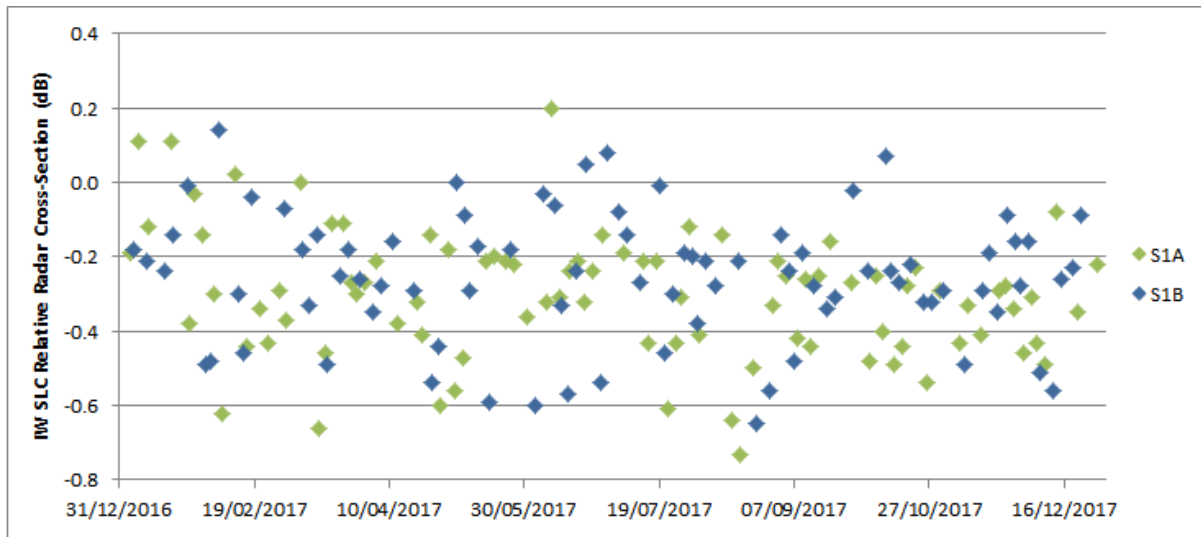


Figure 97: S-1A and S-1B IW SLC Relative Radar Cross-Section for the BAE Corner Reflector

8.1.2. Permanent Scatter Calibration

The following shows a recent IW VV Permanent Scatter Calibration series over Paris. The series covers the period from January 2016 to December 2017 and includes both S-1A and S-1B acquisitions (starting from the end of CP in September 2016), in order to perform a cross-calibration between the sensors. The blue dots (S-1A) show, after the tile 11 issue (June 2016), a small reduction of the calibration constant (about 0.1 dB) and a further step is observed around March 2017 with the deployment of IPF 2.8.2. The red dots show that the calibration constant for S-1B is, at the moment, about 0.2 dB higher than S-1A.

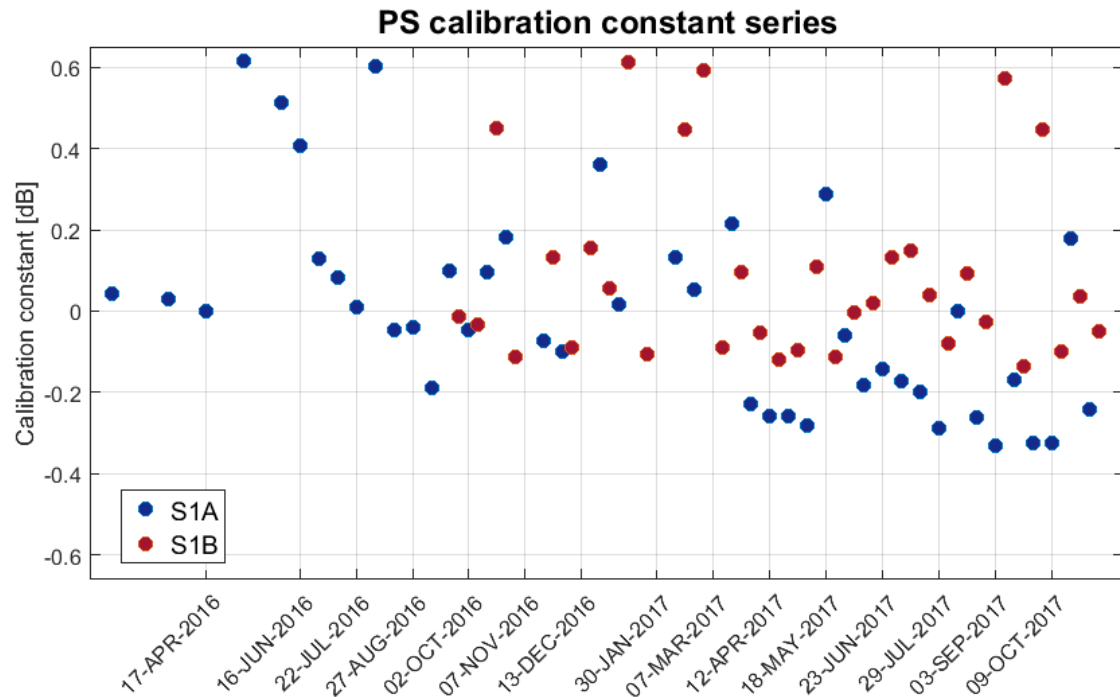


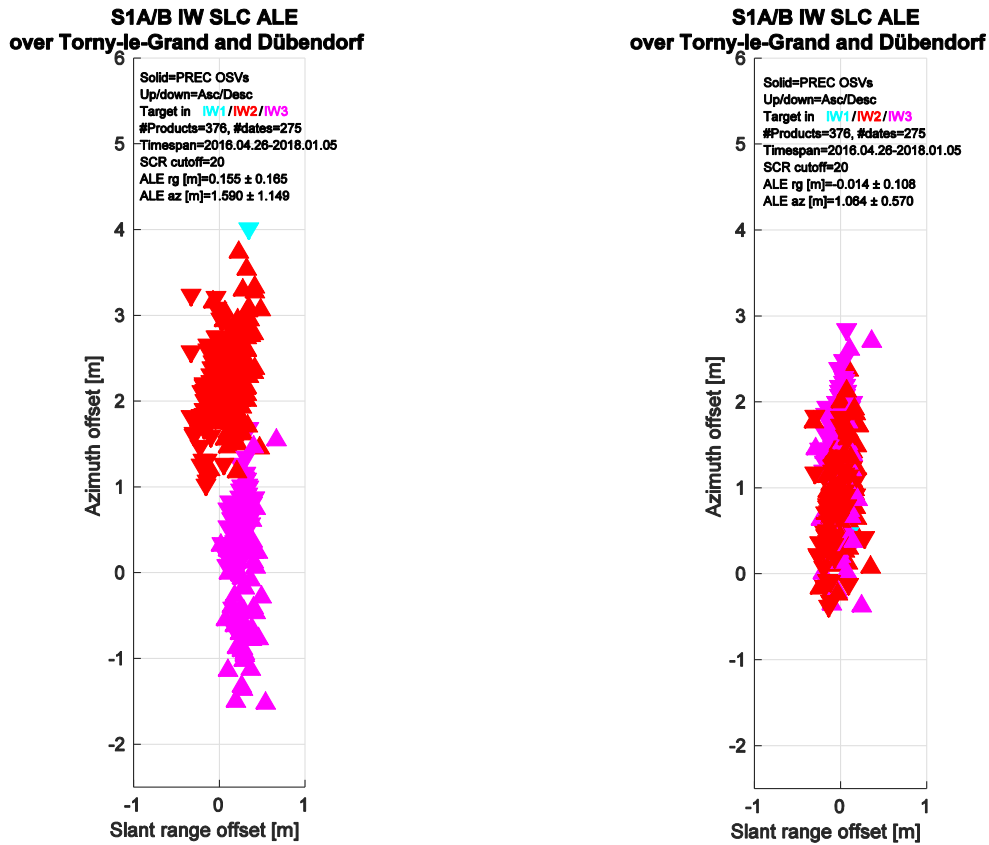
Figure 98: PSCAL time series for IW DV acquisitions over Paris. The colour represents the sensor.

8.2. Geometric Validation

Both S-1A and S-1B geolocation quality was monitored regularly throughout 2017 using IW SLC products. The trihedral corner reflectors (CRs) whose positions had been installed and surveyed with cm-level accuracy at the Swiss test sites *Torny-le-Grand* and *Dübendorf* during S-1B commissioning continued to serve as reference targets in 2017.

Absolute Location Error (ALE) was estimated according to the steps described in section 5.1.3. The ALE estimates are shown for the combined S-1AB IW SLC product time series in Figure 99. It is comparable to Figure 70(c) and (d), but combines estimates from S-1A & -B. To contrast the previous best ALE estimates with the current ones, both results are shown for each mode. In Figure 99(a) the estimates based on the previous methods are shown; Figure 99(b) represents the current estimates. Both the range and azimuth ALE improved for all modes. The elimination of the clear sub-swath grouping visible in (a) was the most significant improvement made to the UZH post-processing chain in 2017.

The ALE plots in Figure 99 indicate that given bias compensations, the localisation performance of both S-1A and S-1B were much better than the original requirements (according to sections 5.5.2.1 and 5.5.2.2 in [S1-RD-09]).



(a) S-1A/BIW SLC (previous ALE scatter)

(b) S-1A/B IW SLC (current ALE scatter)

Figure 99: ALE estimates for S-1A/B IW SLC product time series acquired over the Swiss test sites using precise state vectors (AUX_POEORB). (a) shows ALE using earlier post-processing methods; (b) shows more recent results after improved post-processing. Product date ranges are annotated. Point colours represent beam/sub-swath.

8.3. Interferometric Baseline

Figure 100 shows the three cross-sensor interferometric baseline components (Parallel on top, Normal in the mid and Along-Track on the bottom) evolution during 2017. The baseline components have been evaluated exploiting the PDGS OBS tool, which compares the S-1B orbits with an arbitrary selected S-1A reference cycle (cycle number 60, 30 September - 12 October 2015).

The hot colours represent the maximum baseline value and the cold colours represent the minimum baseline value measured for each orbit. The different colours represent the track number evolving for each cycle from 1 to 175.

The most critical baseline component for the interferometric coherence is the normal one, which shall be lower than a certain threshold named critical baseline (about 5 km for S-1 and depending on the considered swath). The measured normal baseline (mid plot) shows that the worst case coherence loss due to the interferometric baseline is always well below 5%.

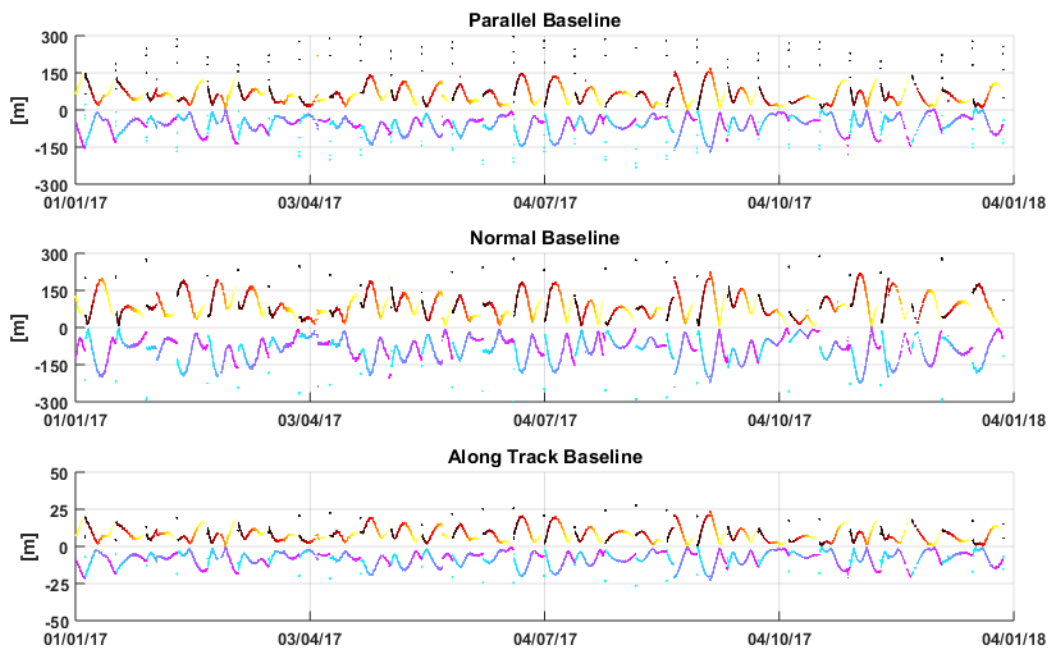


Figure 100: Parallel (top) Normal (mid) and Along-Track (bottom) interferometric baseline during 2017. The hot colours represent the maximum value and the cold colours represent the minimum value for each orbit. The colours represent the track number.

8.4. Instrument Pointing

Figure 101 shows the comparison between the S-1A (blue) and S-1B (red) Doppler Centroid from data during 2017 on a daily basis. The DC difference between S-1A and S-1B is 30 Hz at maximum, corresponding to a loss of coherence for TopSAR interferometry of less than 3%. Some common trends, probably due to seasonal orbit perturbations, can be observed in the data DC evolution. The DC alignment will be verified again after that the attitude patches applied for S-1B during November 2017 will be applied for S-1A as well.

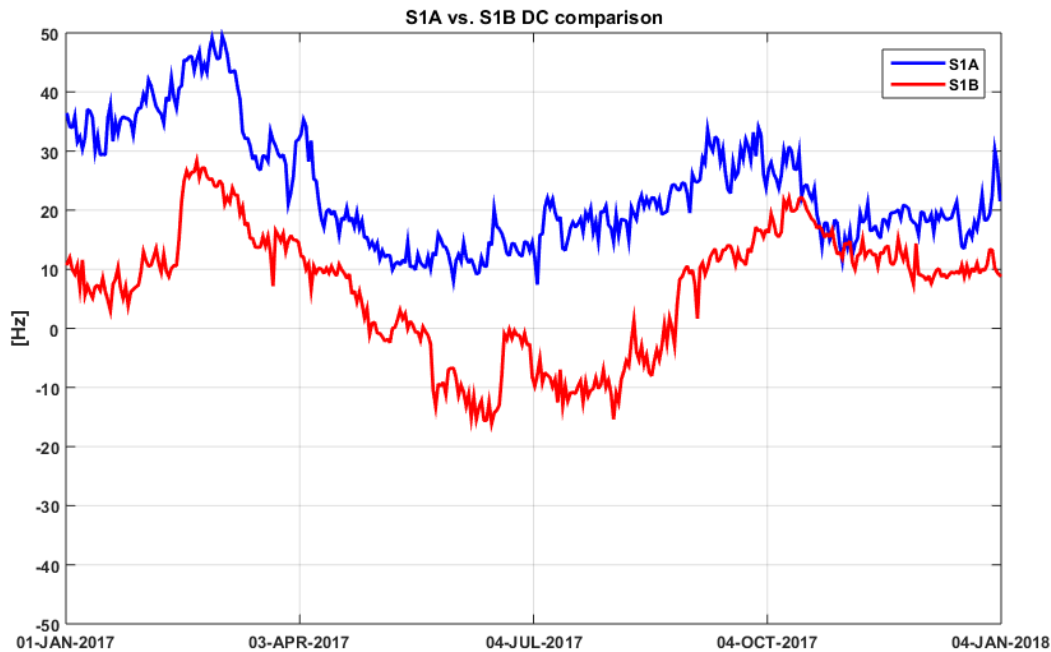


Figure 101: Comparison of S-1A (blue) and S-1B (red) daily average DC from data.

8.5. Cross-interferometry Burst Synchronization

The burst synchronization between repeat pass interferometric acquisitions is relevant for the TOPSAR modes (IW and EW) to provide an indication of the quality of the interferometric phase that can be expected. The SAR acquisition start time is planned over a discrete set of points round orbit with precision down to milliseconds. The performance of the synchronization is monitored by the PDGS OBS tool.

The S-1A and S-1B constellation offers the possibility to perform repeat pass interferometry at 6 days temporal baseline. The following figure shows the S-1B vs. S-1A burst synchronization error over time for IW and EW mode. The colour of the dots represents the number of repeat pass acquisitions falling in a certain temporal and burst synchronization interval (light blue meaning few points and purple meaning many points). The S-1A reference cycle number 60 (30 September - 12 October 2015) has been used as reference. Note that overall synchronization, even though slightly worse than single sensor, is still very good.

The daily average synchronization is reported with a continuous black line. It can be noticed that the average synchronization is always very good with a small seasonal trend (less than 5 ms peak to peak). This is also observed for S-1A (see Figure 28) and S-1B (see Figure 78), suggesting a common origin due to some long term orbit perturbation.

The black dashed lines represent the S-1 synchronization requirement (about ± 7 ms). This value is obtained starting from the timing requirement for single acquisitions (5 ms) and multiplying it by $\sqrt{2}$ due to the fact that all the values in the image are obtained by combining the timing error two independent acquisitions. The synchronization performance is quite good with 95.7% of IW acquisitions and 87.6% of EW acquisitions being better than the timing requirement.

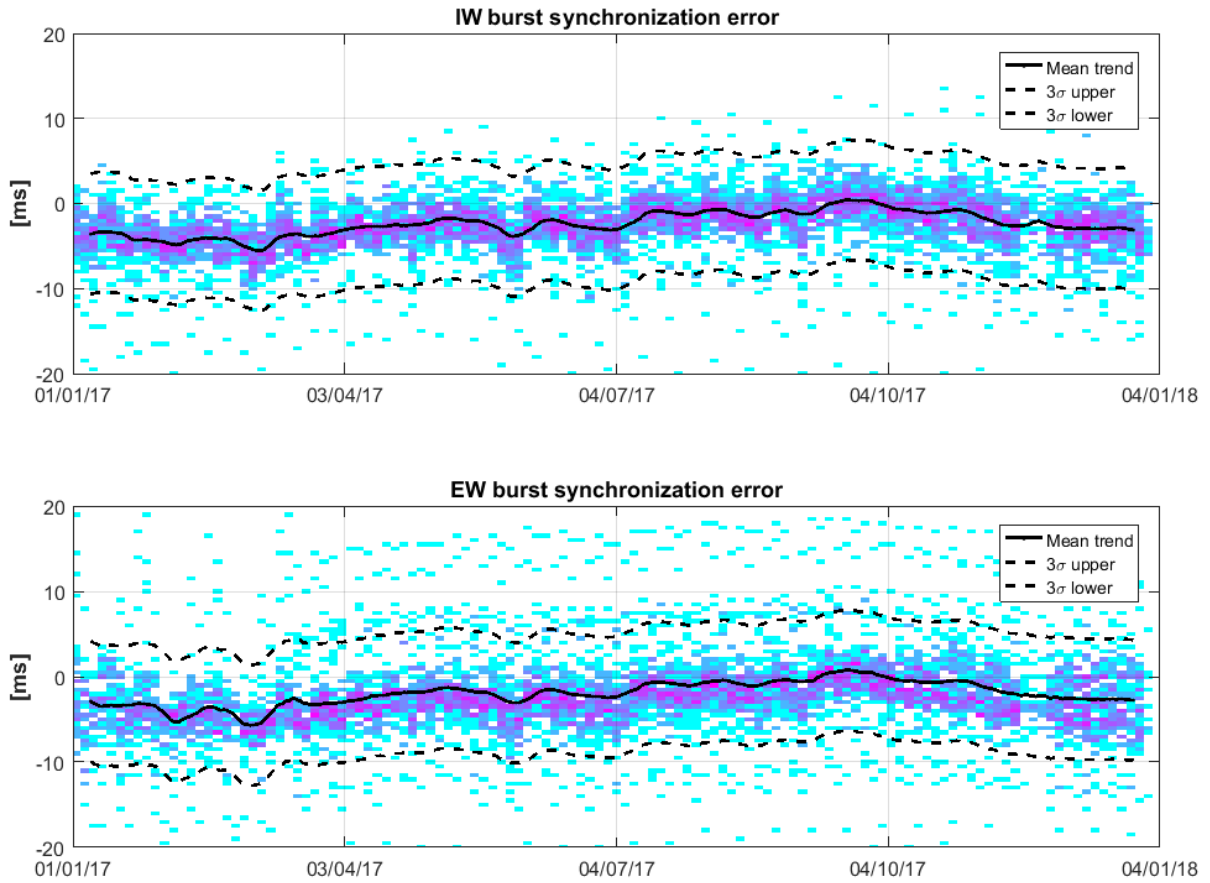


Figure 102: S-1B vs. S-1A burst synchronization error during 2017.



Appendix A - List of Acronyms

AD	Applicable Document
ADF	Auxiliary Data File
CFI	Customer Furnished Item
CP	Commissioning Phase
DC	Doppler Centroid
EAP	Elevation antenna Pattern
ECMWF	European Centre for Medium-Range Weather Forecasts
EFE	Electronic Front End
ENL	Equivalent Number of Look
FDBAQ	Flexible Dynamic Block Adaptive Quantisation
GMF	Geophysical Model Function
IRF	Impulse Response Function
IPF	Instrument Processing Facility
NESZ	Noise Equivalent Sigma Zero
PDGS	Payload Data Ground Segment
PG	Power x Gain
PSC	Permanent Scatterers Calibration
QCSS	Quality Control SubSystem
(N)RCS	(Normalised) Radar Cross Section
RD	Reference Document
RDB	Radar DataBase
RFC	Radio Frequency Characterization mode
RFI	Radio Frequency Interference
SAR	Synthetic Aperture Radar
STT	STar Tracker
TBC	To be confirmed
TBD	To be defined
TRM	Transmit Receive Module



Appendix B - S-1A & S-1B Technical Reports

The following S-1A & S-1B Technical Reports are available on [Sentinel Online Library](#):

Masking "No-value" pixels on GRD products generated by the Sentinel-1 ESA IPF, issue 2.1, 29th January 2018

This technical note describes an approach for masking the "no-pixel" values for GRD products generated by the Sentinel-1 ESA IPF.

Release Note of S-1 IPF for End Users of Sentinel-1 products, MPC-0389, Issue 1.0, 16 January 2018

This document aims to provide the end users of Sentinel-1 products a high level description of the evolutions of the Sentinel-1 products related to successive versions of the Sentinel-1 processor (S-1 IPF). It describes the evolutions introduced by each version of the processor. Notice that each version of the IPF includes the features introduced by previous versions.

Thermal denoising of products generated by the Sentinel-1 IPF, MPC-0392, Issue 1.1, November 2017

This technical note describes the approach for removing the thermal noise contribution (aka product denoising step)

Sentinel-1 RadarSat-2 mutual interference, MPC-0353, Issue 1.0, 28 November 2017

This technical note describes the mutual interference that can occur between Sentinel-1 and the Canadian Radarsat-2 satellite which operates at the same frequency as Sentinel-1. The mutual interferences are observed on specific locations and times of the orbits and only when both instruments are transmitting simultaneously.

This document provides description of (1) the respective orbits of Sentinel-1 and Radarsat-2 is described in Section 2, and (2) examples of the mutual interference given in Section 3. A list of mutual interferences found at the Mission Performance Centre (MPC) Coordination Centre are given in Appendices of the document.

Definition of the TOPS SLC deramping function for products generated by the Sentinel-1 IPF

This document defines the procedure for performing the deramping of Sentinel-1 TOPS IWS and EWS of Level-1 SLC products generated by the Sentinel-1 IPF.

Report on the debris impact on S1-A solar panel on 23rd August 2016

The present technical note discusses the debris collision that occurred on 23rd August 2016 whereby the Sentinel-1A solar panel was struck by a small mm sized particle. The implications for products are given in the report.

Sentinel-1A Antenna Failure - Anomaly Characterization Report

This technical note discusses the impact of the Sentinel-1A tile 11 issue that occurred during June 2016.

Sentinel-1 IPF: Impact of the Elevation Antenna Pattern Phase Compensation on the Interferometric Phase Preservation

The Elevation Antenna Patterns (EAPs) used by the S-1 Instrument Processing Facility (IPF) are derived from the S-1 Antenna Model (AM) which is able to predict with great accuracy the gain and phase patterns.

The EAP correction by the S-1 IPF was at launch only considering the gain, similarly to what was done for ASAR. As an outcome of the S-1A Commissioning Phase, it has been decided to upgrade the S-1 IPF to also compensate for the EAP phase, in order to correct for the induced phase difference between the polarimetric channels.



This correction was introduced in March 2015 with the IPF V243. Performing interferograms between products generated with the IPFV243 and the former version V236 leads to interferometric phase variation in range.

This technical note explains the nature of the phase offset and provides recommendation towards its correction.

Sentinel-1 Radiometric Calibration of Products

This document defines the procedure to radiometrically calibrate Sentinel-1 Level 1 products generated by the Sentinel-1 IPF.

S-1A & S-1B N-Cyclic reports published on <https://sentinels.copernicus.eu/.../sentinel-1-sar/document-library> give information on the S-1 quality on a four-cycle period. These reports aimed to be replaced by the annual performance report of their covering period, when the latter is available.



Appendix C - S-1A & S-1B Instrument Unavailability

The S-1A & S-1B instruments were unavailable during 2017 (a full list since launch can be found in Appendix C of any S-1A or S-1B N-Cyclic Performance Report):

Start Date/Time	End Date/Time	MPC Reference	Summary
16/06/2017 09:09	16/06/2017 12:31	SOB-751	Sentinel-1A Unavailability on 16/06/2017
17/06/2017 11:43	17/06/2017 14:43	SOB-752	Sentinel-1A Unavailability on 17/06/2017
21/06/2017 14:09	21/06/2017 17:35	SOB-753	Sentinel-1A Unavailability on 21/06/2017
07/07/2017 02:20	07/07/2017 10:29	SOB-758	Sentinel-1A Unavailability on 07/07/2017
03/08/2017 13:30	03/08/2017 14:07	SOB-776	Sentinel-1A Unavailability on 03/08/2017
01/10/2017 12:06	01/10/2017 20:01	SOB-796	Sentinel-1A Unavailability on 01/10/2017
25/10/2017 08:25	25/10/2017 10:15	SOB-817	Sentinel-1A planned Unavailability on 25/10/2017

The S-1B instrument was unavailable during 2017 (a full list since launch can be found in Appendix C of any S-1B N-Cyclic Performance Report):

Start Date/Time	End Date/Time	MPC Reference	Summary
21/03/2017 16:23	22/03/2017 11:53	SOB-702	Sentinel-1B SAR issue from 21/03/2017 to 22/03/2017
13/04/2017 15:38	14/04/2017 09:35	SOB-727	Sentinel-1B Unavailability from 13/04/2017 to 14/04/2017
20/04/2017 20:43	21/04/2017 11:32	SOB-729	Sentinel-1B Unavailability from 20/04/2017 to 21/04/2017
12/05/2017 09:03	12/05/2017 10:46	SOB-738	Sentinel-1B Unavailability on 12/05/2017
08/07/2017 05:21	08/07/2017 10:15	SOB-759	Sentinel-1B Unavailability on 08/07/2017
02/08/2017 14:21	02/08/2017 17:32	SOB-779	Sentinel-1B Unavailability on 02/08/2017
25/08/2017 23:29	26/08/2017 09:18	SOB-781	Sentinel-1B Unavailability between 25/08/2017 and 26/08/2017
18/11/2017 20:48	19/11/2017 10:02	SOB-825	Sentinel-1B Unavailability between 18/11/2017 and 19/11/2017



Appendix D - S-1A & S-1B Quality Disclaimers

The following S-1A & S-1B quality disclaimers were issued during 2017:

Number	Description	Start Validity Date	End Validity Date	Issue Status
24	Incorrect Cycle Number in S1-A Products acquired between 12/01/2017 and 24/01/2017	2017-01-12 00:18:59 UT	2017-01-24 06:52:28 UT	Issued
25	Incorrect Cycle Number in S1-B Products acquired between 12/01/2017 and 24/01/2017	2017-01-12 07:48:29	2017-01-24 07:14:46	Issued
26	S-1A products processed with invalid Restituted Orbit Files (AUX_RESORB) between 2017-09-06 and 2017-09-07	2017-09-06 18:57:47 UT	2017-09-07 08:07:45 UT	Issued
27	S-1B products processed with invalid Restituted Orbit Files (AUX_RESORB) between 2017-09-06 and 2017-09-07	2017-09-06 18:07:43	2017-09-07 07:17:41	Issued



Appendix E - S-1A Orbit Cycles

The table below gives the cycle number with start and stop acquisition dates during 2017. The start of a cycle is at approximately 18:00 UT on the dates below.

Cycle	Start Date	End Date
99	10/01/2017	22/01/2017
100	22/01/2017	03/02/2017
101	03/02/2017	15/02/2017
102	15/02/2017	27/02/2017
103	27/02/2017	11/03/2017
104	11/03/2017	23/03/2017
105	23/03/2017	04/04/2017
106	04/04/2017	16/04/2017
107	16/04/2017	28/04/2017
108	28/04/2017	10/05/2017
109	10/05/2017	22/05/2017
110	22/05/2017	03/06/2017
111	03/06/2017	15/06/2017
112	15/06/2017	27/06/2017
113	27/06/2017	09/07/2017
114	09/07/2017	21/07/2017
115	21/07/2017	02/08/2017
116	02/08/2017	14/08/2017
117	14/08/2017	26/08/2017
118	26/08/2017	07/09/2017
119	07/09/2017	19/09/2017
120	19/09/2017	01/10/2017
121	01/10/2017	13/10/2017
122	13/10/2017	25/10/2017
123	25/10/2017	06/11/2017
124	06/11/2017	18/11/2017
125	18/11/2017	30/11/2017
126	30/11/2017	12/12/2017
127	12/12/2017	24/12/2017
128	24/12/2017	05/01/2018



Appendix F - S-1A Transmit Receive Module Failures

The following S-1A antenna Transmit/Receive Modules (TRMs) failed during 2017 (a full list since launch can be found in Appendix B of any S-1A N-Cyclic Performance Report):

TRM	Description	Date of Failure
Tile 11	See below	

On the 16th October 2017 the S-1A antenna was reconfigured to optimize the electronic operation after the tile 11 issue on June 2016. The new antenna configuration, only related to the tile 11, was captured in RDB#6. From the SAR data point of view, the new antenna status is not much different from the previous one and the only observed effects are a slight increase of the PG (less than 0.1 dB) and a modification of the EAP from the S-1 AM (lower then ± 0.1 dB).



Appendix G - S-1A Auxiliary Data Files

The following S-1A Auxiliary Data Files (ADFs) were updated during 2017:

Instrument ADF (AUX_INS)

ADF	Update Reason
S1A_AUX_INS_V20171017T080000_G20171013T101216.SAFE	Update of ADF to be compliant with RDB#6.

Calibration ADF (AUX_CAL)

ADF	Update Reason
S1A_AUX_CAL_V20140406T133000_G20170328T093222.SAFE	Updates of (a) noise calibration factors and (b) Elevation antenna pattern in S1A_AUX_CAL to implement the outcome of recalibration #2 activities performed in preparation to IPF V282 deployment. Related to RDB#1.
S1A_AUX_CAL_V20140616T133500_G20170328T093438.SAFE	Updates of (a) noise calibration factors and (b) Elevation antenna pattern in S1A_AUX_CAL to implement the outcome of recalibration #2 activities performed in preparation to IPF V282 deployment. Related to RDB#2.
S1A_AUX_CAL_V20140908T000000_G20170328T093643.SAFE	Updates of (a) noise calibration factors and (b) Elevation antenna pattern in S1A_AUX_CAL to implement the outcome of recalibration #2 activities performed in preparation to IPF V282 deployment. Related to RDB#3.
S1A_AUX_CAL_V20150519T120000_G20170328T093753.SAFE	Updates of (a) noise calibration factors and (b) Elevation antenna pattern in S1A_AUX_CAL to implement the outcome of recalibration #2 activities performed in preparation to IPF V282 deployment. Related to RDB#4.
S1A_AUX_CAL_V20150722T120000_G20170328T093923.SAFE	Updates of (a) noise calibration factors and (b) Elevation antenna pattern in S1A_AUX_CAL to implement the outcome of recalibration #2 activities performed in preparation to IPF V282 deployment. Related to



	RDB#5.
S1A_AUX_CAL_V20160627T000000_G20170522T132042.SAFE	Updated S1-A SM, IW and EW Elevation Antenna Patterns following the Tile 11 Anomaly in June 2016. Related to RDB#5.
S1A_AUX_CAL_V20171017T080000_G20171013T101200.SAFE	Update of ADF to be compliant with RDB#6.

L1 Processor Parameters ADF (AUX_PP1)

ADF	Update Reason
S1A_AUX_PP1_V20140406T133000_G20170328T093347.SAFE	Update of the processing gains for IW and EW modes to implement the outcome of recalibration #2 activity performed in preparation to IPF V282 deployment. Related to RDB#1.
S1A_AUX_PP1_V20140616T133500_G20170328T093550.SAFE	Update of the processing gains for IW and EW modes to implement the outcome of recalibration #2 activity performed in preparation to IPF V282 deployment. Related to RDB#2.
S1A_AUX_PP1_V20140908T000000_G20170328T093714.SAFE	Update of the processing gains for IW and EW modes to implement the outcome of recalibration #2 activity performed in preparation to IPF V282 deployment. Related to RDB#3.
S1A_AUX_PP1_V20150519T120000_G20170328T093825.SAFE	Update of the processing gains for IW and EW modes to implement the outcome of recalibration #2 activity performed in preparation to IPF V282 deployment. Related to RDB#4.
S1A_AUX_PP1_V20150722T120000_G20170328T093954.SAFE	Update of the processing gains for IW and EW modes to implement the outcome of recalibration #2 activity performed in preparation to IPF V282 deployment. Related to RDB#5.
S1A_AUX_PP1_V20140406T133000_G20171003T120502.SAFE	Processing gains updated for WV mode to introduce an offset compensating the bias characterised by Ifremer for S1A/B WV1 and WV2 through the analysis of data NRCS. Related to RDB#1.
S1A_AUX_PP1_V20140616T133500_G20171003T120626.SAFE	Processing gains updated for WV mode to introduce an offset compensating the bias characterised by Ifremer for S1A/B WV1 and WV2 through the analysis



	of data NRCS. Related to RDB#2.
S1A_AUX_PP1_V20140908T000000_G20171003T120702.SAFE	Processing gains updated for WV mode to introduce an offset compensating the bias characterised by Ifremer for S1A/B WV1 and WV2 through the analysis of data NRCS. Related to RDB#3.
S1A_AUX_PP1_V20150519T120000_G20171003T120730.SAFE	Processing gains updated for WV mode to introduce an offset compensating the bias characterised by Ifremer for S1A/B WV1 and WV2 through the analysis of data NRCS. Related to RDB#4.
S1A_AUX_PP1_V20150722T120000_G20171003T120757.SAFE	Processing gains updated for WV mode to introduce an offset compensating the bias characterised by Ifremer for S1A/B WV1 and WV2 through the analysis of data NRCS. Related to RDB#5.
S1A_AUX_PP1_V20171017T080000_G20171013T101236.SAFE	Update of ADF to be compliant with RDB#6.

L2 Processor Parameters ADF (AUX_PP2)

ADF	Update Reason
S1A_AUX_PP2_V20171017T080000_G20171013T101254.SAFE	Update of ADF to be compliant with RDB#6.

Simulated Cross Spectra ADF (AUX_SCS)

ADF	Update Reason
S1_AUX_SCS_V20171017T080000_G20171016T150910.SAFE	Update of ADF to be compliant with RDB#6.



Appendix H - S-1B Orbit Cycles

The table below gives the cycle number with start and stop acquisition dates during 2017. The start of a cycle is at approximately 18:00 UT on the dates below.

Cycle	Start Date	End Date
27	23/12/2016	04/01/2017
28	04/01/2017	16/01/2017
29	16/01/2017	28/01/2017
30	28/01/2017	09/02/2017
31	09/02/2017	21/02/2017
32	21/02/2017	05/03/2017
33	05/03/2017	17/03/2017
34	17/03/2017	29/03/2017
35	29/03/2017	10/04/2017
36	10/04/2017	22/04/2017
37	22/04/2017	04/05/2017
38	04/05/2017	16/05/2017
39	16/05/2017	28/05/2017
40	28/05/2017	09/06/2017
41	09/06/2017	21/06/2017
42	21/06/2017	03/07/2017
43	03/07/2017	15/07/2017
44	15/07/2017	27/07/2017
45	27/07/2017	08/08/2017
46	08/08/2017	20/08/2017
47	20/08/2017	01/09/2017
48	01/09/2017	13/09/2017
49	13/09/2017	25/09/2017
50	25/09/2017	07/10/2017
51	07/10/2017	19/10/2017
52	19/10/2017	31/10/2017
53	31/10/2017	12/11/2017
54	12/11/2017	24/11/2017
55	24/11/2017	06/12/2017
56	06/12/2017	18/12/2017
57	18/12/2017	30/12/2017
58	30/12/2017	11/01/2018

**Appendix I - S-1B Transmit Receive Module Failures**

The following S-1B antenna Transmit/Receive Module (TRM) failed during 2017 (a full list since launch can be found in Appendix B of any S-1B N-Cyclic Performance Report):

TRM	Description	Date of Failure
Tile 5, Row8	Rx, H	16-January-2017



Appendix J - S-1B Auxiliary Data Files

The following S-1B Auxiliary Data Files (ADFs) were updated during 2017:

Instrument ADF (AUX_INS)

ADF	Update Reason

Calibration ADF (AUX_CAL)

ADF	Update Reason
S1B_AUX_CAL_V20160422T000000_G20170116T134142.SAFE	Updated S1-B noise vectors for IW and EW modes. Related to RDB#1.
S1B_AUX_CAL_V20160422T000000_G20170328T092822.SAFE	Update of noise calibration factors in S1B_AUX_CAL to implement the outcome of recalibration #2 activity performed in preparation to IPF V2.8.2 deployment. Related to RDB#1.

L1 Processor Parameters ADF (AUX_PP1)

ADF	Update Reason
S1B_AUX_PP1_V20160422T000000_G20170116T134234.SAFE	S1B QL scaling LUT updated for SM, IW and EW modes (to be similar to S-1A). Related to RDB#1.
S1B_AUX_PP1_V20160422T000000_G20170328T093014.SAFE	Update of processing gains for IW and EW modes to implement the outcome of recalibration #2 activity performed in preparation to IPF V2.8.2 deployment. Related to RDB#1.
S1B_AUX_PP1_V20160422T000000_G20171003T120152.SAFE	Processing gains updated for WV mode to introduce an offset compensating the bias characterised by Ifremer for S1A/B WV1 and WV2 through the analysis of data NRCS. Related to RDB#1.

L2 Processor Parameters ADF (AUX_PP2)

ADF	Update Reason

Simulated Cross Spectra ADF (AUX_SCS)

ADF	Update Reason
S1__AUX_SCS_V20171017T080000_G20171016T150910.SAFE	Update of ADF to be compliant with S1-A RDB#6.